2017

Limited Bandwidth Wireless Communication Strategies for Structural Control of Seismically Excited Shear Structures

Benjamin Winter
Michigan Technological University, bdwinter@mtu.edu

LIMITED BANDWIDTH WIRELESS COMMUNICATION STRATEGIES FOR STRUCTURAL CONTROL OF SEISMICALLY EXCITED SHEAR STRUCTURES

By

Benjamin D. Winter

A DISSERTATION

Submitted in partial fulfillment of the requirements for the degree of

DOCTOR OF PHILOSOPHY

In Civil Engineering

MICHIGAN TECHNOLOGICAL UNIVERSITY

2017

This dissertation has been approved in partial fulfillment of the requirements for the Degree of DOCTOR OF PHILOSOPHY in Civil Engineering.

Department of Civil and Environmental Engineering

Dissertation Advisor:	*Dr. R. Andrew Swartz*
Committee Member:	*Dr. William Bulleit*
Committee Member:	*Dr. Qingli Dai*
Committee Member:	*Dr. Bo Chen*
Department Chair:	*Dr. David Hand*

To my wonderful family, my wife Eileen and sons, Myles and Henry.

Table of Contents

List of Figures

List of Tables

Preface

The work presented in this dissertation has been part of the research completed between January 2014 and March 2017. Chapters 3, 4, and 5 of this dissertation, though reconstructed and reformatted, include papers that are in review (Chapters 4 and 5) and accepted for publication (Chapter 3) in the Structural Control and Health Monitoring Journal. The author of this dissertation performed the research, experimental work, data analysis, and paper writing with guidance and editing provided by Dr. R. Andrew Swartz.

Chapter 3: Winter B.D., Swartz R.A. Low-force magneto-rheological damper design for small-scale structural control. *Structural Control and Health Monitoring.* 2017; e1990.

Chapter 4: Winter B.D., Swartz R.A. Wireless Structural Control using Multi-Step TDMA Communication Patterning for Static Bandwidth Allocation. *Structural Control and Health Monitoring.* Submitted for review, January 2017.

Chapter 5: Winter B.D., Swartz R.A. Wireless Structural Control using Stochastic Bandwidth Allocation and Dynamic State Estimation with Measurement Fusion. *Structural Control and Health Monitoring.* Submitted for review, February 2017.

Abstract

Structural control is used to mitigate unwanted vibrations in structures when large excitations occur, such as high winds and earthquakes. To increase reliability and controllability in structural control applications, engineers are making use of semi-active control devices. Semi-active control gives engineers greater control authority over structural response versus passive controllers, but are less expensive and more reliable than active devices. However, the large numbers of actuators required for semi-active structural control networks introduce more cabling within control systems leading to increased cost.

Researchers are exploring the use of wireless technology for structural control to cut down on the installation cost associated with cabling. However wireless communication latency (time delays in data transmissions) can be a barrier to full acceptance of wireless technology for structural control. As the number of sensors in a control network grows, it becomes increasingly difficult to transmit all sensor data during a single control step over the fixed wireless bandwidth. Because control force calculations rely on accurate state measurements or estimates, the use of strategic bandwidth allocation becomes more necessary to provide good control performance. The traditional method for speeding up the control step in larger wireless networks is to spatially decentralize the network into multiple subnetworks, sacrificing communication for speed.

This dissertation seeks to provide an additional approach to address the issue of communication latency that may be an alternative, or even a supplement, to spatial decentralization of the control network. The proposed approach is to use temporal decentralization, or the decentralization of the control network over time, as opposed to space/location. Temporal decentralization is first presented with a means of selecting and evaluating different communication group sizes and wireless unit combinations for staggered temporal group communication that still provide highly accurate state estimates. It is found that, in staggered communication schemes, state estimation and control performance are affected by the network topology used at each time step with

some sensor combinations providing more useful information than others. Sensor placement theory is used to form sensor groups that provide consistently high-quality output information to the network during each time step, but still utilize all sensors. If the demand for sensors to communicate data outweighs the available bandwidth, traditional temporal and spatial approaches are no longer feasible.

This dissertation examines and validates a dynamic approach for bandwidth allocation relying on an extended, autonomous and controller-aware, carrier sense multiple access with collision detection (CSMA/CD) protocol. Stochastic parameters are derived to strategically alter back-off times in the CSMA/CD algorithm based on nodal observability and output estimation error. Inspired by data fusion approaches, this second study presents two different methods for neighborhood state estimation using a dynamic form of measurement-only fusion. To validate these wireless structural control approaches, a small-scale experimental semi-active structural control testbed is developed that captures the important attributes of a full-scale structure.

Acknowledgments

A special acknowledgement goes to my advisor, Dr. R. Andrew Swartz, who accepted me into his research group as an undergraduate student and, from then on, has provided wonderful guidance and pushed me to vastly broaden my research and educational foundation.

The circuit designs for the *Martlet* wireless technology used in this dissertation were made by Michael Kane from the University of Michigan. I would like to acknowledge Dr. Jerome Lynch and his group of students at the University of Michigan, including Michael Kane, Courtney Peckins, and Mitsuhito Hirose, for developing core software for the *Martlet*. Additional acknowledgement goes to the Georgia Institute of Technology for Dr. Yang Wang and students Dapeng Zhu and Xinjun Dong for further development and testing of *Martlet* components and code.

I would like to acknowledge the National Security Education Center's Engineering Institute at the Los Alamos National Laboratory for accepting me into the Los Alamos Dynamics Summer School Program. I am grateful for my mentors Chuck Farrar, Eric Flynn, and David Mascareñas and research partners Garrison Stevens and Rex Lu at LANL who have provided support and friendship throughout my Ph.D. and have taught me invaluable skills.

My acknowledgment extends to all of my fellow colleagues and research assistants at Michigan Tech who have helped on the many facets of my lab work: Ehtesham Khan, Baibhav Rajbhandari, Antonio Velazquez, Jiayi Ding, Tianye Yang, Wanbing Bai, John Kmetz, Alice Flanders, Alex Chizmadia, Ben Trojniak, Jacob Bison, and Li Tang. I would also like to thank my student mentees Jamel Foster and Silvio Martinez from Wayne County Community College and Polytechnic University of Puerto Rico, respectively, for helping to accelerate my experimental work during summer outreach opportunities.

I would like to also thank Mark Sloat and Chuck Sannes in the Department of Electrical Engineering at Michigan Tech for circuitry and power supply support for my test setups.

Finally, I would like to acknowledge that this work has been completed thanks to funding provided by Michigan Tech and the National Science Foundation through the Graduate Research Fellowship Program.

1 Introduction

In the past decade, wireless communication for structural control and health monitoring has become more popular in the field of civil engineering [1-4]. This increase in popularity is strongly influenced by the progression of new structural health monitoring techniques and applications. At the same time, structural control devices for civil engineering applications have improved and become more energy efficient, leading to increased interest in using wireless devices to command these devices as the number of them grows. As structural engineers move toward a more sustainable future, control technologies have been developed that leverage small energies to realize large control efforts. These state-of-the-art control technologies, which will be better described in the following chapter, use little energy to give engineers more control of structural response. This technology is known as semi-active control. Though this technology has low energy requirements, the main drawback that exists is the use of extensive cabling to operate these devices. A single semi-active device cannot generate the same magnitude of force that a single active device can to combat the inertial forces of structural floors, therefore multiple must be used per floor on a structural scale [5-7]. In order to supply command signals to all semi-active devices that may be required throughout a structure, more cabling must be used. In a traditional control system with any amount of cabling, the sensors, the cables between sensors, the actuators, and a central data acquisition and actuation module make up what is known as a wired, or tethered control system.

Wireless structural control alleviates the need to physically connect every component in the control system. Wireless technologies have the ability to transmit sensor data throughout a wireless network, thus saving money on cabling for data acquisition and centralization. Wireless control can also improve some measures of reliability versus tethered control because of their intrinsic decentralized nature. Wireless techniques for control can improve reliability during earthquakes and high-wind events because data can still be relayed throughout the network without the worry of loss to sensor cabling. Wireless units are also more reliable because they each perform control calculation and

actuation, thus offering redundant control calculations. In wired systems, if the central data acquisition and actuation module is compromised, control cannot be performed. Wireless nodes for structural monitoring and control applications have been developed that possess both data acquisition and control actuation capabilities [8, 9]. Wireless control technologies possess their own issues, which are presented in the next chapter.

1.1 Motivation

The major drawback to wireless systems for control is communication latency, or the delay between transmission broadcasts and network receipt [10-13]. Communication latency can also be interpreted as a decrease in communication speed. That is, the time necessary to relay all observable data as the wireless network grows increasingly large to accommodate larger structures. A common way for transmitting data throughout a wireless control network is to budget, or schedule, a time by which each wireless sensor must relay its self-acquired data within the control step. Often, if the number of sensors in a structure is large, the control step size must be increased to accommodate the flow of more data, thus slowing down the control process, which introduces significant latency. If the speed of control decreases too much, attenuation of high-frequency dynamics become unreliable.

The most common process of scheduling data communication in wireless structural control networks is the time division multiple access (TDMA) protocol. As demand increases for wireless transmissions within an ever decreasing control step, the conventional technique for expanding the control step and increasing control rates is to spatially decentralize, or breakup the structure into smaller subsystems that use less bandwidth [14-16]. By spatially decentralizing the network, subgroups of sensors will only obtain data from a limited number of sensors. This work seeks to explore additional approaches to transmit sensor data within structural control networks such that all units may receive data from every other sensor in the wireless network, without compromising control speed. Beginning with a static and predefined communication topology and moving to a dynamic, stochastic topology, temporally-decentralized control will be

studied as a means of improving structural control performance using limited wireless communication bandwidth.

1.2 Project Overview and Goals

The area this dissertation seeks to address is communication latencies in wireless structural control. The method chosen to address this issue is to move away from traditional time division transmission scheduling. Specifically, this dissertation will examine how to maintain high speed wireless control with the inevitable increase in communication delays that come with increased sensor network size. In this dissertation, control speed is increased in wireless control network using two techniques: 1) scheduling data communication over multiple timesteps using sensor placement theory-based transmission groups; and 2) programming wireless units to identify when self-acquired data should be transmitted based on dynamically updated importance factors. The two methods will involve static and dynamic allocation of bandwidth, respectively.

Based on the behavior and modal frequencies of a structure, sensor placement can be a difficult task to ensure a controller is given accurate information. Fortunately, sensor placement theory has been developed to address issues related to having a limited number of sensors for monitoring, structural control, and structural health monitoring applications. Sensor placement theory has also been shown to work for placing a budget-limited number of sensors for monitoring and control tasks. On top of choosing a limited number of sensors, sensor placement theory (further described in Chapter 4) can also form the basis of distributed wireless control schemes, and when applied to static bandwidth allocation for multi-step group transmissions, it promotes faster wireless controllers on a structural scale. Sensor placement theory is used to demonstrate how different sensor groups can be formed that provide consistently high-quality output information to the network over multiple timesteps, while still using all sensors in the network. It is found that state estimation and control performance are strongly influenced by the network topology and that sensor placement approaches involving nodal observability provide more useful information that arbitrary sensor groups.

As the number of sensors that are able to transmit in a single timestep decreases (which is associated with the increase in network size), the establishment of transmission priority is necessary. This dissertation discusses a method for prioritizing wireless data that is used in place of a transmission scheduling scheme. This priority based transmission scheme will allocate bandwidth dynamically, as opposed to using a static schedule, to ensure successful transmission of highly important data. If it is not necessary to transmit data to maintain observability (*e.g.,* sensor readings or state estimation has not changed between timesteps), it would not be feasible to transmit data from a particular, or multiple units. Therefore, if units could prioritize their own data based on importance, then bandwidth would be more available, or the control system could be made to run at a faster speed. Large wireless networks, even with prioritized transmissions, run into the risk of data collision without a TDMA communication protocol. When there is a high demand for units to allocate a small transmission window, communication media are considered highly saturated/contented. Contention exists when two or more wireless units may wish to communicate at the same time. In the event that units do communicate at the same instant, carrier sense multiple access with collision detection or avoidance (CSMA-CD or -CA) techniques may be used to predict and prevent multiple contended units' data from colliding and becoming lost or misreported. In Chapter 5, a modified CSMA-CA approach is explored that strategically prioritizes data transmissions from the most useful sensors in a contended medium. The method defined in Chapter 5 relies heavily on a dynamic measurement fusion approach programmed within each wireless sensor. Both Chapters 4 and 5 of this dissertation are shown to lead to the development of wireless control algorithms that can handle different combinations of sensor data while providing accurate state estimates, which are shown to improve control performance.

The methods in Chapters 4 and 5 have been performed in simulation using a 20 degree-of-freedom (DOF) structure and validated by simulating and experimentally testing their performance on a 9-DOF small-scale test-bed that has been developed to emulate tests that are performed in more expensive laboratories. The following subsection will present

the scope of this dissertation, the objectives of this work, and the research approach taken to complete this work along with the organization of the document.

1.2.1 Goals and Objectives

The aim of this dissertation is to enhance structural control techniques for wireless systems to improve their performance relative to tethered/wired control approaches, thereby promoting the greater adoption of wireless technology in the structural control community. Wireless control has been proven to be a promising alternative to traditional tethered control, however, several challenges exist when using control components that are not centralized. The main issues in the application of wireless structural control include: limited bandwidth for relaying data, communication latency between wireless nodes, capacity limitations that negatively impact necessary data storage, and computation speed. Previous work in wireless structural control has suggested that an improvement of wireless capabilities and embedded control algorithms would help wireless networks to better contend with wired control systems. This dissertation develops and validates novel temporally decentralized communication approaches for wireless structural control that address the issue of slow control speeds using wireless technology by strategizing wireless transmissions using nontraditional methods.

The first objective for this dissertation is to develop a structural control testbed that is highly modular. This testbed should consist of an excitation platform for inputting earthquake ground records and other signals. Additionally, the testbed should contain a structure that can be reconfigured with varying degrees of freedom, multiple floor heights, different column stiffness, and variable mass per floor. The test-bed structure should be equipped feedback control technology including dampers/actuators, wired sensors, a centralized data acquisition and actuation system for wired control, and wireless sensing/actuation units.

With a working testbed, the second objective of this dissertation can be explored, which is to investigate the most appropriate wireless communication schemes for improved

control speed and estimation accuracy in large sensing and control networks assuming static bandwidth allocation is still feasible (*i.e.,* network size is not so large as to fully prevent wireless transmissions in a timed fashion). To achieve this objective, this dissertation examines the effect that the number of sensors and sensor placement has on estimator and control performance. Additionally, this dissertation examines the impact of sensor grouping and geometry/combinations on control performance and state estimation and develops a method for designing improved communication topologies using sensor placement theory.

The third objective for this dissertation is to develop an adaptive, dynamic priority-based communication scheme that addresses how to strategically transmit data if timed transmissions, or static bandwidth allocation, is no longer feasible. Given a fixed transmission window and a large number of wireless sensors, it is important to determine when to send data based on importance so that multiple transmissions do not collide and become corrupted. For this objective, the derivation of state-space estimator gains that can handle time-varying sensor input sets and the development of algorithms for fusing random sets of measurements is important.

1.3 Contributions to the Field

Broadly speaking, this dissertation offers two major contributions to the field of structural engineering. The first unique contribution is to provide a rational strategy for communicating all sensor data throughout a large wireless network without spatial decentralization. Spread over multiple timesteps, wireless estimators and controllers are able to observe data from the entire structure as opposed to receiving data from a single subset of units. This approach is to be applied in larger structures where traditional centralized wireless structural control would not be feasible at high speeds.

The second unique contribution is the development, verification, and validation of a new means for contention-based dynamic allocation of bandwidth in large wireless structural control networks. If a data point from a particular or multiple sensor(s) does not need to

be transmitted, then it would be a waste of valuable bandwidth to transmit it, along with other less important data, on a schedule. The uniqueness in this topic is the removal of a schedule and the addition of autonomous prioritization of transmissions over saturated bandwidth where TDMA is no longer possible. This prioritized transmission scheme is paired with estimators that make use of random measurements from units throughout the structure as opposed to fixed groups of measurements.

1.4 Research Approach and Document Organization

Beyond Chapter 1, which provided an introduction and motivation for the projects conducted as part of this dissertation, this dissertation will first present a literature review in Chapter 2 of the relevant history of structural control leading to the present state of the art, along with methods of wireless structural control and estimation. This literature review will describe three broad categories of structural control: passive, active, and semi-active control. The structural control portion of the literature review will emphasize semi-active control due to the popularity of these devices for use in civil engineering seismic control test-beds and their synergy with wireless sensors. Chapter 2 will elaborate on methods of handling slow data transmission and reception in wireless structural control networks. In large networks, often fewer sensors are used to estimate states, this review will discuss how reduced order models are incorporated into the control process to improve controller performance. Chapter 2 will also include shortcomings and useful aspects of spatially-decentralized control, frequency division approaches, reduced-order state feedback control, sensor placement problems, and handling data in both timed and stochastic manners.

Following the literature review, Chapter 3 summarizes the construction of the structural control test-bed used to perform experimental validation for the methods discussed in Chapters 4 and 5, as well as the design and model development for small-scale semi-active magneto-rheological (MR) fluid dampers. Chapter 3 also introduces the wireless technology used in Chapters 4 and 5 and demonstrates the successful use of a small-scale

damper for control testing applied to a 3-DOF small-scale test-bed shear structure, and it introduces the modularity of a structural test.

Chapter 4 focuses on methodology aimed toward handling a large network of sensors using a fixed topology that spreads communication across multiple timesteps to improve observability given the lack in ability to fully centralize data from all units in a wireless network.

Chapter 5 addresses the issues highlighted earlier, by building off of methodology in Chapter 4. This chapter examines a scenario where fewer sensors can transmit data, consistent with larger wireless networks, and an approach had to be developed to prioritize when data should be transmitted and how to handle random sets of data for estimation and control purposes.

Finally, Chapter 6 will provide conclusions and identify future directions for related work. The research approach for this dissertation is represented in Figure 1.1. This figure depicts the dissertation organization, starting with the broad overview of structural control methods and approaches to address the highlighted issues motivating this project, and ending with Chapters 4 and 5, which provide unique contributions to the field of structural control.

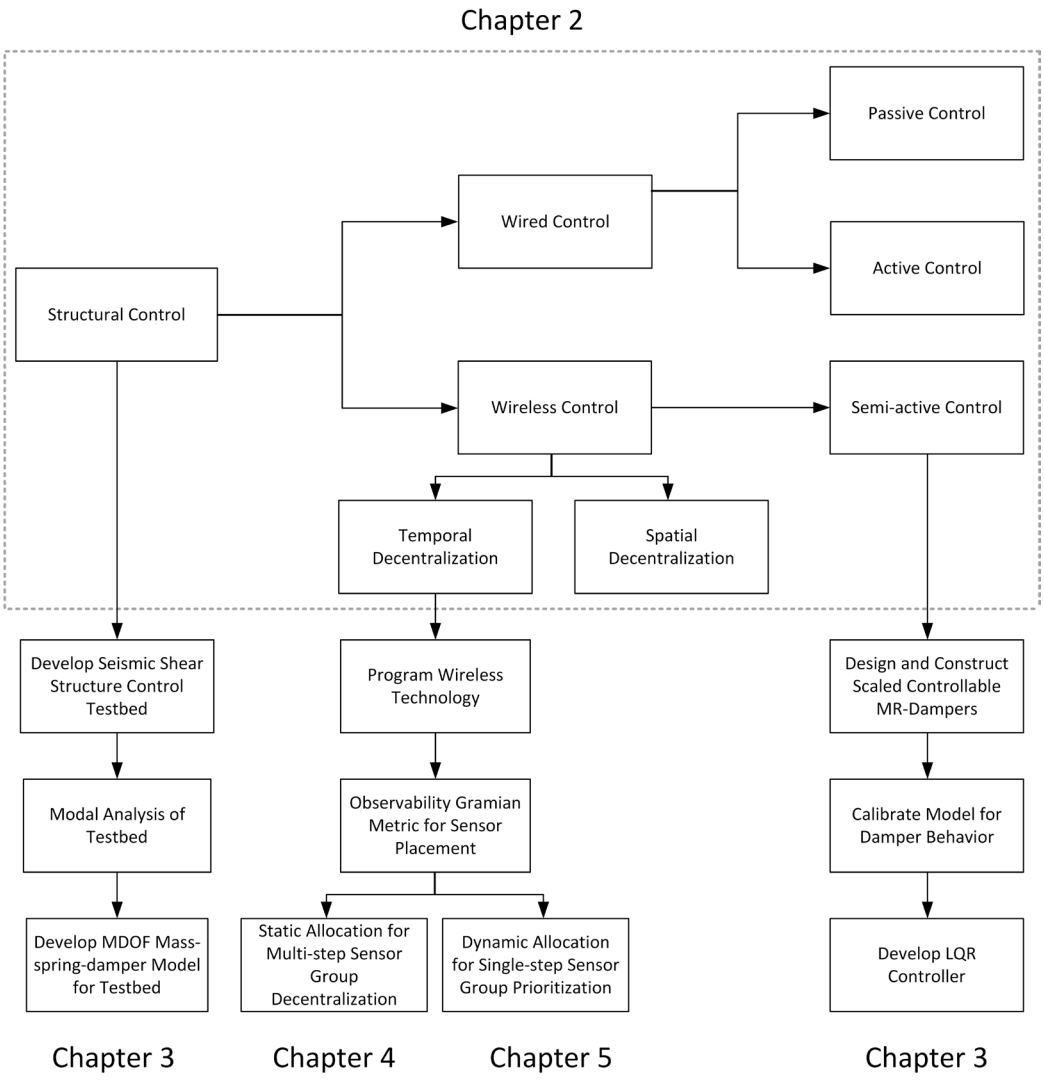

Figure 1.1: Research approach for dissertation project

2 Literature Review

Interest in wired structural control is steadily growing for improving structural stability during seismic and high-wind events and to provide occupant comfort. Wireless sensing and actuation networks are becoming more popular for use in civil structures for structural health monitoring [17-19], damage detection [1, 20, 21], parameter estimation [4] and structural control [2, 3, 22, 23] and have been designed to carry out both functions [8, 9, 15]. While researchers are exploiting control capabilities of wireless networks in lieu of tethered control schemes, the control elements used remain the first topic of discussion in this chapter. To understand the purpose of semi-active control technologies used within the later chapters of this dissertation, this literature review will discuss the progression of control elements leading to the state of the art. In response to this increased attention in semi-active devices and to build a small-scale test-bed for wireless structural control applications, this literature review identifies that magneto-rheological fluid dampers are an appropriate semi-active technology for emulating control elements used in larger testing facilities. Later in this chapter, wireless technology for structural related activities are discussed, and the benefits are weighed against wired control. The wireless aspect of the topics in this dissertation arises from the large number of semi-active dampers required to fully control large structures under earthquake loading. In the field, when magneto-rheological devices are used to control inter-story drift, extensive cabling is required for one damper. However, one commercially sold damper is not capable enough to attenuate all drift expected by large structures with equally large inertial forces. Therefore, the amount of cabling increases to match the demand for more dampers. Thus, wireless technology is even more necessary to combat cost and reliability associated with wired installation. At the end of this chapter, techniques to address the shortcomings of wireless control are discussed and compared, highlighting the areas for improvement that can be made using this dissertation.

2.1 Actuators for Structural Control Application

Structural control involves the provision of actuators to minimize seismic or wind excitation to protect structures and ensure occupant comfort. Properly implemented, structural control elements also help to improve structural stability and dynamic performance. Structural control technologies are generally categorized into three broad groups: passive, active, and semi-active control [24-27]. Each category respectively builds off of the shortcomings of the prior control type. The state-of-the-art structural control consists of hybrid passive and active control systems, as well as semi-active control devices. This subsection will discuss the principles behind each type of structural control approach, give examples of each technology, and describe the shortcomings associated with each.

2.1.1 Passive Control

Under the passive control paradigm, a system or structure is controlled using principles of energy balance [28]. This control can be achieved through the use of elements that passively counter system response (*e.g.,* implementing a tuned mass-spring-damper system with the structure to bring the dynamic response to a desired stable response). Energy balance can also be achieved through the use of interconnecting components to provide additional paths of energy transfer and damping in the structure [28, 29]. At these interconnections, passive control elements can be introduced that dissipate energy. Another way to think of passive control is to consider the two primary components of these systems: an elastic element to store energy and a damper to dissipate it, neither of which impart additional energy to the structure [28, 29].

The practice of using passive control elements to dissipate the energy introduced into a structure as a result of earthquake excitation has been observed in buildings for over 100 years. Passive structural control was first documented in western journals by John Milne, who explained that large pendulums in Japanese Pagoda structures were used for energy dissipation [30]. The use of these pendulums was simple, relying on cantilever oscillation

of the pendulum as a method of attenuating structural energy. The pendulum would strike the inside of a cylindrical hole, converting mechanical energy in the structure to some other forms [30]. Thus, the structure released energy from the system into the air and back into the ground upon earthquake excitation.

Some examples of modern passive control elements include base isolation, friction and metallic yield dampers, viscoelastic dampers, and tuned mass/liquid dampers. Each of these devices relies on a different form of energy balance. Isolation systems are passive dampers that use two components to prevent energy transfer to the controlled system. Base isolation possesses the unique blend of damping and stiffness provided through a mechanical system (*e.g.,* large rubber and lead bearing columns to support a structure) [24, 31]. These elements isolate the structure from ground excitations, thus limiting the energy transferred to the structure. Over a thousand structures in Japan have base isolation systems installed including the Dowa Kasai Phoenix Building in Osaka and the Ando Nishikicho Building in Tokyo [32].

Friction dampers and metallic yield dampers convert mechanical energy into heat energy through friction or plastic deformation as they deform under structural or seismic loading [33]. Finally, tuned mass/liquid devices counter structural motion to balance system response (*e.g.,* story drift) under earthquake or wind loading [34]. Examples of structures that use tuned mass dampers include the Washington National Airport Control Tower, the Petronas Towers, Taipei 101, the Citicorp Tower, and the John Hancock Tower among others reviewed in [32, 35]. Structures that make use of tuned liquid damper include the Crystal Tower Building in Chicago [36], the Nagasaki Airport and the Yokohama marine tower [37], along with other hotel towers and airports in Japan [32].

Though these control techniques are used because of the ease of implementation, relatively low cost, and their effectiveness, they do come with shortcomings. One of the chief disadvantages of passive control is that each device is calibrated to control specific excitations or behaviors (*e.g.,* a tuned mass damper that targets a specific modal

frequency) [38]. Out of this range, the control device may not function properly, or might fail completely. Even when devices are intended to yield as a form of energy dissipation, these are other shortcomings associated passive control devices, namely fatigue and high replacement rates [24]. Due to these shortcomings, newer technologies have been investigated for structural control that do not require frequent replacement and are able to be effective over a broader range of conditions and excitation frequencies.

2.1.2 Active Control

Active control devices, as opposed to passive control devices, actively impart counter-excitation frequencies or forces into a structure to control system response [24, 29]. Active control devices are often used to alleviate wind induced inter-story drift and passive dampers are primarily used to perform seismic and wind mitigation activities [25-27, 37, 39]. Examples of active control include active mass dampers and active tuned mass dampers. Active mass dampers rely on large amounts of electricity to actuate a mass to control structural behavior based on detected structural behavior. Similarly, active tuned mass dampers use actuation methods and large power consumption to impart counter frequencies or forces onto structures. An example of a structure with an installed active mass damper is the Kyobashi Seiwa Building [37].

The chief advantages active systems have over passive systems include the ability to react in short time intervals and provide a greater range of forces adequate for many different seismic excitations. Active control devices are effective at reducing story drift. Passive systems are still used for structural control. However, active control systems are used to eliminate undesired disadvantages of the passive systems. The chief disadvantages of active dampers is instability (*i.e.,* overuse/estimation of required actuation can impart more counter loads, thus imparting more energy into the system) [40], the large cost associated with first time incorporation of the systems, the external power consumption (which may be insufficiently supplied during an actual earthquake), and non-adaptability (*i.e.,* these devices require significant structure-specific design effort). These limitations

have led to the exploration of control techniques that use similar principles of structural control with low electrical demands.

2.1.3 Semi-active Control

To overcome the limitations of active control, semi-active control strategies have emerged. Semi-active control devices operate under similar principles to fully-active control elements. The term semi-active, however, implies the use of less energy and the particular way these devices create control forces indirectly. Unlike active control, semi-active devices control structural parameters (*e.g.,* stiffness and damping) in real time to modify structural behavior [41-43]. Researchers have given significant attention to this attribute of semi-active devices and have recognized the associated benefits of generating large forces from small input energy, and inherent stability (*i.e.,* forces are indirectly applied through altering structural parameters and as such, do not destabilize or introduce more energy into the structure) [44-47].

Even with low power consumption, the effective structural forces are very large, which makes these devices particularly useful for civil structural control. Also, because of their low power requirements, semi-active control can still function in the event of a power outage by using a backup battery. The passive nature and reliability of these devices allow for guaranteed stability, with proper equipment, and real-time structural control [29].

Examples of semi-active control devices include active variable stiffness (AVS) dampers, active bracing systems (ABS), aerodynamic appendages, piezo-ceramics or piezo-stack actuators, shape-memory alloy members, and rheological devices. AVS systems can be used to alter the full system stiffness continuously in real-time throughout an earthquake as different frequencies are detected [48]. Active bracing systems use various bracing members, typically pre-stressed tendons linking two floors in a structure with electro-hydraulic actuator components [24]. Aerodynamic appendages are active control for wind excitation. However, these devices do not address the issue of seismic

excitation of a structure [24]. Piezo-ceramics or piezo-stack actuators use small electrical charges to change element length, effectively altering the stiffness to achieve attenuation of vibrations and even counter vibrations by actuating deflections [49]. Similarly, shape-memory alloys can be used to construct a part of a structure to add or release stresses, by modifying shapes of elements using electricity or heat. This shape change can lead to increased or decreased damping effects by manipulation of structural stiffness [50]. Finally, other forms of semi-active control devices have a rheological damping component, or plastic/viscous flow or solidity that can change under various excitation stimuli. Rheological devices that are used for structural control are magneto- or electro-rheological fluid and elastomeric devices. The prefixes refer to the type of excitation (*e.g.,* magneto-rheological (MR) devices respond to a change in magnetic flux, and electro-rheological (ER) devices respond to a change in and electric field). Examples of structures with semi-active dampers installed include the Shiodome Tower and the Roppongi Hills Mori Tower which use semi-active oil dampers, the Kajima Research Institute which has 6 AVS devices installed, and many others reviewed in [51].

Because of the low-power consumption of semi-active dampers, specifically MR-dampers along with the high-force yield, this form of control has become a popular choice for civil structural control applications and test-beds. Furthermore, these devices are controllable over a broad range of frequencies and are guaranteed to be stable in their operation. MR-dampers exhibit non-linear, hysteretic behavior, leading to numerical modeling complications [52, 53]. These complications are independent of scale, making a low-force MR-damper a good stand-in for the full-scale dampers in laboratory experiments.

2.2 MR-Dampers for Structural Control

This subsection presents an introduction to MR-damper technology including a description of MR-fluid and its behavior, as well as descriptions of a number of damper configurations based on MR principles. The effectiveness of each of these configurations for small-scale damping applications is reviewed. Typical constituents that make up MR-

fluid devices are the MR-fluid, steel pistons, steel damper housing, an electromagnetic coil (or multiple coils), and a fluid leak prevention system (*e.g.,* either seals or an absorbent foam matrix). Steel is used for the piston and damper housing due to its high magnetic susceptibility. Since steel has high magnetic saturation properties, it can support magnetic moments, which play a role in maximum achievable force in MR-dampers. Saturation of the damper's internal magnetic circuit is a critical design property that depends on the material and geometric properties of the damper and is discussed further in the theoretical portion of this report. Three typical types of MR-dampers are used in many different mechanical and civil engineering applications: single-ended, double-ended, and sponge-type MR-dampers. These different types are presented in the following parts of this section with a description of their shortcomings related to use for small-scale test-beds.

2.2.1 Single-ended MR-fluid Piston-type and Valve-type Dampers

Single-ended MR-fluid piston-type dampers use the main constituents previously described, and are arranged such that the piston moves through the MR-fluid, as seen in Figure 2.1 (a). The electromagnetic piston, once power is supplied, experiences resistive forces as the MR-fluid attracts to the piston and a magnetic circuit is formed through the fluid, steel housing, and piston. Diverting from the traditional single-ended piston MR-fluid damper, a valve-type damper includes a fluid escape path from the main housing. The fluid travels through a smaller enclosure and experiences a change in viscosity as an electromagnetic valve is activated, see Figure 2.1 (b). The forces acting on the piston can be controlled in real-time by changing the levels of applied current to the piston or electromagnetic valve, which strengthens the magnetic circuit and stiffens the MR-fluid greater. This single-ended configuration only uses one seal to prevent fluid leak, whereas later configurations use two seals. Seals are a major shortfall of this technology when developing a device to be used in affordable small-scale experimentation.

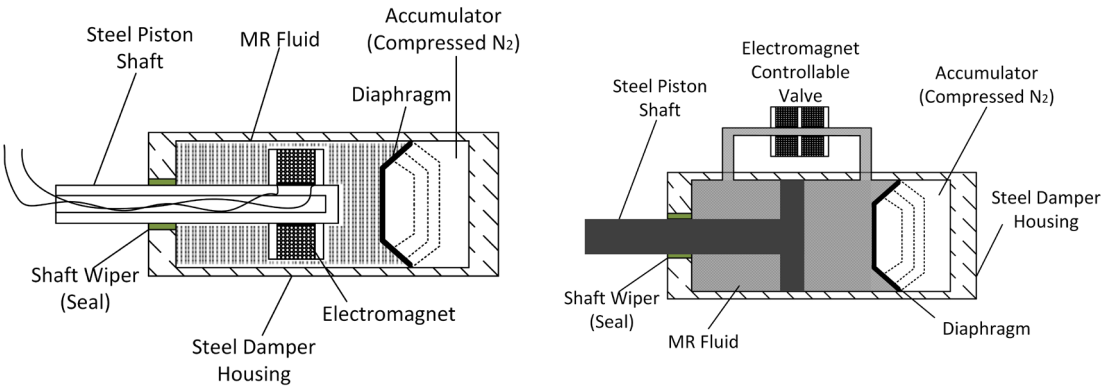

(a) (b)

Figure 2.1: Single-ended damper (a); MR-valve type damper with fluid escape path (b)

Seals are a major source of undesired friction which limits the lower end of small-scale achievable forces (not an issue for commercial devices because they operate on the kN scale). For the single-ended damper configuration, another shortcoming with constructing small-scale devices is the need for an accumulator and a diaphragm. The diaphragm folds to provide more volume for the excess fluid on the non-shaft side as the piston and electromagnetic coil moves inward, and vise-versa for the piston's outward motion. The diaphragm is stabilized by use of a compressed gas (*e.g.,* Nitrogen) acting as a pressure differential to help guide the piston in the fluid chamber. Additional major shortcomings associated with this design for small-scale low-force applications include the use of high pressured gases and the cantilever geometry of the piston that is difficult to support in the horizontal application intended in this dissertation [44].

2.2.2 Double-ended MR Piston Damper

The next type of MR-fluid damper is a double-ended configuration as shown in Figure 2.2. Rather than using an accumulator to stabilize the piston, a double-ended piston damper employing two seals are used, one at each end, to allow the inner piston shaft to protrude from both ends of the damper. With these seals at each end, support is provided, thus eliminating the need to provide cantilever support for the piston. However, this approach necessitates two seals, further degrading the minimum controllable forces of the device achievable for small-scale construction [44].

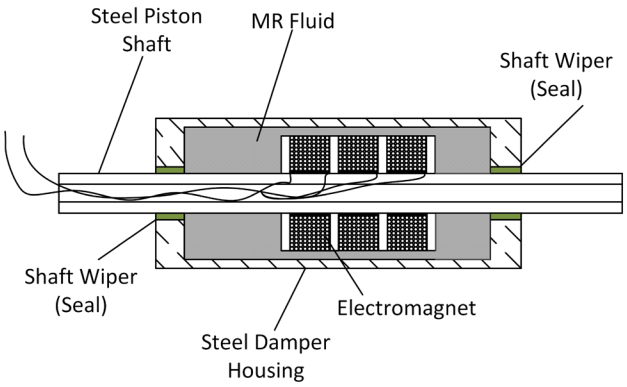

Figure 2.2: Double-ended damper and constituents

This design was found to be more promising for horizontal control applications due to ease of constructability in comparison to the single-ended damper design due to better piston support and the elimination of compressed gases and accumulators. However, the friction created by the pair of seals needed by this damper is quite large. In fact, this friction proved to be too high for effective use in small-scale test-bed control, later discussed in Chapter 3. To eliminate these seals, a new approach is needed.

2.2.3 Sponge-type Dampers

Sponge-type dampers are used in a number of mechanical engineering applications in two forms: expulsion or extraction. Expulsion, in this context, refers to fluid being expelled out of an absorbent matrix (*e.g.,* polyurethane foam) through positive pressure. The expulsion of fluid, in the presence of a magnetic field, creates shear stresses that initiate damping forces (Figure 2.3). Extraction refers to fluid being drawn out of an absorbent matrix and attracted to a source of magnetic field, thus activating viscous shear forces in the damper.

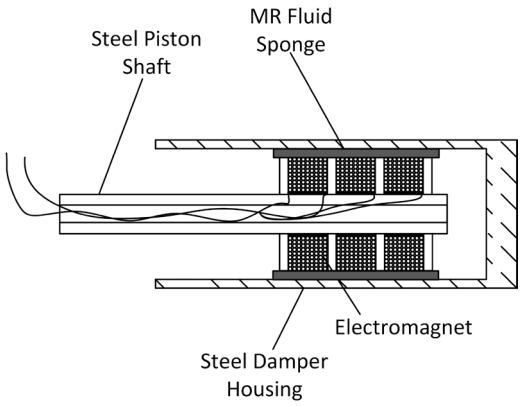

Figure 2.3: Expulsion sponge-type MR-damper

The absorbent matrices within expulsion sponge type dampers are typically made of polyurethane foam. This damper type relies on the presence of the same cantilever anchorage for horizontal applications as is needed in single-ended devices. However, these devices do not contain seals to prevent fluid from leaking. Typically, sponge-type MR-dampers are single-ended, but they do not require an accumulator because the sponge, or foam, guides the piston in the housing (and there is no pressure compensation required) [54]. Polyurethane foam required for expulsion dampers is very affordable, however, it is easily torn [55-58] and replacement of this matrix is very difficult in this type of damper. To avoid the tendency of the foam to tear as often, the foam thickness has to be relatively thin, thus limiting the amount of volume and increasing the stiffness of the foam. Finally, the polyurethane foam surrounding the piston adds friction to the damping force, which is not controllable and is undesired for small-scale devices. The extraction device, shown in Figure 2.4, presents more promising attributes for this dissertation.

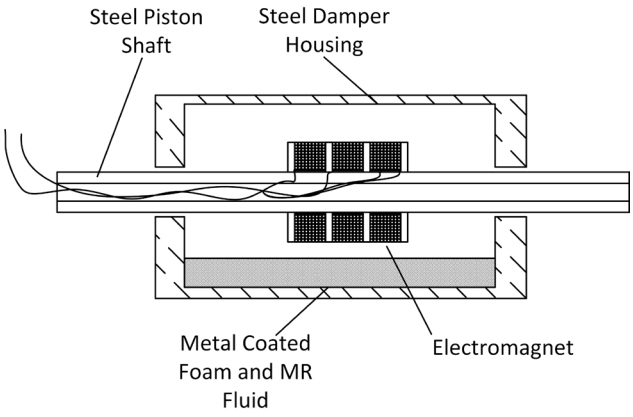

Figure 2.4: Extraction sponge-type MR-damper

Extraction sponge-type dampers use metal coated polyurethane foam as the MR-fluid absorbent matrix. Like normal polyurethane foam, metal coated foam, with small pore sizes, can retain MR-fluid. However, as the pore size increases, the ability for MR-fluid to be extracted increases. The metal coating process has already been performed and this foam is available commercially for purchase [57]. The polyurethane foam is a skeleton for a metal powder to latch on using a bonding agent. Some examples of the different types of metal foams that are available are steel composite foam, aluminum iron composite foam, aluminum foam, copper foam, and vitreous carbon foam [57]. Basic properties of metal foams of interest for this dissertation include absorbency and magnetic saturation. Metal foam extraction sponge-type dampers allow for seal-less construction, comparable to the expulsion-type dampers.

2.3 Wired Structural Control

Wired structural control refers to a system installed on a structure (*e.g.,* buildings, bridges, *etc.*) that gathers data from sensors throughout the structure, makes decisions with a control algorithm in a centralized computational core, and actuates voltages to active or semi-active devices. These systems generally work well and are feasible for smaller structures with limited density of sensors and actuators. The main advantage to wired control is the direct connectivity between the computational core and all sensors throughout the structure. This presents some difficulty during anomalistic loading such

as earthquakes, tornadoes, and hurricanes when sensors may become disconnected or damaged. Another advantage to wired control systems is the relative high speed of computation performed in the centralized computational core. High computation speeds, data acquisition speeds, and actuation speeds all allow wired control to monitor and attenuate higher frequency dynamics in a structure.

2.3.1 Wired vs. Wireless Control

Wireless networks are a great alternative to their wired counterparts due to ease of installation, lack of space-burdening cables, inherent decentralized and redundant computations, and low power consumption. Wireless technologies allow sensors, or sensing units, to communicate to one another rapidly to perform damage detection algorithms and initiate control schemes. These advantages are ultimately why researchers have focused on developing newer wireless technology for civil applications. Collecting data in wireless sensing nodes spread throughout a structure becomes more important as the structure grows in size and the number of sensors applied to the structure increases. Though broadly wireless technology helps to alleviate the high cost of installation associated with wired networks, wireless technology suffers in applications requiring near real-time dual processes, such as data acquisition and voltage actuation. Wireless technology is constantly improving to address this issue, especially with the demand for semi-active technologies increasing. As mentioned earlier, semi-active devices must be installed in dense networks throughout a structure to achieve the same force as active devices. The large control device density and sensor density would further increase the cost of traditional wired control networks, thus making wireless control even more desirable, despite its lack of capabilities toward real-time applications.

2.4 Wireless Structural Control

This subsection will discuss different methods for performing structural control using wireless systems. The field of wireless sensing and actuation is getting more attention because it presents an economic solution to high cost for installation and maintenance

traditionally associated with wired control systems. Wireless control systems are considered to be novel approaches to structural vibration control utilizing microprocessors for combining sensing, actuation, and data centralization. The main shortcoming wireless systems have is communication latency. The next sub-subsections discuss methods to address reducing the effects of communication latency of wireless control systems by spatially decentralizing the system, communicating data across different communication channels, and reducing the model size and amount of data required for computation of control gains.

Structural control is moving toward using low-power wireless microcontroller units in lieu of traditional tethered data acquisition systems. Altogether, wireless networks have been reliably used for structural control and health monitoring, including the use of wireless units to command MR-dampers [2, 23, 59]. Due to the complexity and high cost associated with wiring sensors and actuators to a central control system, wireless technologies provide a more feasible avenue for engineers to deploy dense wireless networks for control [60]. While wireless sensing, wireless control, and in-network computing have all advanced in the past decade, scaling these technologies from a single system to a network or grid remains an open challenge. The aforementioned studies all address wireless structural control of limited degree-of-freedom (DOF) structures. Each study points out how traditional centralized control is costly for wired control and infeasible for wireless control, ultimately leading to the use of decentralized wireless structural control.

Attempts to increase the speed of control systems have been summarized as decentralized structural control, frequency-division multiplexing, and reduced order structural control. These methods have their distinct advantages, however, each possess shortcomings. This section will highlight the main benefit to using each, present the drawbacks, and identify and discuss the gaps that this dissertation fills.

2.4.1 *Spatially Decentralized Control*

When communication is sparse or nonexistent between nodes, the centralized control scheme performs poorly. To compensate for slow data transmission rates and missed data, decentralized control for response reduction has been shown to be comparable to fully centralized control [14, 15, 23]. The spatial decentralization of control systems is the act of dividing sensing and control networks into multiple subsystems, or subsets of wireless units, depicted in Figure 2.5.

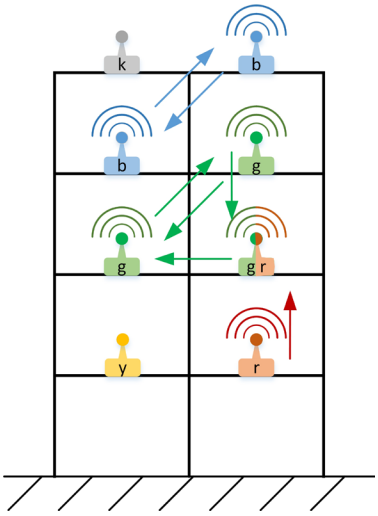

Figure 2.5: Diagram of a control network spatially decentralized into subnetworks

In this architecture, each data processing system uses locally obtained data which may or may not contain information regarding other nodes in the system. Embedded controllers and estimators are common among several units within each subsystem and require only the subsystem sensor data to perform the necessary calculations for full system state estimation. Thus, a large network can be broken down into many subsystems and eliminate the contention over communication channels. Without any communication between units, or any communication of sensor data throughout the network, the control system is fully decentralized. Partial decentralization of the entire structure into subsystems and considering inter-story response as subsystem input, has yielded similar control performance with centralized schemes [61-63]. It has also been shown that additional information passed between nodes and subsystems improves the performance

of estimators in both centralized communication schemes with dropped packets [64, 65] and partially decentralized communication schemes of varying size [14, 66]. Work has been done to control structural response based on triggered events to minimize power consumption and the necessity to transmit data [22]. Slower wireless technology often magnifies the issues associated with communication latency and some research groups have had to develop methods for carrying out a control process with incomplete data sets in spatially decentralized networks [67].

Law, Swartz *et al.* [14] have shown that centralized control requires low frequency sampling to relay all sensor data throughout a wireless network. As the sampling and control frequency decreases, to accommodate larger structures with more sensors, the modal behavior of the system can no longer be represented fully. Decentralized control decreases accuracy in state estimation, but has been shown to increase control performance by decreasing latency due to wireless transmission time, thus increasing the observable bandwidth of modal frequencies in the structure [14]. Because reduced communication increases the control speed, a partial or fully decentralized wireless controller can outperform a centralized controller that operates at a slower rate in large systems. Partially-decentralized control schemes have improved upon decentralized control by providing enhanced control speeds over centralized schemes while also reducing the error in state estimates consistent with fully-decentralized schemes. However, as the full system increases in size, to a point where demand for high control speed limits the number of partially decentralized subsystems, the capability of broadcasting all data within a single timestep diminishes even at the subsystem level [68].

Centralized wireless control is commonly used to compare control techniques with tethered systems. In a fully-centralized communication scheme, data from different sensors may contain redundant observable information [68]. It is beneficial to have all sensors transmit data throughout the network for full accuracy, but the exchange is not necessarily important and may waste valuable bandwidth [68]. Large networks using centralized control architectures operate at slower speeds and traditionally use a time

division multiple access (TDMA) protocol to handle data transmissions and reduce packet loss due to collisions by limiting the likelihood of multiple nodes transmitting at the same time. While packet collisions are only one of the numerous causes of packet loss, a TDMA protocol can help to improve reliability [69]. However, in large networks, this requires extensive resources that are not capable by conventional and affordable hardware. If, however, partially decentralized wireless structural control is performed with a TDMA data transmission schedule, speed can be increased and hardware can become more efficient.

Decentralization of the wireless control scheme has presented beneficial performance over centralized wireless and wired control. Decentralized control at faster control rates can achieve nearly the same, if not better, control performance compared to centralized control at slower rates. By increasing the number of channels units communicate to one another on, contention is reduced on a single channel. If communication is eliminated altogether, the control rate of the system can be effectively improved by a factor of the number of nodes in the network. Control rate, which involves sampling rate, is important because system natural frequencies that are excited in a structure may not be correctly observed when using the wrong rate (*i.e.,* a rate below the Nyquist rate appropriate for not aliasing dominant modal frequencies).

2.4.1.1 Transitioning from Spatial to Temporal Decentralization

The central drawback to the decentralized approach is that the overall controller stability is not guaranteed on structures that are nonlinear or have many coupled degrees of freedom. Additionally, the basis for studying decentralized control that is adaptable to any system is difficult to establish. Distributed control has been explored, which helps to address this issue of model uncertainty by sharing state vectors and information vectors, which indirectly pass measurements from units outside of fixed sensor subnets. Distributed control does not, however, ensure the best observability required for understanding full-structural response. Observability is the key gap in any degree or form of spatially decentralized wireless control approach. The work in this dissertation fills

this gap by examining how to strategically pass information throughout the wireless network using observability as the basis of forming transmission groups, Figure 2.6, and to prioritize transmissions.

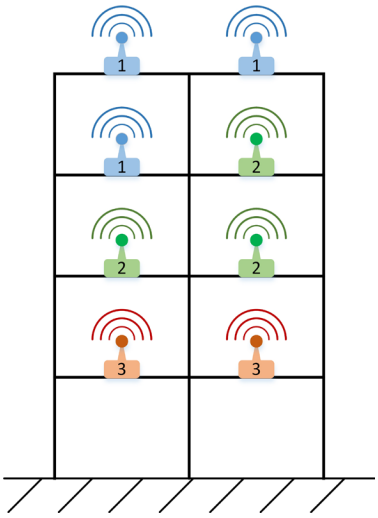

Figure 2.6: Diagram of a control network divided into muti-step communication groups

2.4.2 Frequency-division Multiplexing

It is recognized that spatial decentralization techniques fall short in estimation accuracy by not allowing subgroups to access data from other sensors in the wireless network. To extend the standard approach of spatial decentralization, studies have made use of frequency division multiple access (FDMA) protocols, or frequency-division multiplexing (FDM), to communicate data from each unit to the wireless network using different communication frequencies, or channels. This has been done to partially transfer data between subnetworks with overlapping subgroups so that a single or multiple unit(s) communicate on multiple channels simultaneous [62, 63, 70]. This approach starts to address the lack of accuracy in spatial decentralization. Expanding on the method of FDM within overlapping subnetworks, studies have shown potential for all units to communicate on different channels to the entire wireless network [71-73]. The receiving units in this fully-FDM network would gather data simultaneously from all units in the network in a non-time-budgeted manner. The main benefit to partial and full FDM approaches is the maintenance of spreading information throughout the

network. Additionally, as the network approaches a fully-FDM scheme, the communication latency is minimized. The main disadvantages to approaches like these is the complexity of managing multiple channels of communication to each receiving units and the finite number of channels that can be generated. Eventually, the discrete number of channels will limit FDM from sufficiently addressing large network data centralization. This dissertation is inspired by the divergence of this technique from spatial decentralization, but seeks for other means to maintain data centralization and control speed.

2.4.3 Reduced Order Modeling for Control Enhancement

When using a state-space controller to penalize undesired behavior of a structure, often times the full-order model realization of the structural properties is used. However, using the full-order model naturally presents an obvious drawback to performance speed when considering wireless control in large networks. Alternatively, controllers of much lower dimension have been used to produce nearly concise and satisfactory performance when compared to the full-ordered system [23]. Also, the dimension of the mathematical model of a system is limited by the ability to still accurately characterize the plant's dynamic behavior. The model may incorporate marginal effects that drastically increase the dimension of the model without really improving the accuracy of the model.

Common methods for reducing the order of the state-space realization include: a modal analysis approach, static condensation, and an aggregation method. The modal analysis approach is used to retain the dominant poles so as to approximate the behavior of a full-order system with both dominant and far-off poles. The aggregation method is similar in that important eigenvalues are chosen from the original system and nonessential user identified eigenvalues are neglected. The two methods may perform similarly, but the aggregation method gives the user a better ability to control the model size, whereas the modal analysis approach relies on determining dominant modes that must be retained (often limiting the smallest achievable reduced order model).

Controllers, such as the linear quadratic regulator (LQR) used in Chapters 3, 4, and 5 of this dissertation, perform best when provided adequate real-time state response data used to compute control forces. Direct state-feedback (*e.g.,* velocity, displacement, and drift feedback) is not always feasible in a real-life setting due to instrumentation cost and availability. To address this difficulty, state estimation can make use of more common sensor data (*e.g.,* acceleration) to calculate a state vector for determining control forces. Using various decentralized control schemes defined by Wang, Swartz *et al.* [15], sensing and actuation units can be commanded to eliminate localized structural response without communicating to other units. This technique is beneficial because it reduces control force updating time by eliminating communication latency. However, without full knowledge of the structural response, each unit could be performing counterproductive control for the remainder of the structure. Work by Swartz [3] has described that control and communication latencies presented in wireless control studies are hardware specific. *Martlet* wireless sensing/actuation units now exist that have been designed to address latent communication and control behavior described in [9]. Kane, Zhu *et al.* [9] have designed these actuator nodes to handle larger models with more degrees of freedom with much less communication and computational latencies. However, a tradeoff between actuation speed and state-space model size must be shown to validate an increased performance capability of *Martlet* units.

Controller model reduction is becoming common for addressing practical and technical issues like information transfer networks, data acquisition, sensing, computing facilities and the associated cost of each when using a full order controller design. Studies have suggested that reduced order dominant state controllers would be feasible to address these issues [74-78]. However, these reduced order controllers have been applied to theoretical systems that have perfect information. The simulations used in each study do not incorporate time latencies that may be associated with data acquisition systems, wireless communication, and computation speed. Swartz [3] has shown that changing the domain of the control system can speed up the computations associated with feedback control

using a full and reduced order model (*i.e.,* switching to the modal domain can allow mode shapes to be identified and removed from the model).

The main issue that exists with reduced-order, specifically modal space, control systems is how state responses of the controlled structure may be underestimated if the effects of control forces on the certain modes are neglected (*i.e.,* modal-domain control forces may increase the magnitude of frequency contributions to disregarded modes of the system) [79]. The advantage that any reduced-order model control technique has over traditional modal space controllers (*e.g.,* independent modal space and dependent modal space control) is simplicity. The simple transformation can even be performed prior to embedding the system realization into a wireless setting. The accuracy of the state estimator remains dependent upon the participation of the ignored modes in the response of the structure. With the reduced representation, a new LQR control law has to be calculated along with the discrete-time plant model. If you only consider the first few mode shapes, control speed may not need to be fast when using reduced-order modal space control. As the wireless network grows large, a reduced number of modes has been shown to decrease the efficiency of the controller. If the network grows to have many nodes, then fewer mode shapes may not be sufficient to accurately capture the structural behavior for attenuating the structural response. In the case of flexible structures where the number of degrees of freedom are infinite, wired control using reduced-order models are reasonable. However, when considering reduced-order modeling in a wireless setting with limited bandwidth and high necessity for observability, these techniques cannot fully address the present issue (*i.e.,* control speed) inherent to wireless structural control of large systems. Continued work in this area is suggested and carried out in this dissertation.

3 Low-Force Magneto-Rheological Damper Design for Small-Scale Control*

Civil engineers implement control elements to improve the performance of structures during seismic and high wind events. Active control devices are often used to alleviate wind induced inter-story drift (*e.g.,* active mass dampers), and passive dampers are primarily used to perform seismic and wind mitigation activities [24-27, 29, 37, 39]. Researchers have given significant attention, however, to semi-active controllers for use in civil applications because these devices control structural parameters (*e.g.,* stiffness and damping) in real time to modify structural behavior [28, 41-43, 80]. By doing so, the amount of power needed by these devices to impart large control forces can be provided by a battery [45, 52, 81, 82], thus ensuring continued operation during weather anomalies and/or seismic events that may interrupt the local power supply grid. Magneto-rheological (MR) fluid dampers are becoming a more widely used semi-active damper type in the fields of civil and mechanical engineering [15, 29, 83-86]. MR-dampers can be used to alter system damping in real time through rapid changes of applied current within an internal electromagnet [24, 52, 87, 88]. These changes in magnetic field alter the viscosity of MR-fluid contained within the damper. Internal components are arranged to take advantage of these changes to produce controllable damping forces to the structure. These devices produce forces at a smaller scale than traditional control devices (*e.g.*, active mass dampers) necessitating the coordinated use of many such devices. Recent research studies have focused on accomplishing this task using wireless sensor networks to reduce costs and increase reliability [3, 11, 23, 59].

Traditionally, control testbeds that are used to validate the performance of MR-fluid dampers for use in civil structures are somewhat large and expensive to operate [89]. Researchers have shown the usefulness of semi-active structural control validation

---

* The material contained in this chapter has been accepted for publication in Structural Control and Health Monitoring.

studies on a smaller scale [27, 45, 90, 91]. Small-scale control tests allow for safe, affordable, and repeatable state-feedback control experiments, particularly scale-independent studies focused on control laws, decentralized control strategies, and timing issues for wireless communication problems. Since these problems involve timing and not physical scale, they are well suited for a low-cost, small-scale experimental environment. However, the range of forces produced by prior MR-damper devices used in field applications (kilonewton scale) is not appropriate to perform control tests for small-scale laboratory experiments.

There are several types of MR-fluid damper geometries that may be characterized by the configuration of the two main components: the electromagnet and the MR-fluid containment system. Each geometric configuration enables an MR-damper to impart a range of control forces. Typical commercial MR-fluid dampers used for full-scale (kN) control tests are made in two piston-type configurations: double-ended and single-ended, where a piston is surrounded by MR-fluid contained within the damper housing. These commercial devices can actuate a broad range of forces with small changes in magnetic flux provided by the electromagnetic piston. It has been shown that commercial MR-fluid dampers have been effectively used for control experiments conducted on large-scale testbed structures with inertial story accelerations of 1 $\mathrm{m/s^2}$ [15, 52, 59, 82, 92].

MR-dampers have not been used in small-scale laboratory control experiments as low-force ranges are difficult to achieve (*e.g.,* 0-10 N force) from these devices. Work has been done, however, to control small-scale mechanical systems, such as washing machines and rotary caliper breaking systems using MR-valve [93] and sponge-type dampers [54, 94] where the generation of finely-tuned control forces is not critical. In the sponge-type MR-damper configuration, the MR-fluid is contained in an absorbent matrix (*e.g.,* polyurethane foam). When a change is made in the magnetic flux applied to the MR-fluid, it is expelled from the pores of the matrix in order to generate a controllable viscosity similar to more conventional piston-type MR-fluid devices.

MR-fluid possesses an inherent nonlinear hysteretic restoring force that provides controllable damping forces at low velocities (*i.e.,* linear damping does not impart force without velocity; the restoring component of MR-fluid sustains an amount of resistive and damping force). However, such nonlinear hysteretic behavior is the cause for numerical modeling complications [29, 52, 53, 82]. When designing a small-scale analog for commercial devices, the desired force range must be achieved, but this model complexity must also be maintained to provide a fair and consistent comparison. The expulsion behavior of scale MR-dampers has demonstrated similar nonlinear hysteretic characteristics when compared with full-scale commercial MR-dampers [54, 95]. The controllable force range of typical expulsion devices exists between 50-150 N [54, 95, 96]. Though the force range provided by the polyurethane foam MR-fluid expulsion-type dampers is closer to the desired level for performing small-scale control experiments, work by Hoyle, Arzanpour *et al.* [97] has been done to lower the controllable damping levels of foam-type MR-fluid devices to between 20-50 N for use in adjusting actuator piston constraints. Also, Yi, Dyke *et al.* [98] have successfully used a non-annular volume MR-fluid saturated foam in structural control tests and were able to reliably produce a controllable force range between 5-25 N.

In studies using polyurethane foam, the low durability of the foam has been the main shortcoming cited in previous literature [55-58]. Metal coated polyurethane foam has been proposed and tested to produce similar results for rise-time and performance [55, 99] when compared to conventional MR-fluid dampers and expulsion-type dampers. Since the foam is coated in metal (*e.g.,* aluminum, copper, and iron), the damper cannot operate under conditions consistent with expulsion-type dampers. The MR-fluid actuation of the metal foam type dampers is initiated by attracting iron particles, suspended in the MR-fluid, out of the foam and completing a magnetic circuit through the fluid, the foam, the steel housing, and the piston. This form of actuator can be referred to as a double-ended piston-type MR-fluid extraction damper. It has been shown that these devices can produce between 10-30 N of controllable force with nonlinear characteristics consistent with the polyurethane foam counterpart [55].

The concerns that are common among these types of MR-fluid dampers are the containment of the fluid within the device, as well as accurately modeling the behavior of these devices. The housing allows movement of the piston through an opening that must be sealed to prevent fluid loss. This seal is the main source of friction in the damper and can hinder truly controllable low-scale forces. In this chapter, a damper device is enlarged to better contain the fluid and the seals are eliminated. After eliminating the seals for fluid containment, a prototype small-scale (0-10 N) MR-fluid damper has been constructed based on the configuration of double-ended piston-type extraction dampers. It is hypothesized that this low-force MR-fluid damper can be modeled consistently with commercial devices using techniques used in preceding literature. Additionally, it is hypothesized that this device can be used as a semi-active actuator to control and attenuate inter-story drift and velocities in a small-scale laboratory shear structure using a traditional control law.

The main objective in this chapter is to characterize and validate the performance of a novel double-ended piston-type MR-fluid extraction damper as an actuator for use in small-scale structural control testbed applications, for not only the case study in this chapter, but also the validation of methods in Chapters 4 and 5 of this dissertation. It is anticipated that this damper will enable the operation of a multi-degree-of-freedom (MDOF) structural control platform (1-9 DOF) that is based on a relatively inexpensive shaking table that may provide meaningful information for researchers. In this chapter, theoretical background information is provided including an MR-fluid damper model (previously validated for commercial dampers) that is matched to the prototype damper. In addition, a basic linear-quadratic-Gaussian (LQG) state-space control algorithm for a 3-story lumped-mass model is presented that will calculate optimal control forces to be provided using the damper. Following that, details of the design and construction of the low-force MR-damper design are provided and its properties characterized. Performance of the extraction-type damper for use in small-scale structural control is validated and presented, followed by results of the validation case study, and conclusions for this chapter.

3.1 Constraints for the Desired Performance of a Prototype MR-fluid Damper

Challenges in developing a damper to meet the desired properties for this dissertation arose specifically from the need to achieve low damping forces for the small-scale test-bed. When developing dampers for low-forces, production of damping forces dominated by magneto-rheological (MR) effects is important. Dampers that harness smart fluid properties must prevent fluid loss due to the cost associated with fluid replacement and environmental/cleanliness concerns within the test structure and testing facility. Techniques that are effective to prevent the leakage of fluid in full-scale dampers include vertical or angled orientation of the damper and piston shaft wipers [100]. Seals, as well as gravity, play a role in increasing undesired friction, thus on a small-scale, hindering the practical controllable range of the damper. Another issue related to building dampers is that the constituents can become damaged. The electromagnet that is an integral part of a MR-damper construction requires use of small-diameter magnet-wire (*e.g.,* 30 AWG). This wire is very delicate and can break with excess force and also fatigues easily. Also, magnet-wire has equally delicate coating (*i.e.,* to avoid the use of typical wire casing, a non-conductive coating is used) which can wear away. The likelihood of two overlapping wires with worn coating is very high because any motion between layers can wear adjacent surface coating. When both wires with worn coating touch a short is formed in the electromagnet, which drastically reduces the magnetic field that it can produce. Such a short will usually require that the magnetic component of the piston be entirely rebuilt. These challenges can be avoided by purchasing commercially-available MR-damper technology, but both cost and technical barriers exist to adopting these components in small-scale studies. Therefore, novel and customized design approaches were necessary to achieve the goal of a small-scale test-bed that approximates the behavior of larger-scale systems. Scaling issues represent the most serious challenge to such a goal.

3.2 Environment/Damper Conditions

Technical challenges extend past the construction and calibration of these devices. The environment, in which the two main components exist (the electromagnet and MR-fluid), presents problems related to corrosion and leakage. Careful measures must be taken to waterproof the electromagnetic wires, such as applying two-part epoxy to the wires. Application of low viscosity superglue and a bond accelerant after coiling each layer can prevent wire movement and loss of magnet-wire coating. Prevention wear of this coating will prevent short circuits and also prevent the wires from being exposed to MR-fluid. Waterproofing and the wearing of the non-conductive coating are also issues in the piston shaft as it is hollow in order to allow the wires to escape the damper housing. As such, similar measures must be taken to ensure that MR-fluid does not leak into the piston shaft and also to prevent the wires from becoming disconnected in the core of the piston.

3.3 Exploration of Two Damper Designs

With these technical challenges and the shortcomings noted earlier that are associated with each MR-fluid damper type, two designs were attempted to make a damper suitable for this dissertation. The preliminary design is based on a double-end configuration MR-damper with seals that guide the piston and prevent fluid loss. The final design is based on an extraction sponge-type MR-damper, which does not require any extra measures that prevent fluid loss beyond the sponge itself. The expected behavior of the preliminary design was based on an adaptive search technique developed by in [100] which defines the relationships between fluid volume, gap thickness, and damping force. Based on this work developed for determining damper parameters and their relationships to desired damper forces, the initial damper design (based on the double-ended configuration) was expected to achieve an output range of 0 to 25 N forces at magnetic saturation for typical damper velocities. The actual results for the preliminary design did not reflect what was expected. The results demonstrate that the friction forces, which limit the lower end of the controllable range of the damper, are generally as high as 3.5 N. Also, the magnetic saturation occurs at low current inputs (100 mA). Efforts aimed at ameliorating these

friction forces (by the use of composite Teflon/steel pistons) were not successful. The Teflon ends can replace weakly magnetized portions of the steel piston (*i.e.,* at the ends, far from the coil); therefore, the MR-force would not be affected, but the friction at the seals would be lowered. These efforts were able to produce modest reductions in friction forces, but not as much as was hoped.

To achieve the desired low-friction behavior, it became necessary to eliminate these seals entirely. The final design uses metal foam extraction to contain the MR-fluid. Additionally, there exists a unique interaction between the MR-fluid and metal foam that serves to add extra shear stresses to the damping system for higher input currents. These alterations were made in order to have a damper that met the requirements for the work in this dissertation. The alterations increased the controllable range on both ends of the preliminary force curve. The seal-less design provides approximately 0 N low-forces when no current is applied and greater damping forces when power (varying levels of current) is present.

3.4 Damper Prototype, Model calibration, and Experimental Setup

Extraction-type dampers can operate on a low-force range (10-30 N) [55]. The goal for this chapter is to develop a damper with controllable force range of 0-10 N, to be used in this dissertation. The metal foam used in previous designs of MR-fluid extraction dampers is porous nickel metal foam with 110 pores per inch (ppi) [55]. From this foam, MR-fluid was extracted by a moving piston via electromagnetism (actuated by a DC motor). The thickness of the foam used was 2 mm to prevent pore clogging and to allow for material magnetic saturation (necessary for completing the magnetic circuit) [55]. For this dissertation, a damper was selected that has a less dense (20 ppi) aluminum (6101-T6 Alloy) coated foam to contain the MR-fluid to allow fluid to be drawn more quickly from the foam. The selected foam is 12.7 mm thick and has lower porosity so that the fluid can flow freely through the foam when the damper is not active. The prototype damper is 17.8 cm long and contains 100 mL of MR-fluid. The actuator dimensions are highlighted in Figure 3.1.

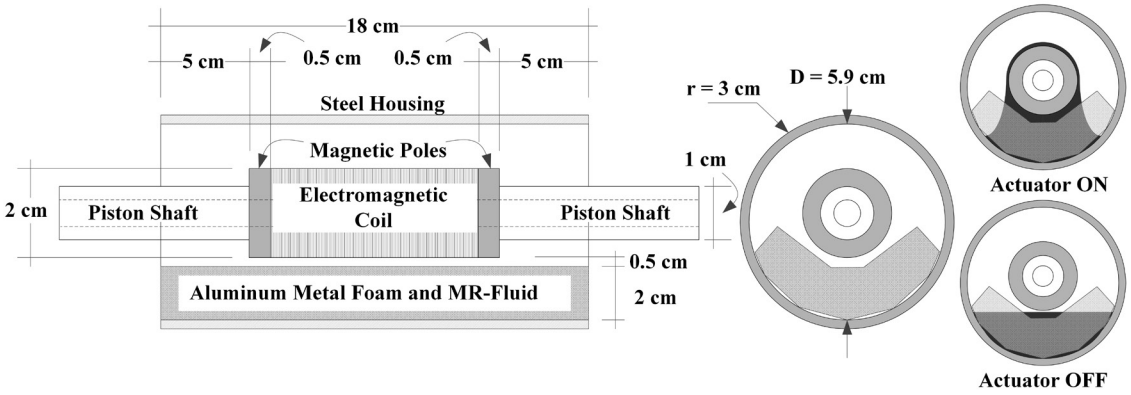

Figure 3.1: Schematic of MR-fluid extraction damper prototype

A photograph of the prototype damper is provided in Figure 3.2. When the damper is active, the fluid becomes adhered to the metal foam and steel housing, initiating a controllable smart friction and viscosity. In comparison to previous designs, the steel housing has a similar inner diameter, but the wall thickness has been reduced. Thicker walls can increase the magnetic saturation of the wall material, which can increase the MR-fluid iron particle attraction. However, it was desired to minimize the mass of the damper to keep the test bed within the limits of the shaker. Also, the magnetic circuit saturation (which limits the maximum achievable damping), is defined by the weakest point. In this case was found to be the link between the magnetic poles and the piston [44, 82, 95, 100, 101]. Therefore, the additional wall thickness did not contribute additional damping. The overall length of the damper was increased to help contain the MR-fluid in the housing without the use of seals (*i.e.,* shaft wipers to prevent fluid loss), which are the main source of friction in MR-fluid dampers. Eliminating this source of friction extended the range of controllable forces down near the zero-force zone.

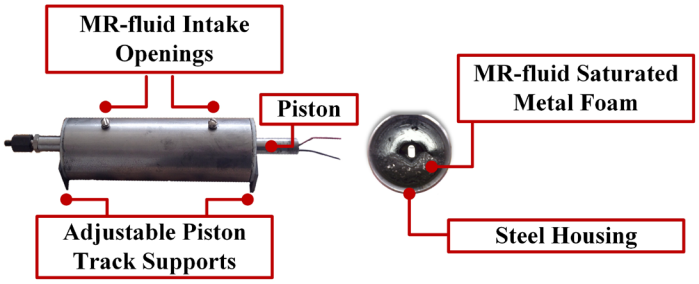

Figure 3.2: MR-fluid extraction damper prototype housing and saturated foam

3.5 Devising Control Scheme with the Prototype MR-Damper

The theory behind the model used to characterize this damper prototype is reviewed in this section. For the control portion of this chapter, some background on linear-quadratic-Guassian (LQG) control is also provided.

3.5.1 Bouc-Wen Nonlinear Hysteresis Model Development

Magneto-rheological (MR) fluid dampers provide damping and axial forces to a structure through both viscous and inelastic restoring forces. When combined, these forces possess nonlinear characteristics that have been most accurately modeled using a Bouc-Wen hysteresis model [82, 102]. This phenomenological model can be used for modeling the damping behavior of the MR-fluid extraction damper prototype at varying input current levels. Before using the prototype low-force damper for structural control of the small-scale laboratory test structure, the various Bouc-Wen model components must be calibrated.

3.5.1.1 Bouc-Wen Model Identification and Look-up Table

To command the MR-damper used in this chapter, and later the dampers used in Chapters 4 and 5, first a Bouc-Wen model, previously applied to larger scale dampers [2, 102], is fit using a recursive nonlinear filter developed by Lin, Chung *et al.* [92]. The Bouc-Wen derivation uses the previously collected force-displacement data from the MR-fluid damper [92]. The damper force, $F(t)$, can be expressed as follows:

$$F(t) = C(V)\dot{x}(t) + \xi(t) \tag{3.1}$$

where $C(V)$ is the damping coefficient that varies with a change in command voltage, V, $\dot{x}(t)$ is the relative velocity between the damper housing and the piston, and $\xi(t)$ is the nonlinear hysteretic restoring force.

$$\dot{\xi}(t) = A\dot{x}(t) + \beta|\dot{x}(t)||\xi(t)|^{n-1}\xi(t) + \gamma\dot{x}(t)|\xi(t)|^{n} \tag{3.2}$$

Here, A, β, and γ are all variables that can be used to calibrate the shape of the hysteresis [103]. Parameter A controls the slope of the hysteresis loop. When A is increased, the model system natural frequency is increased. β is the parameter that defines strain hardening and softening behaviors when combined with the γ term. The behavior is governed by the relative sign of the summation of β and γ terms [103]. When β is increased, the response amplitude is decreased. As the parameter γ varies from negative to positive, the system frequency response curves gradually vary from hardening to quasi-linear, respectively. Ultimately, it is desired to utilize low-power wireless sensing units in future work to command these MR-dampers. For faster calculation of actuation forces, Eq. (3.2) can be discretized into a look-up table [15, 92]. The first step in discretizing this model is shown below:

$$\dot{\xi}(t) = A\dot{x}(t) + \sum_{n=1}^{N} a_n(\beta|\dot{x}(t)||\xi(t)|^{n-1}\xi(t) + \gamma\dot{x}(t)|\xi(t)|^n) \qquad (3.3)$$

where a_n is binary for all N (*i.e.,* a_n is a toggle for each n from 1 to N to determine the power representing the curvature of the nonlinear hysteresis). Since there is an intrinsic inelastic memory that calls on previous system state, the Bouc-Wen model can be further discretized to reference the previous time-step as a prediction for the next or active time-step using numeric integration [92]:

$$\xi_k = \xi_{k-1} + \Delta t\left(A\dot{x}_{k-1} + \sum_{n=1}^{N} a_n(\beta|\dot{x}_{k-1}||\xi_{k-1}|^{n-1}\xi_{k-1} + \gamma\dot{x}_{k-1}|\xi_{k-1}|^n)\right) \quad (3.4)$$

In Eq. (3.4) k is the time-step to which damping force will be applied, $k-1$ is the previous (or *a priori*) time-step, and Δt is the sampling time (reciprocal of the sampling frequency, f_s) of the data acquisition system used to collect the force-displacement data. Once parameters A, β, and γ are chosen, they can be estimated for use in an adaptive learning algorithm to fit a full time series data set [92, 103]. The approximation starts by defining two vectors: Φ defined by Eq. (3.5); and Θ defined by Eqs. (3.6-3.8).

$$\vec{\Phi}_{k-1} = \begin{Bmatrix} \phi_0 \\ \phi_1 \\ \phi_2 \\ \phi_3 \\ \phi_4 \\ \cdots \\ \phi_{2N-1} \\ \phi_{2N} \end{Bmatrix}_{\mathrm{k-1}} = \Delta \mathrm{t} \begin{Bmatrix} \dot{x}_{k-1}|\xi_{k-1}|^0 \\ |\dot{x}_{k-1}||\xi_{k-1}|^0\xi_{k-1} \\ \dot{x}_{k-1}|\xi_{k-1}|^1 \\ |\dot{x}_{k-1}||\xi_{k-1}|^1\xi_{k-1} \\ \dot{x}_{k-1}|\xi_{k-1}|^2 \\ \vdots \\ |\dot{x}_{k-1}||\xi_{k-1}|^{N-1}\xi_{k-1} \\ \dot{x}_{k-1}|\xi_{k-1}|^N \end{Bmatrix} \tag{3.5}$$

$$\vec{\mu}_k = \vec{\Theta}_{k-1} - \frac{\gamma_0}{\beta_0 + ||\Phi_{k-1}||^2} e_{k-1}\vec{\Phi}_{k-1} \tag{3.6}$$

Here $\vec{\Phi}_{k-1}$ is a vector of system measurements, $\dot{x}_{k-1}$ and ξ_{k-1}, for time $k-1$, and $||\cdot||$ represents the Euclidean norm, $\vec{\mu}_k$ is the projection of $\vec{\Theta}_{k-1}$ onto the span of $\vec{\Phi}_{k-1}$ [92]. The projection is simplified using two design learning parameters: γ_0 (user selected learning rate $\gamma_0 > 0$) and β_0 (design parameter: in previous literature as $\beta_0 = 1\text{x}10^{-5.5}$) [92]. $\vec{\Theta}_k$ is defined using Eq. (3.8) and is the approximation of the parameters that generate the shape of the Bouc-Wen hysteresis. $e_k \forall\, k \geq k_0$ is the error between the actual force-velocity restoring component and the approximated hysteretic shape using $\vec{\Theta}^*$ and $\vec{\Theta}_k$, respectively. $\vec{\Theta}^*$ is a vector that stores the chosen values for A, β, and γ (*i.e.,* $\vec{\Theta}^* = \{A \quad a_1\beta \quad a_1\gamma \quad \dots \quad a_{n-1}\beta \quad a_{n-1}\gamma \quad a_n\beta \quad a_n\gamma\}^T$).

$$e_k = \vec{\Phi}_{k-1}{}^T\vec{\Theta}_k - \vec{\Phi}_{k-1}{}^T\vec{\Theta}^* \tag{3.7}$$

$$\vec{\Theta}_k = \begin{cases} \vec{\mu}_k & \text{if } ||\vec{\mu}_k|| \leq M_\theta \\ \frac{M_\theta}{||\vec{\mu}_k||}\vec{\mu}_k & \text{if } ||\vec{\mu}_k|| > M_\theta \end{cases} \tag{3.8}$$

$\vec{\Theta}_k$ is a piecewise function between $\vec{\mu}_k$ and $\frac{M_\theta}{||\vec{\mu}_k||}\vec{\mu}_k$, where M_θ is the Euclidean norm of $\vec{\Theta}^*$. This use is meant to aid in stability of the filter and to limit $\vec{\Theta}_k$ as time progresses to prevent estimates of shape parameters from approaching infinity. Once shape parameter estimates are achieved for each time-step in the entire time series (*i.e.,* $\exists\, \vec{\Theta}_k \forall\, k \geq k_0$), $\vec{\Theta}_{k_f}$ will then represent the adapted shape factor that characterizes the nonlinear behavior

of every time-step. $\vec{\theta}_{k_f}$ can then be used to for the last step in the discretization of the Bouc-Wen model:

$$\xi_{k+1} = \xi_k + \Delta t \sum_{i=1}^{5} \theta_i(I_k)\phi_{i_k} \tag{3.9}$$

$$I_k = \frac{V_k A_V}{R_{eq}} \tag{3.10}$$

In Eq. (3.9), ξ_{k+1} can be obtained given $\theta_i(I_k)$ for $i = 1 \ldots 5$ and the provided input current at the current time-step, I_k. Together each θ_i helps estimate the continuous time parameters of the solution to the partial differential equation, Eq. (3.3). Also, Eq. (3.9) involves the restoring force components: $\phi_{1_k} = \dot{x}_k$, $\phi_{2_k} = |\dot{x}_k|\xi_k$, $\phi_{3_k} = \dot{x}_k|\xi_k|$, $\phi_{4_k} = |\dot{x}_k||\xi_k|\xi_k$, and $\phi_{5_k} = \dot{x}_k|\xi_k|^2$. The remainder of the ϕ values from Eq. (3.5) and corresponding θ values are neglected because they add no additional accuracy in approximating ξ [92].The input current I_k can be calculated using the amplifier command voltage, V_k, the damper equivalent resistance, R_{eq}, and the operational amplifier gain value, A_V. Finally, a look-up table can be generated using the theta equations and damping coefficients for each current level:

$$\begin{cases} \theta_1(I_k) = -77.53 - 6.71I_k + 19.9{I_k}^2 - 14.98{I_k}^3 + 4.77{I_k}^4 - 0.7{I_k}^5 \\ \theta_2(I_k) = -24.23 - 9.27I_k + 13.96{I_k}^2 - 9.23{I_k}^3 + 2.80{I_k}^4 - 0.4{I_k}^5 \\ \theta_3(I_k) = -38.70 + 7.86I_k - 13.83{I_k}^2 + 8.37{I_k}^3 - 2.48{I_k}^4 + 0.35{I_k}^5 \\ \theta_4(I_k) = -14.62 - 6.35I_k + 3.32{I_k}^2 - 0.68{I_k}^3 - 0.03{I_k}^4 + 0.02{I_k}^5 \\ \theta_5(I_k) = -23.89 + 1.19I_k - 10.45{I_k}^2 + 8.59{I_k}^3 - 2.96{I_k}^4 + 0.46{I_k}^5 \\ C(I_k) = 11.73 + 54.74I_k - 11.04{I_k}^2 + 0.84{I_k}^3 \end{cases} \tag{3.11}$$

$$\begin{bmatrix} \theta_1(I_{k_1}) & \theta_1(I_{k_2}) & \ldots & \theta_1(I_{k_P}) \\ \theta_2(I_{k_1}) & \theta_2(I_{k_2}) & \ldots & \theta_2(I_{k_P}) \\ \vdots & & \ddots & \vdots \\ \theta_5(I_{k_1}) & \theta_5(I_{k_2}) & \ldots & \theta_5(I_{k_P}) \\ C(I_{k_1}) & C(I_{k_2}) & \ldots & C(I_{k_P}) \end{bmatrix} \tag{3.12}$$

The look-up table from Eq. (3.12) is comprised of discrete values of current from 0 mA to I_P to be used as a reference within an embedded or wired control system in place of

the set of equations in Eq. (3.11). The discretization speeds up control time and algorithm evaluation. Ultimately, based on the ampacity of the damper's electromagnet, and to have a reasonably sized look-up table, this dissertation employs 13 discrete current levels defined at 50 mA increments.

3.5.2 State-Space Control

The control portion of this chapter employs a small-scale lumped-mass structure that can be approximated as a linear time-invariant (LTI) system, to which linear-quadratic-Gaussian (LQG) control applies directly. Using linear assumptions, discrete-time control, n lumped mass degrees-of-freedom, and m dampers ($m \leq n$), the state-space equation is as follows:

$$\boldsymbol{A} = \begin{bmatrix} 0 & I \\ -\boldsymbol{M}^{-1}\boldsymbol{K} & -\boldsymbol{M}^{-1}\boldsymbol{C}_d \end{bmatrix} \in \mathbb{R}^{2n\times 2n}$$

$\boldsymbol{B} = \begin{bmatrix} 0 \\ -\boldsymbol{M}^{-1}\boldsymbol{L} \end{bmatrix} \in \mathbb{R}^{2n\times m}$ and $\boldsymbol{L} \in \mathbb{R}^{n\times m}$ is the actuator location matrix

$\boldsymbol{C} \in \mathbb{R}^{q\times 2n}$; $\boldsymbol{D} \in \mathbb{R}^{p\times m}$; $\boldsymbol{E} = \begin{Bmatrix} 0 \\ -\mathbf{1} \end{Bmatrix} \in \mathbb{R}^{2n\times 1}$; and $\boldsymbol{F} \in \mathbb{R}^{q}$

$$\boldsymbol{z}_{k+1} = \boldsymbol{\Phi}\boldsymbol{z}_k + \boldsymbol{\Gamma}\boldsymbol{p}_{k-\ell} + \boldsymbol{\Lambda}\ddot{\boldsymbol{x}}_{\boldsymbol{g}} \tag{3.13}$$

where $\boldsymbol{z}_{\mathrm{k}} = \begin{Bmatrix} \boldsymbol{x}_k \\ \dot{\boldsymbol{x}}_k \end{Bmatrix} \in \mathbb{R}^{2n\times 1}$ is the state vector in discrete-time, $\ddot{\boldsymbol{x}}_g$ is the ground acceleration disturbance, $\boldsymbol{p}_{k-\ell} \in \mathbb{R}^{m\times 1}$ is the control force vector delayed by time ℓ, and q is the number of observable states. When discretizing the state-space representation, using a zero-order hold approximation, $\boldsymbol{\Phi} = e^{\boldsymbol{A}T_s} \in \mathbb{R}^{2n\times 2n}$ is the discrete system matrix, where T_s is the sampling time, $\boldsymbol{\Gamma} = \int_0^{T_s}(e^{\boldsymbol{A}\tau}\boldsymbol{B})\,d\tau \in \mathbb{R}^{2n\times m}$ is the discrete actuator control matrix, and $\boldsymbol{\Lambda} = \int_0^{T_S} e^{\boldsymbol{A}\tau}\boldsymbol{E}\,d\tau \in \mathbb{R}^{2n\times 1}$ is the discrete-time disturbance matrix. $\boldsymbol{I}$ is the identity matrix, $\boldsymbol{M}$ is the diagonal measured lumped mass matrix, $\boldsymbol{K}$ is the lumped mass dynamic stiffness matrix of a three degree-of-freedom (DOF) system with floor, and $\boldsymbol{C}_d$ is formed with 1% modal/Rayleigh damping. For the discrete-time state-space

model, the control force ($\boldsymbol{u} \equiv \boldsymbol{p}_{k-\ell}$) is used to minimize the quadratic cost function, J.

$$J = \sum_{k=0}^{\infty} \boldsymbol{z}_{\mathrm{k}}^{T} \boldsymbol{Q} \boldsymbol{z}_{\mathrm{k}} + \boldsymbol{u}^{T} \boldsymbol{R} \boldsymbol{u} \tag{3.14}$$

Here $\boldsymbol{Q} = {\boldsymbol{C}_{\mathrm{LQR}}}^{T} \boldsymbol{C}_{\mathrm{LQR}}$ ($\boldsymbol{C}_{\mathrm{LQR}} \in \mathbb{R}^{2n \times 2n}$: the linear transform $\boldsymbol{z}_{\mathrm{k}} \longrightarrow \boldsymbol{y}_{\mathrm{k}}$) and $\boldsymbol{R} \in \mathbb{R}^{m \times m}$ is a symmetric positive definite matrix that is used to set importance levels on output response and control effort [3, 104, 105]. The matrix $\boldsymbol{C}_{\mathrm{LQR}} = \boldsymbol{I}_{2nx2n}$ is used for minimizing both relative displacement and velocity. Putting emphasis on either velocity or displacement can be done by increasing the weight of the diagonal terms of the $\boldsymbol{I}$ matrix (*e.g.,* $\boldsymbol{C}_{\mathrm{LQR}} = \begin{pmatrix} \boldsymbol{I}_{3x3} & \boldsymbol{0}_{3x3} \\ \boldsymbol{0}_{3x3} & 10\boldsymbol{I}_{3x3} \end{pmatrix}$ is used to target relative velocity with more emphasis while still penalizing displacement). For the $\boldsymbol{Q}$ matrix to penalize displacement drift:

$$\boldsymbol{C}_{\mathrm{LQR}} = \begin{pmatrix} 1 & 0 & 0 & \\ -1 & 1 & 0 & \boldsymbol{0}_{3x3} \\ 0 & -1 & 1 & \end{pmatrix}$$

similarly, to penalize velocity drift:

$$\boldsymbol{C}_{\mathrm{LQR}} = \begin{pmatrix} & 1 & 0 & 0 \\ \boldsymbol{0}_{3x3} & -1 & 1 & 0 \\ & 0 & -1 & 1 \end{pmatrix}$$

for the case study in this chapter:

$$\boldsymbol{C}_{\mathrm{LQR}} = \begin{pmatrix} 14 & 0 & 0 & \\ -4 & 4 & 0 & \boldsymbol{I}_{3x3} \\ 0 & -4 & 4 & \end{pmatrix}$$

which is set up to mainly target displacement drift and relative displacement for each floor, while still penalizing relative velocity. To determine the control force trajectory two things are necessary: the gain matrix, $\boldsymbol{G} \in \mathbb{R}^{m \times 2n}$, and the state vector, $\boldsymbol{z}_k \in \mathbb{R}^{2n \times 1}$.

Lastly,

$$\boldsymbol{u}_k = -[[\boldsymbol{R} + \boldsymbol{\Gamma}^{\boldsymbol{T}} \boldsymbol{P} \boldsymbol{\Gamma}]^{-1} \boldsymbol{\Gamma}^{\boldsymbol{T}} \boldsymbol{P} \boldsymbol{\Phi}] \boldsymbol{z}_k = -\boldsymbol{G} \boldsymbol{z}_{\mathrm{k}} \tag{3.15}$$

$$\boldsymbol{P} = \boldsymbol{\Phi}^T[\boldsymbol{P} - \boldsymbol{P\Gamma}[\boldsymbol{R} + \boldsymbol{\Gamma}^T\boldsymbol{P\Gamma}]^{-1}\boldsymbol{\Gamma}^T\boldsymbol{P}]\boldsymbol{\Phi} + \boldsymbol{Q} \tag{3.16}$$

where $\boldsymbol{P} \in \mathbb{R}^{2n\times 2n}$ is the Riccati matrix defined by Eq. (3.16). The traditional LQG Controller consists of the previously defined LQR gain and Kalman state estimates to produce an input into the system. However, the prototype actuator brings rise to a modification to the LQG controller, Figure 3.3, where $y(t)$ is the output response, $\hat{x}(t)$ is the estimated state, and $u(t)$ is the desired control force. With an imperfect controller, such as an MR-fluid damper, the block diagram is altered such that the LQR gain only impacts what force, $F(t)$, is determined to be provided by MR-damper through the use of the Bouc-Wen look-up table (which defines the actuator characteristics and varying levels of command voltage, $V(t)$).

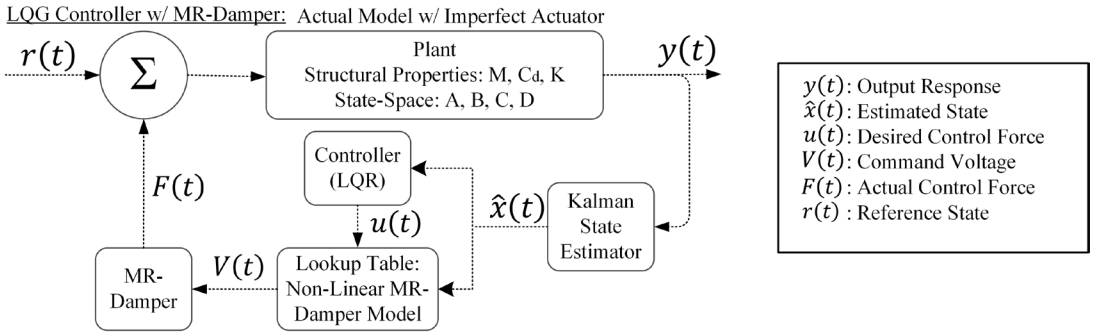

Figure 3.3: LQG controll block diagram with added MR-fluid extraction damper

3.5.3 Experimental Setup for Isolated Damper Tests and Bouc-Wen Model Calibration

Magneto-rheological (MR) fluid dampers have complex nonlinear hysteretic behavior that can be modeled using Bouc-Wen models [82]. The prototype damper used in this chapter, which is used to develop the dampers for use in later chapters, possesses similar characteristics to commercial devices and therefore may be modeled in the same way. The calibration of Bouc-Wen model parameters was performed on an isolated damper excited by a Quanser Shake Table II. The piston was connected via a threaded rod to an HSS6x6x5/8 steel column that is assumed to be fully rigid. The damper force was measured using an in-line force transducer (see Figure 3.4). A sinusoidal chirp excitation

(0-30 Hz in 30 seconds) was applied to the damper using the shaking table for a number of tests. These individual tests were performed using multiple damper current input levels supplied by an Agilent Technologies U3606A power supply. With damper command levels ranging from 0-600 mA, the Bouc-Wen parameters were derived. The sensors used to measure the force-displacement relationship were PCB Piezotronics 333B50 accelerometers, MTS C-Series Core Linear Position Transducers (LPT) 551020, and PCB Piezotronics 208C01 force transducers connected to a NI PX1-6255 data acquisition card. Additional experiments on the isolated damper were used to validate the Bouc-Wen model accuracy and repeatability of the response to sinusoidal excitations at each current level.

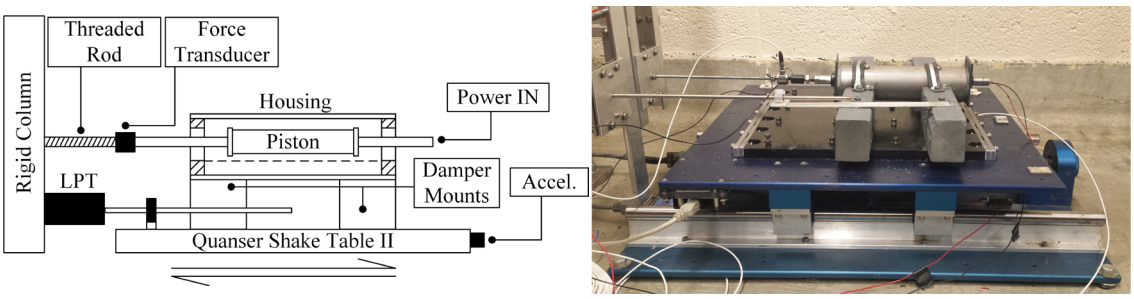

Figure 3.4: Damper characterization apparatus and sensor placement

The magnet wire used for the dampers in this dissertation was 30 AWG and wrapped 2880 times, with a maximum safe current rating of 870 mA when exposed freely to air and 520 mA when enclosed [106]. Though wire used in electromagnets is enclosed, the length of time needed to power the coil is not sufficient to damage the wire by exceeding the enclosed ampacity. Each chapter discusses using the dampers with variable control, and the maximum amperage, or working ampacity is 600 mA, just slightly higher than the maximum current for enclosed wire due to short test durations. Therefore, the damper behavior is characterized between 0 and 600 mA.

3.5.4 Experimental Setup for Control Tests

The experimental setup used for control tests involved several components: a shake table for simulating seismic excitation, the prototype magneto-rheological (MR) fluid extraction damper, and a data acquisition/actuation system. Figure 3.5 (a) shows the assembly of the testbed, while Figure 3.5 (b) depicts the instrumentation used in this chapter.

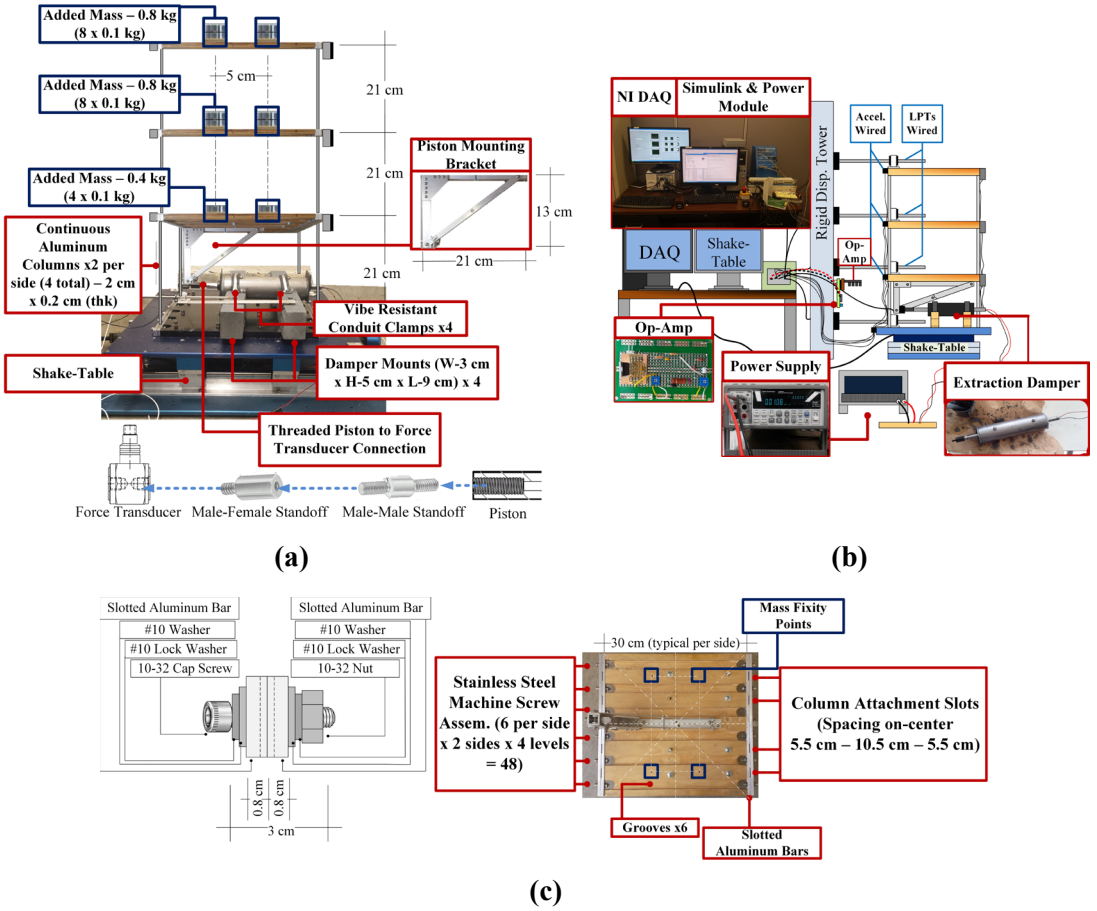

Figure 3.5: Test-bed assembly schematic (a); 3-DOF control setup (b); floor design (c)

The structure floors are made from Baltic birch plywood plates, with grooves cut in the bottom to reduce weight, and are connected to one another using four rectangular aluminum columns that are clamped to the ends of the floors in their weak-axis bending direction (shown in Figure 3.5 (c)). Additional mass was added to each floor to shift the

natural frequencies of the system to those more closely matching full-scale structures. A National Instruments (NI) DAQ NI PXIe-1071 running LabVIEW was used to acquire story accelerations and compute the linear-quadratic-Gaussian (LQG) state-space control algorithm to determine control forces. A voltage-to-current converter was fashioned to convert voltage signals from a NI PXI-6713 actuation card to the appropriate current levels (50 mA increments) for the MR-fluid damper. For the control portion of this chapter, an LQG controller was derived for the three degree-of-freedom (DOF) structure based on identified modal properties. Acceleration signals were measured using the same PCB accelerometers used for the damper characterization and were used to estimate the relative story velocities and displacements for state feedback.

The system properties of the three degree-of-freedom (DOF) testbed were obtained using a sinusoidal linear chirp signal excitation. The band of identified modal frequencies fell between 0 and 12 Hz. Since the mass was known prior to testing, the stiffness was calibrated and recorded in Table 3.1 for the three degrees of freedom to match the measured resonant frequencies. The results from the case study in this chapter identified three modal frequencies at 1.400, 4.670, and 8.000 Hz, depicted in Figure 3.6.

Table 3.1: Modal properties of testbed

Floor	*Mass (kg)*	*Stiffness (N/m)*	*Resonant Frequency (Hz)*	
1	1.750	582.0	1.400	(1st Mode)
2	1.800	834.0	4.670	(2nd Mode)
3	1.800	1975	8.000	(3rd Mode)

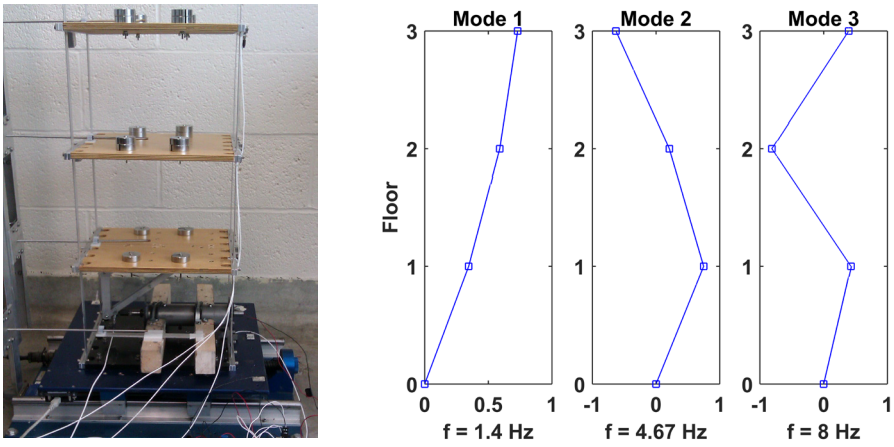

Figure 3.6: Three degree-of-freedom testbed and lumped mass model mode shapes

The control tests were also performed on the Quanser Shake Table II system that was itself controlled using the manufacturer's software in conjunction with Simulink. Using the NI DAQ, both LQG state feedback and passive control were executed. For comparison, both passive (damper fully-on) and LQG (varying current) control were performed on the 3DOF small-scale test structure excited by the El Centro ground-record from the Imperial Valley 10/15/79 El Centro Array #5, 150 – USGS Station 962. The results are plotted and recorded in the following section including: inter-story drift and acceleration response of the structure to El Centro, along with the total structural energy. The total energy is the sum of the kinetic and potential energy in the structure and is estimated using:

$$TE = PE + KE = \sum_{i=1}^{n} \frac{1}{2} \boldsymbol{k}_i x^2 + \frac{1}{2} \boldsymbol{m}_i \dot{x}^2 \tag{3.17}$$

where $\boldsymbol{k}_i$ is the story stiffness and $\boldsymbol{m}_i$ is the mass for each story, i, from the 1st to the n^{th} story, x^2 is a vector of square entries for the displacement time history, and $\dot{x}^2$ is a vector of square entries for the velocity time history.

For passive damping tests, the MR-damper was set to a constant 600 mA current for the entire duration of the simulated seismic event. For LQG control, the current range is broken down in thirteen increments and a Bouc-Wen lookup table was employed to allow the system to find the closest force to desired control forces during state feedback. The discrete levels of current that characterize the lookup table are better for embedding in low-power controllers, that may be used on small-scale testbeds, such as wireless control sensors [92]. The command voltage was recorded along with the desired control and achieved control forces. The measured force in this setup included the inertial force of the damper piston (which is not negligible at this scale), which had to be calculated and removed to reveal actual force provided by the damper. This process can be expressed as follows:

$$F_{t_n} = F_{d_n} + m_{p_n} \ddot{x}_n \tag{3.18}$$

where F_{t_n} is the total force measured in the force transducer for the damper applied directly to the n^{th} degree-of-freedom. The transducer force is composed of the resistive force of the damper (used to compare to the desired control force), F_{d_n}, which absorbs dynamics acting between floors, and the piston inertial force, which is equal to the piston mass, m_{p_n}, multiplied by the acceleration of the piston and the n^{th} floor, $\ddot{x}_n$.

3.5.5 Modularity of Structural Control Testbed

The structural testbed described in the previous sub-subsection was made of components that are highly modular. Each of the floors can be separated by a user defined distance, additional mass can be mounted to each floor, and the column thickness and lengths can be adjusted. In Chapters 4 and 5, this same testbed is used, but the column thickness is increase by 50% and the overall test-bed structure's height is doubled. For both Chapters 4 and 5, structural floor separation is decreased and the total number of floors increases. Overall, the testbed is made to support a wide range of research projects, from structural control and health monitoring of single-DOF small-scale buildings, to damage detection testing on multi-DOF small-scale buildings.

3.5.6 Use of Martlet Wireless Structural Control Technology

The calibration of the prototype MR-damper and the validation for its use in this chapter were both performed in a wired structural control and excitation setup. However, the end goals of this dissertation are to have a structural control testbed that can validate new means for wireless structural control to address communication related issues in large control networks. The wireless control units used in this dissertation are *Martlet* units developed by the University of Michigan, Michigan Technological University, and the Georgia Institute of Technology. *Martlet* units are collocated wireless sensing and control actuation nodes that utilize Piccolo F28069 Microcontrollers capable of running the main CPU and a control-law accelerator simultaneously, making them effectively dual core [9]. These units are a newer generation wireless structural control technology consisting of a faster processor capable of true floating point calculations in the control-law

accelerator, modularity toward a wide variety of applications (*i.e.,* depending on the sensor type needed for monitoring and/or the power requirements for that sensor type, a different *Martlet* attachment "wing" can be added to interface with the required sensors), a Joint Test Action Group (JTAG) debugging interface to make embedded program development more rapid, and external memory for large data storage (*i.e.,* an 8 or 16 GB microSD card) [9]. There are several wings under development and validation at the University of Michigan and Georgia Tech for monitoring data at ultrasonic speeds [107], hydronic sensing, strain sensing [108], and tri-axial acceleration sensing [9]. For more general applications and applications involving both data acquisition and control, an analog-to-digital conversion/digital-to-analog conversion (ADC-DAC) wing was developed to use with the base *Martlet* board. The base *Martlet* board, or motherboard, which connects to the various wings, the JTAG debugging board, and a power supply/battery board is shown in Figure 3.7 (a).

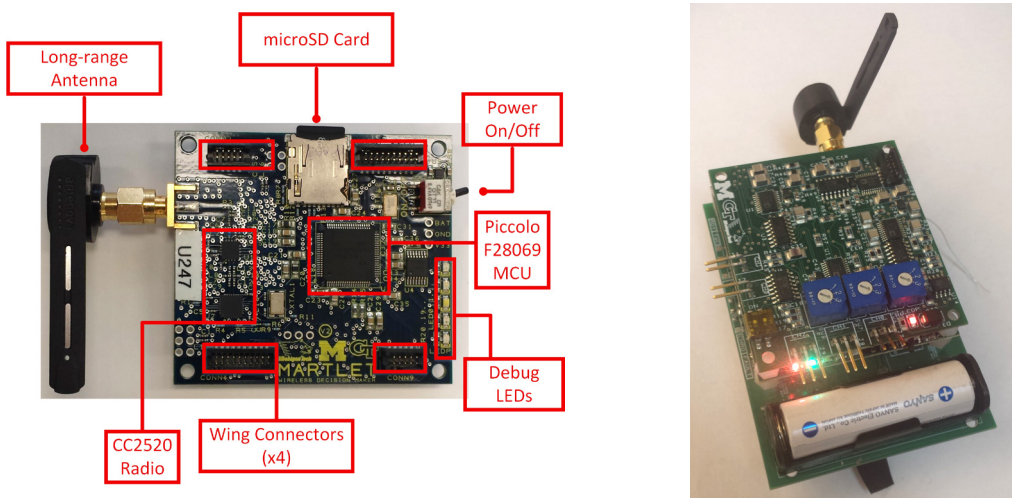

(a) **(b)**

Figure 3.7: *Martlet* motherboard configuration (a) and *Martlet* full assembly (b)

Along with JTAG debugging capabilities, a main feature to the *Martlet* motherboard is the row of LEDs. The LEDs can be turned on and off during code execution to indicate successful progression and/or failure. The microcontroller to microSD card data storage can be performed in one of two ways: byte-wise register allocation or using a file

allocation table (FAT) file system (similar to file saving on a PC). A FAT file system makes data storage and retrieval possible without wireless communication, but is not explored in this dissertation to focus on issues related to wireless data centralization, large data storage, and large data retrieval. Power is supplied to the *Martlet* motherboard from the bottom of the board shown in the full assembly Figure 3.7 (b), and power along with commands are bussed to additional sensing/actuation wings through the four wing connectors indicated in Figure 3.7 (a). Also, the *Martlet* motherboard uses a CC2520 radio which can transmit data between civil structures outdoors and between multiple floors indoors [9]. The long range antenna and range extender (CC2591) on the *Martlet* board may be used increase transmission distances with or without clear line of sight. The main boards used in this dissertation are *Martlet* motherboards, which store the embedded software for control tests, 5-AA battery power supply boards, a debugging board, and the general purpose ADC-DAC wings. These four boards are shown in Figure 3.8.

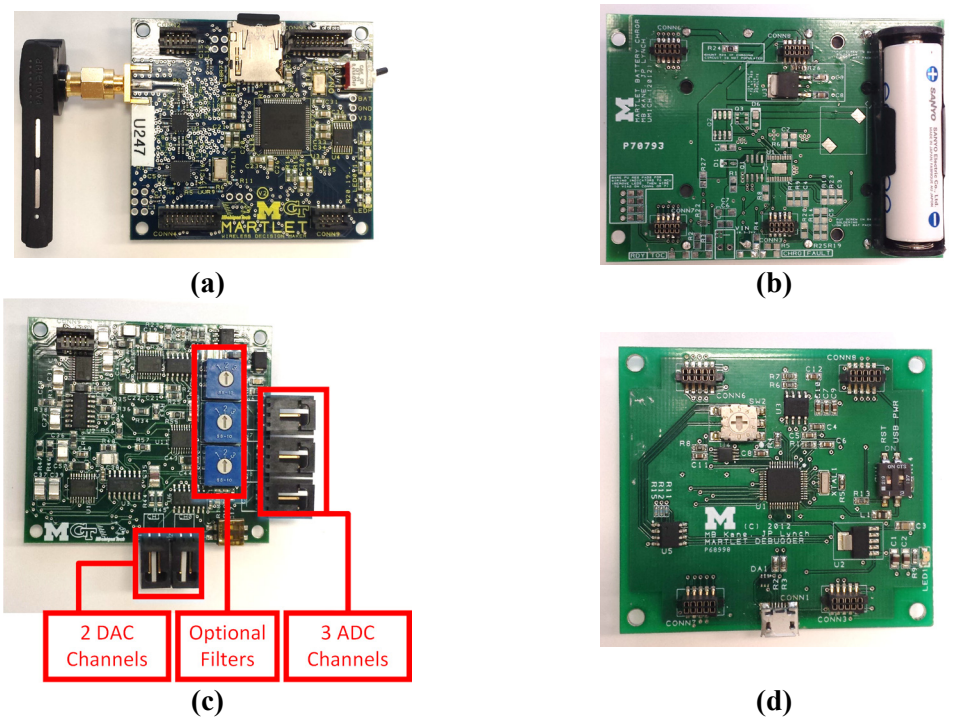

Figure 3.8: *Martlet* components – motherboard (a), battery board (b), ADC-DAC wing (c), and JTAG debugging board (d)

The battery board in Figure 3.8 (b) contains circuitry that can allow for solar power recharging of the 5 AA batteries (1 battery shown, the remaining 4 batteries are not shown and are located on the bottom of the board) and can provide sustainable power for permanent installation applications. The ADC-DAC wing, shown in Figure 3.8 (c), can interface with three sensors (ADC channels), where analog signals are converted to digital signals with 12-bit resolution and can be passed through optional 4^{th}-order Bessel low-pass filter (variable cut-off frequency) or a 2^{nd}-order unit-gain low pass filter (fixed 25 Hz cut-off frequency). The optional filters are not used in this dissertation. The DAC channels on the ADC-DAC wing output pulse-width modulated (PWM) signals that approximate desired analog signals for actuation and motor control.

For this dissertation, *Martlet* units are used to communicate data between floors and throughout the wireless network contained in the structural control testbed. The control-law accelerator is primarily used in Chapter 5 for switching the control law associated with different incoming data sets. The microSD card is used to store large data sets during tests for both Chapters 4 and 5.

3.6 Results

The damper model was characterized between 0 mA and the ampacity, 600 mA. Figure 3.9 shows an overlay of the modeled response and the experimentally measured response for three input-current levels (0, 300, and 600 mA) to a uniaxial sinusoidal input. Averaged hysteresis curves are provided in Figure 3.10 to illustrate the nonlinear shape of the damper response with respect to displacement and velocity.

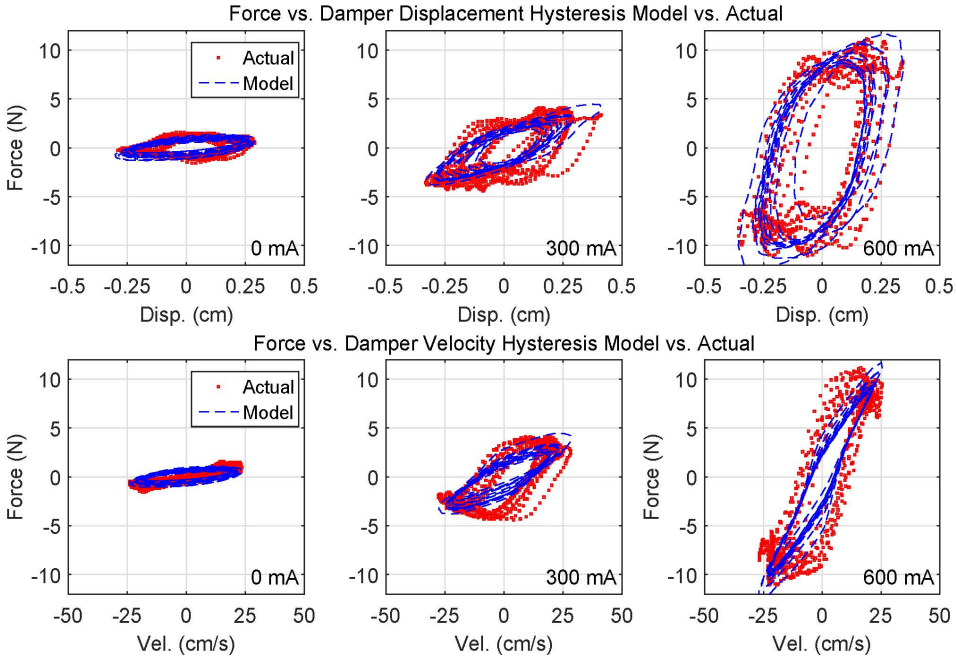

Figure 3.9: Bouc-Wen model and experimental data for damper force vs. velocity curves

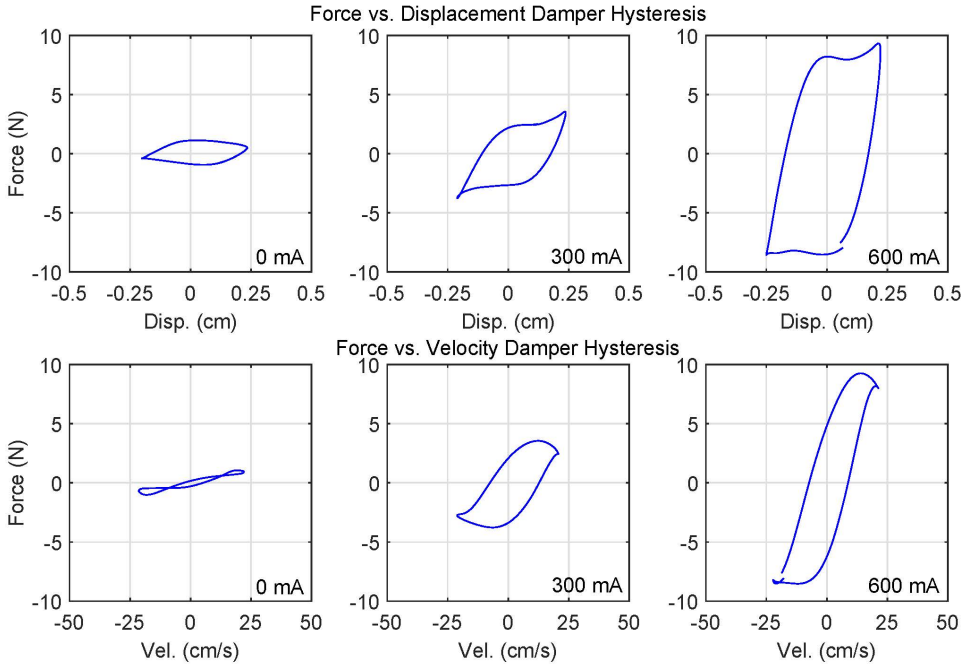

Figure 3.10: Averaged force vs. damper displacement and velocity hysteresis curves

In the multi-degree-of-freedom (MDOF) control portion of this chapter, the prototype magneto-rheological (MR) fluid extraction damper was used to control the response of a

3DOF small-scale shake structure. The Bouc-Wen lookup table was coupled with linear-quadratic-Gaussian (LQG) control to determine how well the actuator could provide the optimal force to minimize system acceleration and displacement. These damper forces are shown in Figure 3.11 superimposed with the desired control force determined from the LQG gain and output response. The actual/actuated force of the MR-damper appears more dramatic than desired, which is in part due to the force transducer noise spectrum and the accelerometer associated with the piston. The second source of inconsistency between the desired and actual damper force is due to disturbance introduced by the piston-to-force transducer connection. The connection consists of two standoffs featuring threaded members, shown in Figure 3.5, which introduce chatter and possibly other nonlinear disturbances such as torsional vibrations (connection slip).

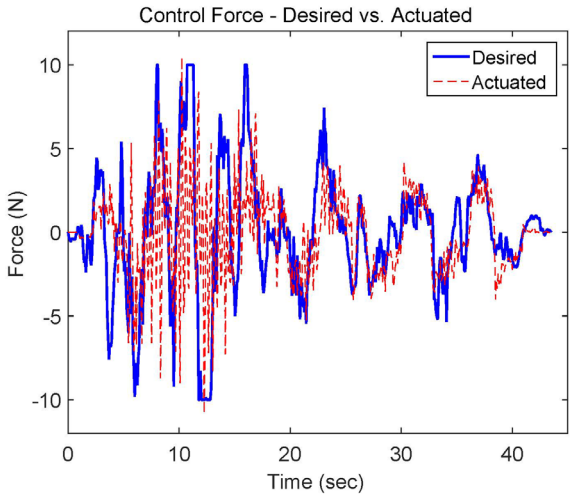

Figure 3.11: Desired vs. actual actuator control force

Figure 3.12 shows the controlled and uncontrolled inter-story drift time histories that indicate that a reduction in drift was achieved using the controller in its passive-on mode and a further reduction using the LQG controller. When passively controlled, the peak drift reductions for the first, second, and third floors are 37%, 27%, and 55%, respectively. The peak drift reductions using LQG are 74%, 41%, and 66% for the first, second, and third floors, respectively. Figure 3.13 show the comparison between controlled and uncontrolled acceleration response of the small-scale structure. The

maximum peak velocity reductions were observed at the first floor and were 51% for LQG control and 38% for passive control of the second floor. The maximum reductions in acceleration were 44% for LQG and 55% for passive control of the second and third floors, respectively. The peak values for the above performance metrics (*i.e.,* drift, velocity, and acceleration), as well as relative displacement between the structural story and the shake table, are shown in Figure 3.14 (in this case, maximum 2nd story drift is very close in magnitude to the maximum 2nd story displacement when the structure is controlled and uncontrolled, and close in magnitude for the 3rd story for the uncontrolled structure owing to the relatively smaller magnitude of the 1st story displacements).

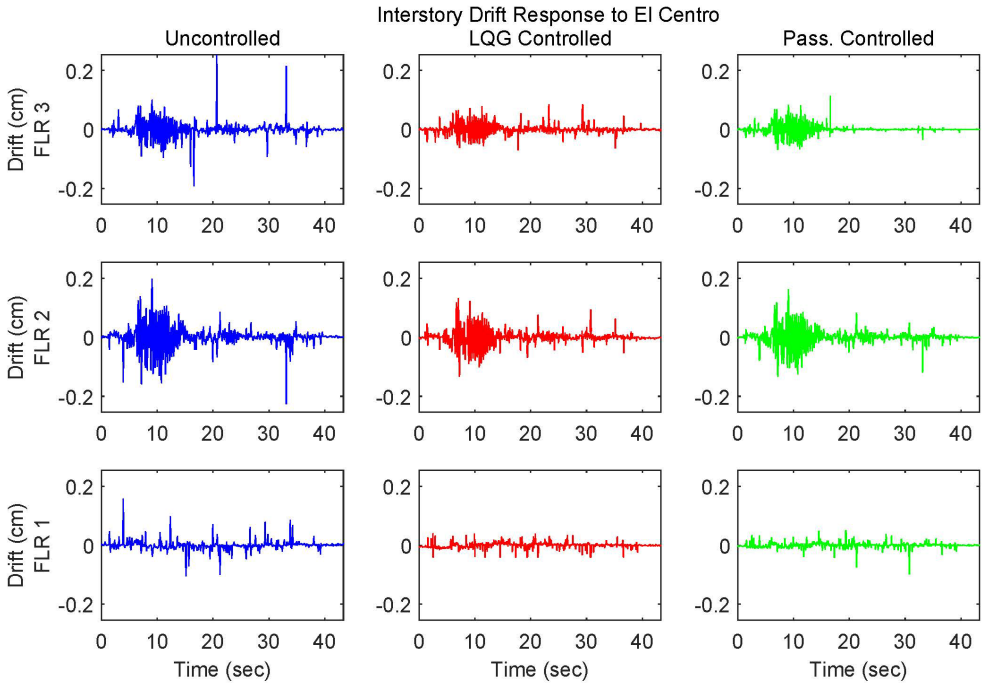

Figure 3.12: Story drift response time history

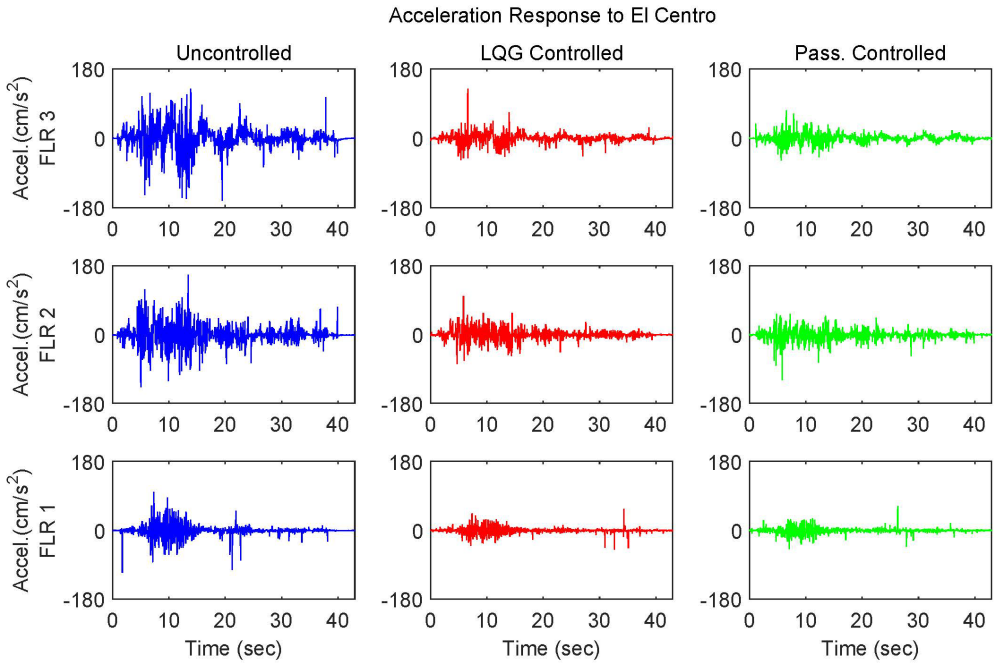

Figure 3.13: Story acceleration response time history

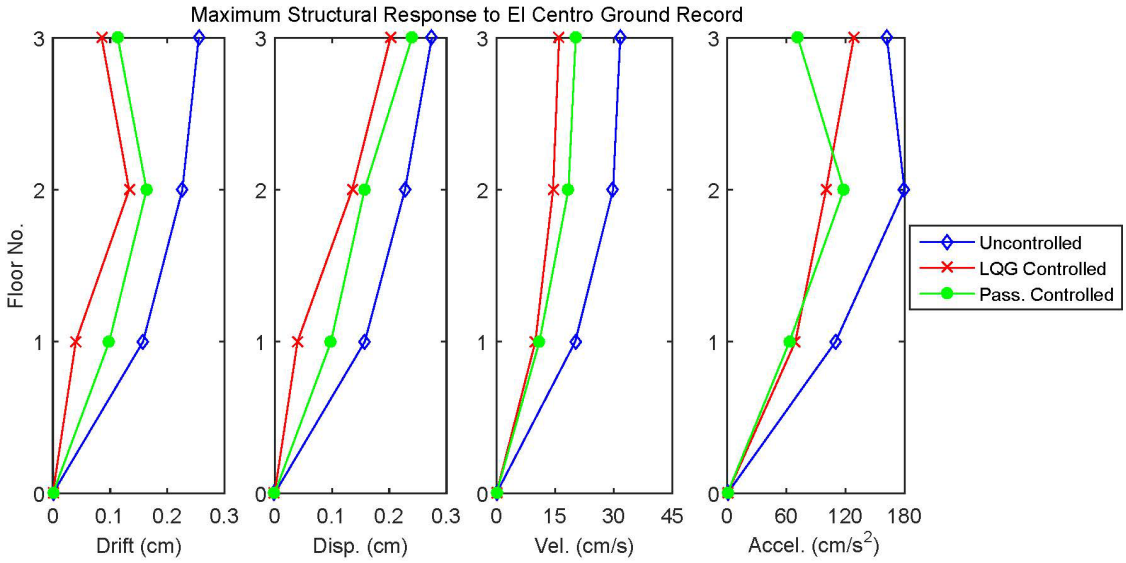

Figure 3.14: Maximum structural response metrics

A 67% combined reduction of peak total mechanical energy (*i.e.,* combined potential and kinetic energy) was observed for LQG control and 48% for passive control of the three degrees-of-freedom over the uncontrolled structure (both observed for the second floor). Figure 3.15 shows the corresponding time histories for the total mechanical energy.

Overall, the LQG controller performs slightly better with drift, displacement, and velocity reduction than using the MR-damper in a passive-on state. The two methods perform closely because they both are providing damping as the method for removing dynamics from the system. This characteristic of semi-active dampers has been fully examined by Ou and Li [109]. In a passive-on state, the damper located at the bottom of the structure caused locking of the lower level, which generated higher drifts in the upper levels compared to the LQG controller.

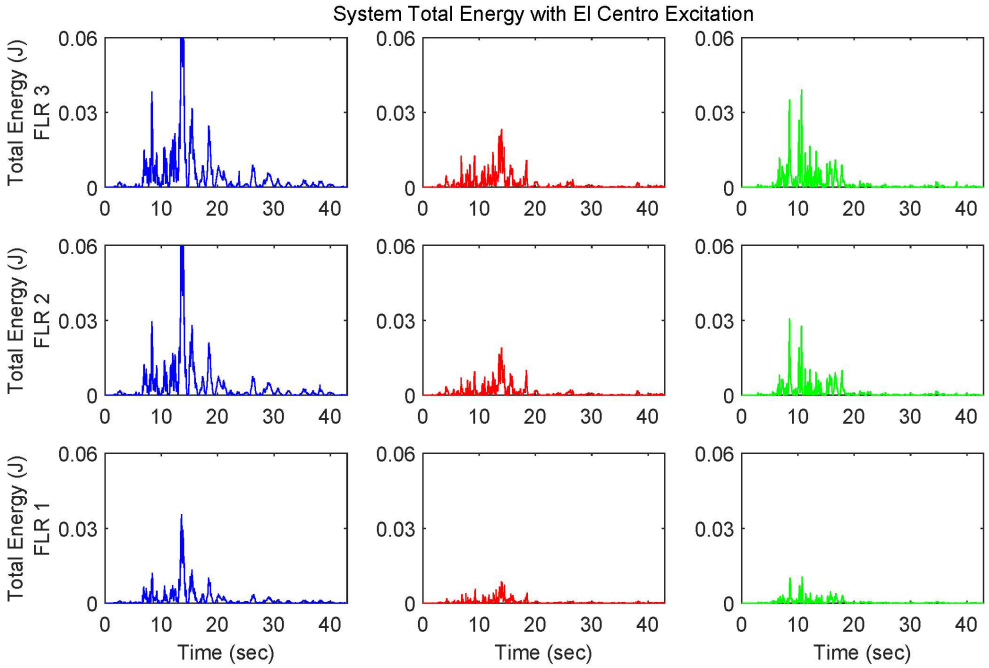

Figure 3.15: Total energy response El Centro time history

3.7 Conclusions

Semi-active damping devices are of particular interest in civil engineering, however, experimentation using these devices can be prohibitively expensive at full scale. In this chapter, to enable the development of a small-scale testbed for semi-active control tests for the case study in this chapter, and later use in this dissertation, a prototype low-force (0-10 N) double-ended piston-type magneto-rheological (MR) fluid extraction damper was investigated. MR-fluid extraction was chosen because literature has shown that this

form of actuation can provide a low-force range. For consistency with large-scale testbed and civil structural control applications, this prototype damper was designed to exhibit the same inherent complex nonlinear hysteretic behavior comparable to a full-scale commercially available MR-fluid damper. This chapter has shown that a small-scale device can be made to have comparable attributes to large-scale commercial devices. This force relationship differed from previously established forces because of the existence of effective friction, or shear reactions, between the MR-fluid and the metal foam. Also, the force range was smaller than other devices because the material properties were altered from those found in previous literature and seals were not needed to prevent fluid loss.

The MR-fluid extraction damper also demonstrated the ability to reduce inter-story drift of a three degree-of-freedom (DOF) testbed structure at the scale of interest. The damper was used to control a 3DOF structure using linear-quadratic-Gaussian (LQG) control strategies and a passive-on control strategy. The two forms of control performed with similar reductions acceleration and total energy. However, the LQG controller gave greater drift, displacement, and velocity reduction in the upper stories when compared to the passive-on MR-fluid damper.

4 Wireless Structural Control using Multi-Step TDMA Communication Patterning for Static Bandwidth Allocation[†]

As a structure increases in size, traditional wired, or tethered, data acquisition and structural control becomes prohibitively expensive [110]. Also, centralized computational systems can become inoperable due to degradation of system components or loss of power during a natural hazard. In the past decade, researchers have given significant attention to the use of wireless data acquisition for structural health monitoring and control applications in lieu of wired methods [1-4, 9, 15, 17-23]. Wireless control improves upon tethered control in terms of cost and its inherent decentralized nature can improve reliability during disasters, but it introduces issues related to centralizing data for computations. When communication is sparse or nonexistent between nodes, the centralized control scheme performs poorly. To compensate for slow data transmission rates and missed data, decentralized control for attenuation of undesired structural response has been shown to be comparable to fully centralized control [14, 15, 22, 23, 61, 67]. Decentralized control typically involves spatially dividing the wireless network into subnetworks. Each subnetwork can communicate on a different channel, communicate with different personal area network identifiers, or communicate out of the range of other subnetworks on the same channel or network identifier. In these subnetworks, embedded controllers and estimators are consistent and require only data from subnetwork units to perform the associated calculations. Thus, a large network can be broken down to eliminate the contention over communication channels. The control system is considered fully decentralized in the absence of data communication between units in the network. It has been shown, however, that additional information passed between nodes greatly improves the performance of estimators in fully decentralized networks and networks with unreliable communication [14, 64-66].

[†] The material contained in this chapter has been submitted to Structural Control and Health Monitoring.

Law, Swartz *et al.* [14] have shown that centralized control requires low frequency sampling to relay all sensor data throughout a wireless network due to communication bandwidth limitations. As the sampling and control frequency decreases to accommodate larger structures with more sensors, the complete lumped-mass modal behavior of the system can no longer be represented by acquired measurements. All things being equal, decentralized control decreases accuracy in state estimation, but has been shown to increase performance through increased control speed, which increases the observable bandwidth of modal frequencies in the structure [14]. Because reduced communication increases the control speed, a partial or fully-decentralized wireless controller can outperform a centralized controller that operates at a slower rate in large systems. Unlike fully-decentralized networks, partially-decentralized networks can sacrifice some communication, thus increasing speed, but pass more data to each unit in subnetworks. However, as the overall wireless network becomes too large, the ability to broadcast data quickly in large subgroups also diminishes.

Diverging from typical decentralization techniques to address congested bandwidth issues consistent with large networks, progress has been made to relay data between subnetworks with overlapping subgroups so that a single or multiple unit(s) communicate on multiple channels simultaneous [62, 63, 70], thereby increasing the spread of information throughout the wireless network and decreasing the number of subgroups overall. Expanding on this method, the issue of congested bandwidth has been examined by having each unit communicate on a different channel to the entire wireless network to maintain control speed without adding more transmission delays [72, 73]. This approach, and the previous approach with overlapping subgroups, is referred to as a frequency division multiple access (FDMA) protocol, or frequency-division multiplexing (FDM), which provides truly simultaneous data transmissions and reception without the use of transmission budgeting (*i.e.,* a time division multiple access, or TDMA protocol). This approach of layering transmissions to avoid time delays has previously been validated and used for control on a laboratory 3-story small-scale structure with multiple wireless units [72]. In the spirit of divergence from typical spatial decentralization, this chapter is

aimed toward developing another technique to maintain wireless control speed. However, this chapter presents a method for transmitting data to the entire wireless network over multiple time steps without spatially decentralizing (in which subgroups do not receive data from other subgroups in the network), or FDM with subgroups passing some data with units overlapping across multiple subgroups, or centralization with FDM to simultaneously transmit more data in a single time step. Staggered communication of data, or temporal decentralization, when properly executed can accomplish this objective.

In this chapter, it will be shown that the communication pattern employed for the wireless medium access control (MAC) protocol directly affects control performance when multiple time steps are needed to communicate sensor data. Optimized communication patterns can also minimize the state estimation errors exhibited by decentralized estimators. Updating state estimates with data from other nodes throughout the entire system is necessary to maintain estimation accuracy and to improve control performance. However, with high levels of contention in a wireless network, all data in a large network cannot be transmitted in a single time step. One feasible approach would be to choose the best (highest observability) sensors from the wireless network to transmit every time step. This is an approach that has been explored for structural health monitoring applications to manage transmissions in a single time step [111]. Additionally, the concept of accuracy with sensor placement has been demonstrated in [112], which shows how structural health requires information from throughout the structure to be strategically monitored. However, in wireless networks, cases arise where it is desired to utilize all deployed wireless units over multiple time steps (*e.g.,* to avoid highly-nonuniform battery depletion). The goal for this chapter is to show that a multi-step communication scheme can be found using methods developed for sensor placement that can yield control performance that is nearly equal to that of a fully-centralized case. In this chapter, each time step is treated as a new sensor placement problem where the observability of the system is maximized over all time steps as opposed to a single time step.

This chapter is organized as follows. First, chapter describes how the wireless state estimator can be manipulated to make use of an arbitrary subset of outputs (*i.e.,* estimator formulation for varying levels of sensor network decentralization). This chapter then shows how multi-step TDMA transmission groups are developed using sensor placement theory. Then, the subject of the verification case study, a 20 degree-of-freedom (DOF) structure, is presented. Simulation results demonstrate how various wireless communication schemes perform (*e.g.,* centralized/full communication, fully decentralized/no communication, and patterned/staggered communication). A 9-DOF small-scale experimental test-bed is used to validate the simulation results. Finally, the results are presented to compare estimator/control performance and show their dependency on communication topology for both the 20-DOF and 9-DOF case.

4.1 Control and Estimation with Communication Schemes

This chapter explores the development of wireless sensor groups that can be communicated over multiple time steps to show how passing information over time can maintain control speed and control performance. Multi-step sensor groups are generated using sensor placement theory. To build up to the main contribution of this chapter, this section first describes the standard theory for the continuous-time and discrete-time state-space representations of a multi-degree-of-freedom (MDOF) structure. This section then proceeds by showing the standard derivation of a linear-quadratic-Gaussian (LQG) controller (*i.e.,* a linear-quadratic regulator and Kalman estimator). To emphasize the contribution of this chapter, sensor placement theory is described for the development of reduced observability multi-step sensor groups and the associated impact to Kalman estimation.

4.1.1 State-space Representation of a Multi-Degree-of-freedom Structure

The following theory in this subsection is standard theory for representing the behavior of a MDOF structure in state-space form. The dynamic equilibrium of a linear, time-invariant (LTI) lumped-mass structure with n degrees of freedom is as follows:

$$\dot{\boldsymbol{z}}(t) = \boldsymbol{A}\boldsymbol{z}(t) + \boldsymbol{B}\boldsymbol{u}(t) + \boldsymbol{E}\ddot{x}_g(t) \tag{4.1}$$

where $\dot{\boldsymbol{z}}(\boldsymbol{t}) = \begin{Bmatrix} \boldsymbol{x} \\ \dot{\boldsymbol{x}} \end{Bmatrix} \in \mathbb{R}^{2n\times 1}$, $\boldsymbol{x} \in \mathbb{R}^{n\times 1}$ is the vector of floor displacements, $\dot{\boldsymbol{x}} \in \mathbb{R}^{n\times 1}$ is the vector of floor velocities, $\ddot{x}_g$ is the ground acceleration, and:

$$\boldsymbol{A} = \begin{bmatrix} 0 & I \\ -\boldsymbol{M}^{-1}\boldsymbol{K} & -\boldsymbol{M}^{-1}\boldsymbol{C}_d \end{bmatrix} \in \mathbb{R}^{2n\times 2\mathrm{n}} \tag{4.2}$$

$$\boldsymbol{B} = \begin{bmatrix} 0 \\ -\boldsymbol{M}^{-1}\boldsymbol{L} \end{bmatrix} \in \mathbb{R}^{2n\times m};\ \boldsymbol{E} = \begin{Bmatrix} 0 \\ -\boldsymbol{1} \end{Bmatrix} \in \mathbb{R}^{2n\times 1}$$

where $\boldsymbol{I}$ is the identity matrix, $\boldsymbol{M}$ is the diagonal mass matrix, $\boldsymbol{K}$ is the dynamic stiffness matrix, $\boldsymbol{C}_d$ is the damping matrix formed using modal/Rayleigh damping [113], $\boldsymbol{L} \in \mathbb{R}^{n\times m}$ is an actuator location matrix, and m is the number of actuators. In state-space form, measurements are represented as a linear sum of the observed state response, the influence of the control force attenuating the structural response, and the inertial acceleration:

$$\boldsymbol{y}(t) = \boldsymbol{C}\boldsymbol{z}(t) + \boldsymbol{D}\boldsymbol{u}(t) + \boldsymbol{F}\ddot{x}_g(t) \tag{4.3}$$

where $\boldsymbol{C} \in \mathbb{R}^{q\times 2n}$; $\boldsymbol{D} \in \mathbb{R}^{q\times m}$; and $\boldsymbol{F} \in \mathbb{R}^{q}$, with q being the number of observable states.

Using the zero-order hold approximation, the continuous-time state-space representation can be brought into the discrete-time domain for LTI systems as follows:

$$\boldsymbol{z}_{k+1} = \boldsymbol{\Phi}\boldsymbol{z}_k + \boldsymbol{\Gamma}\boldsymbol{u}_k + \boldsymbol{\Lambda}\ddot{\boldsymbol{x}}_{\boldsymbol{g}} \tag{4.4}$$

$$\boldsymbol{y}_k = \boldsymbol{C}\boldsymbol{z}_k + \boldsymbol{D}\boldsymbol{u}_k + \boldsymbol{F}\ddot{x}_g$$

where $\boldsymbol{\Phi} = e^{\boldsymbol{A}T_s} \in \mathbb{R}^{2n\times 2n}$; $\boldsymbol{\Gamma} = \int_0^{T_s}(e^{\boldsymbol{A}\tau}\boldsymbol{B})\,d\tau \in \mathbb{R}^{2n\times m}$; $\boldsymbol{\Lambda} = \int_0^{T_S} e^{\boldsymbol{A}\tau}\boldsymbol{E}\,d\tau \in \mathbb{R}^{2n\times 1}$; and T_s is the sampling time. The state-space model of the structure is used to derive the controller that minimizes vibrations due to seismic effects in the building.

4.1.2 Centralized Linear-quadratic-Gaussian Controllers

In LTI systems with complete state knowledge, the linear-quadratic regulator (LQR) provides an optimal control law that trades off control effort for performance. For a discrete-time state-space model, the discrete-time LQR control solution calculates a control force trajectory that minimizes the quadratic cost function, $\boldsymbol{J}$ [114].

$$\boldsymbol{J} = \sum_{k=0}^{\infty} \boldsymbol{z}_{\mathrm{k}}^{T} \boldsymbol{Q} \boldsymbol{z}_{\mathrm{k}} + \boldsymbol{u}^{T} \boldsymbol{R} \boldsymbol{u} \tag{4.5}$$

$\boldsymbol{Q}$ and $\boldsymbol{R}$ are used to set importance levels on output response and control effort, respectively [104]. Using $\boldsymbol{Q} = \boldsymbol{C}_{\mathrm{LQR}}{}^{T} \boldsymbol{C}_{\mathrm{LQR}}$ ($\boldsymbol{C}_{\mathrm{LQR}} \in \mathbb{R}^{2n \times 2n}$: the linear transform $\boldsymbol{z}_{\mathrm{k}} \longrightarrow \boldsymbol{y}_{\mathrm{k}}$) and $\boldsymbol{R} \in \mathbb{R}^{m \times m}$ is a symmetric positive definite matrix gives the control designer the ability to target the controller to minimize undesired vibrations in the structure. If the $\boldsymbol{C}_{\mathrm{LQR}}$ matrix, which regulates response using state variables, is configured as the identity matrix, $\boldsymbol{I}_{2nx2n}$, it minimizes both displacement and velocity for the state-space formulation in Eq. (4.4). Emphasizing specific values of either velocity or displacement can be accomplished by increasing the weight of the associated diagonal terms in $\boldsymbol{C}_{\mathrm{LQR}}$:

$$\boldsymbol{C}_{\mathrm{LQR}} = \boldsymbol{I}_{2nx2n} \boldsymbol{\Psi} \tag{4.6}$$

where $\boldsymbol{\Psi} = \begin{Bmatrix} \boldsymbol{\Psi}_d \\ \boldsymbol{\Psi}_v \end{Bmatrix}$ contains the weighting factors for each floors displacement, $\boldsymbol{\Psi}_d \in \mathbb{R}^{n \times 1}$, and velocity, $\boldsymbol{\Psi}_d \in \mathbb{R}^{n \times 1}$.

Minimization of interstory drift can be targeted as an approach that minimizes the possibility of collapse in a full-scale building. To assemble the $\boldsymbol{Q}$ matrix that penalizes drift and velocity, the following configuration of $\boldsymbol{C}_{\mathrm{LQR}}$ is used:

$$\boldsymbol{C}_{\mathrm{LQR}} = \begin{pmatrix} \boldsymbol{c}_{nxn} & \boldsymbol{0} \\ \boldsymbol{0} & \boldsymbol{I}_{nxn} \end{pmatrix} \boldsymbol{\Psi} \tag{4.7}$$

where:

$$\boldsymbol{c} = \begin{pmatrix} 1 & 0 & \cdots & 0 & 0 \\ -1 & 1 & & 0 & 0 \\ 0 & -1 & & 0 & 0 \\ \cdots & \vdots & \ddots & \vdots & \vdots \\ 0 & 0 & & 1 & 0 \\ 0 & 0 & \cdots & -1 & 1 \end{pmatrix} \tag{4.8}$$

To determine the control force trajectory two things are necessary: the control gain matrix, $\boldsymbol{G} \in \mathbb{R}^{m\times 2n}$, and the state vector, $\boldsymbol{z}_k \in \mathbb{R}^{2n\times 1}$. The control gain matrix is derived using the equation:

$$\boldsymbol{u}_k = -[[\boldsymbol{R} + \boldsymbol{\Gamma}^{\boldsymbol{T}}\boldsymbol{P}\boldsymbol{\Gamma}]^{-1}\boldsymbol{\Gamma}^{\boldsymbol{T}}\boldsymbol{P}\boldsymbol{\Phi}]\boldsymbol{z}_k = -\boldsymbol{G}\boldsymbol{z}_k \tag{4.9}$$

where $\boldsymbol{P} \in \mathbb{R}^{2n\times 2n}$ is the discrete Riccati matrix [114]:

$$\boldsymbol{P} = \boldsymbol{\Phi}^T[\boldsymbol{P} - \boldsymbol{P}\boldsymbol{\Gamma}[\boldsymbol{R} + \boldsymbol{\Gamma}^T\boldsymbol{P}\boldsymbol{\Gamma}]^{-1}\boldsymbol{\Gamma}^T\boldsymbol{P}]\boldsymbol{\Phi} + \boldsymbol{Q} \tag{4.10}$$

The state is known through direct measurement, or using an estimator. In civil structures, direct measurement of the state is problematic, necessitating the estimation of state values from sensor measurements. Eq. (4.9) requires accurate measurements or estimates of the entire state vector, $\boldsymbol{z}_{\mathrm{k}}$, in order to calculate optimal control forces. When direct measurements of state variables are not available, an estimator can be implemented to estimate the state vector, $\hat{\boldsymbol{z}}_k$ instead. The Kalman state estimator uses a series of measurements and assumes a base input of a zero-mean, broad-band excitation into the system, $\boldsymbol{w}_{\boldsymbol{k}}$, :

$$\boldsymbol{z}_{k+1} = \boldsymbol{\Phi}\boldsymbol{z}_k + \boldsymbol{\Gamma}\boldsymbol{u}_k + \boldsymbol{\Lambda}\boldsymbol{w}_k \tag{4.11}$$

It is assumed that the output measurements of the system are corrupted by white noise, $\boldsymbol{v}_k$:

$$\boldsymbol{y}_k = \boldsymbol{C}\boldsymbol{z}_k + \boldsymbol{D}\boldsymbol{u}_k + \boldsymbol{v}_k \tag{4.12}$$

The estimator first estimates the state, $\bar{\boldsymbol{z}}_k$, of the current time step, k, using the previous estimate, $\hat{\boldsymbol{z}}_{k-1}$, and the previous applied control force, $\boldsymbol{u}_{k-1}$:

$$\bar{\boldsymbol{z}}_k = \boldsymbol{\Phi}\hat{\boldsymbol{z}}_{k-1} + \boldsymbol{\Gamma}\boldsymbol{u}_{k-1} \tag{4.13}$$

Finally, the estimator can update this estimate using the current measurement error:

$$\hat{\boldsymbol{z}}_k = \bar{\boldsymbol{z}}_k + \boldsymbol{\mathcal{L}}_k(\boldsymbol{y}_k - \boldsymbol{C}\bar{\boldsymbol{z}}_k + \boldsymbol{D}\boldsymbol{u}_{k-1}) \tag{4.14}$$

where $\boldsymbol{\mathcal{L}}_k \in \mathbb{R}^{2n \times q}$ is the time varying estimator gain matrix.

The separation principle [115] allows the stable controller derived in Eqs. (4.5-4.10) to be combined with the stable estimator from Eqs. (4.11-4.14) into a stable estimator control network where both elements are derived separately.

4.1.3 Communication Bandwidth Limitations & Decentralization

This chapter utilizes the capabilities of the *Martlet* wireless sensing units [9]. Data transmission times for small packets (*i.e.,* a payload of one single-precision floating-point value) typically require transmission times of approximately 1.2-1.5 ms using this device. Conservatively focusing on the upper end of this range, a time division multiple access (TDMA) rule set was designed assuming 1.5 ms data transmission windows. Consequently, if a controller is set to update at a rate of 100 Hz, for example, only 5 units would have sufficient time to broadcast their data during each 10 ms time step (allowing 2.5 ms for computation of state estimates, control forces, and actuator command voltages). When faced with similar limitations, a number of strategies have been employed to accommodate networks that consist of more nodes than can be accommodated in a single time step.

One common approach, uses spatial decentralization of the total control network into local subnetworks, which reduces the observability within these subnetworks [14, 15, 116-118]. This approach uses different groups of data in different corresponding estimators. If data is intentionally not communicated from specific degrees of freedom (DOF), the rows associated with those degrees of freedom in the output matrix, $\boldsymbol{C}$ in Eq. (4.14), are zeroed, and similarly the corresponding rows from the feedthrough matrix, $\boldsymbol{D}$, are zeroed, when formulating the Kalman estimator matrices [15]. At the extreme end, a fully decentralized control scheme can be derived, when $n - 1$ rows of $\boldsymbol{C}$ are zeroed and

each wireless unit uses only locally measured data. The manipulation of the output and feedthrough matrices, to generate reduced observability estimators, is as follows:

$$\hat{\boldsymbol{z}}_k = \bar{\boldsymbol{z}}_k + \widehat{\boldsymbol{\mathcal{L}}}_{k_{ts}}(\boldsymbol{y}_k - \widehat{\boldsymbol{C}}_{ts}\bar{\boldsymbol{z}}_k - \widehat{\boldsymbol{D}}_{ts}\boldsymbol{u}_{k-1}) \tag{4.15}$$

$$\widehat{\boldsymbol{C}}_{ts} = (\boldsymbol{C}^T\boldsymbol{\Theta}_{ts})^T; \widehat{\boldsymbol{D}}_{ts} = (\boldsymbol{D}^T\boldsymbol{\Theta}_{ts})^T$$

where $\widehat{\boldsymbol{\mathcal{L}}}_{k_{ts}}$ is the time varying estimator gain matrix unique to each sensor time step group output matrix, $\widehat{\boldsymbol{C}}_{ts}$, where the rows of the original output matrix, $\boldsymbol{C}$, are toggled (*i.e.,* multiplied by 1 or 0) using:

$$\boldsymbol{\Theta}_{ts} = \sum_{i=1}^{n} \boldsymbol{\Upsilon}_i g_{ts} \boldsymbol{\gamma}_i \tag{4.16}$$

which is also known as the diagonalization of a column vector, where $\boldsymbol{\Upsilon} \in \mathbb{R}^{n\times n\times n}$ is a tensor where the diagonal entry $[i,i]$ of each matrix $\boldsymbol{\Upsilon}_i \in \mathbb{R}^{n\times n}$ is 1 and the other entries are 0, $\boldsymbol{\gamma} \in \mathbb{R}^{nxn}$ is a matrix where the i^{th} entry for each row $\boldsymbol{\gamma}_i \in \mathbb{R}^{1\times n}$ is 1 and the other entries are 0, and $g_{ts} \in \mathbb{R}^{n\times 1}$ is a column vector populated with 1's and 0's to identify which sensors are transmitting in a subnetwork. Eq. (4.15) uses $\widehat{\boldsymbol{\mathcal{L}}}_{k_{ts}}$, $\widehat{\boldsymbol{C}}_{ts}$, and $\widehat{\boldsymbol{D}}_{ts}$ matrices of the same size as $\boldsymbol{\mathcal{L}}_k$, $\boldsymbol{C}$, and $\boldsymbol{D}$ but contain 0's that negate the effect of each row corresponding to a non-observable state of a particular time step.

Spatial decentralization, whether fully decentralized or with sub-network communication, remains a static process, *i.e.,* each subgroup of units only listens to and communicates on a specific channel or channels (*e.g.,* frequency division multiple access or FDMA). Estimation of state variables can be further improved if there is overlapping communication of between subnetworks (*e.g.,* a single unit may communicate on two channels). Sharing state vectors and measurements between channels is a form of distributed control and has been used by Wang, Law *et al.* [119] and Qu, Huo *et al.* [70] to improve control performance with higher accuracy estimation. Dynamic subnetworking can better still integrate measurements from subnetworks.

To integrate data from units outside of the static subnetworks that are common within

spatially decentralized networks, this chapter will use temporal decentralization, defining sub-network communication groups that have staggered transmissions over multiple time steps. The main advantage of temporal decentralization over spatial decentralization is that all units in the network are listening to each staggered communication group and all units are able to communicate their data over time to the full network, just not at every time step. Temporal decentralization relies on using a different reduced observability estimator, defined by Eq. (4.13) and Eq. (4.15), for each time step that will accommodate the pattern of the units that are permitted to transmit on that step.

On its face, temporal decentralization appears to create an asynchronous, or multi-rate control network, with control steps taking place at every time step, but with measurements from individual sensors becoming available at a slower rate. Methods for addressing slow data transmissions and arrivals have been investigated and data fusion techniques, which account for lost data and integrate old or slow with current measurements, have been used to aid estimator and controller performance [10, 65, 67, 120]. However, unlike like an old data integration problem, temporal decentralization uses the estimated state vector, updated every time step, and a measurement update, which is also acquired every time step (as opposed to making use of old transmitted data that is delayed to a later time step).

Decentralization does have some limitations that must be considered. With decentralization, whether spatial or temporal, as the size of the subnetwork sensor group decreases (due to increases in control frequency or transmission delay times), the observability of the estimators decreases, negatively impacting control performance. In the case of temporal decentralization, a larger amount of on-board memory is necessary to store the complete set of estimator matrices needed for each communication group. Finally, sensor topology must be considered when the subnetwork groups are formed, because it affects control performance. The remainder of this chapter will focus on investigating these effects and will utilize sensor placement techniques as a rational means to form subnetwork groups.

4.1.4 Sensor Placement Techniques for Temporal Decentralization

Sensor placement approaches generally focus on maximizing observability [121]. A linear system is observable if any given state can be determined by the output of the system at the same instant in time [114]. Meeting the minimum requirement for observability is typically not a challenge for lumped-mass shear building systems, however observability can function as a measure of how closely system outputs are related to one another. Different outputs and combinations of outputs will vary in their level of correlation to the states of the building in a manner that can be predicted by the modal properties of the system. Generally, an LTI system is only observable if the observability Gramian, $\boldsymbol{W}_O$, is regular (*i.e.,* for some power, p, $\boldsymbol{W}_O^p$ has positive entries).

$$\boldsymbol{W}_O(t_f) = \int_0^{t_f} e^{\boldsymbol{A}^T\tau}\boldsymbol{C}^T\boldsymbol{C}e^{\boldsymbol{A}\tau}d\tau \tag{4.17}$$

Although the rank of the full $\boldsymbol{W}_O$ matrix determines if a system is observable, the relative size of $\boldsymbol{W}_O$ for a given $\boldsymbol{C}$ matrix gives a measure of the relative observability of the corresponding sensor group. It is apparent that the best output matrix, $\boldsymbol{C}$, uses data measured from each degree of freedom. Due to limitations in communication speed, it is infeasible to use all sensors in the network in a single time step. To overcome this challenge, wireless communication can be treated like a series of sensor placement problem. Several methods using the observability Gramian matrix have been summarized by Singh and Hahn [121] that provide meaningful metrics for determining strategic sensor locations. For this chapter specifically, the $trace$, or diagonal summation, of the inverse of the observability Gramian matrix was chosen, which is the second observability metric discussed by Singh and Hahn [121]:

$$\mu = \frac{2n}{trace(\boldsymbol{W}_0^{-1})} \tag{4.18}$$

This metric is used to rate the various patterns of sensors that could exist in the output matrix, $\boldsymbol{C}$. For every new combination of sensors, the metric changes, and a greater μ value represents a higher degree of observability, yielding, among other things, higher

signal-to-noise ratios for a given state vector realization. Even though, for instance, a 20-DOF structure might be able to affordably employ 20 wireless sensors, the sensor placement technique can address the limited ability of the network to transmit or observe all wireless sensors in a given time step.

For a single timestep, or for identifying the best group of units of a limited size, ℓ_v, the maximum observability group can be found by identifying the largest observability Gramian metric from $\frac{n!}{\ell_v!(n-\ell_v)!}$ combinations of ℓ_v sensors. If a different group of sensors is chosen for each time step (*e.g.,* to ensure uniform battery usage of the wireless sensor nodes), the state estimators for each time step would be naturally less efficient than the previously mentioned single best subset of sensors. To optimize the total observability over all time steps, the following objective function can be used:

$$Z = \max \sum_{ts}^{\eta} \mu_{ts} \tag{4.19}$$

where μ_{ts} is the observability Gramian for each possible subset of units that is defined by manipulating the entries in $\boldsymbol{C}$. The subscript ts represents a time step, and η represents the total number of subsets required to transmit data from each sensor. With the new set of observability metrics, μ_{ts}, an efficient pattern can be determined that can allow all time steps to exhibit maximum potential for observability in staggered communication. This optimization takes the form of a mixed-integer optimization problem. Such a problem can be solved by wide array number of search algorithms. In this case a genetic algorithm is employed. The integers involved are the indices for the rows of $\boldsymbol{C}$, which correspond to the sensors on the structure. If a given sensor is chosen for the communication pattern, the respective row of $\boldsymbol{C}$ is multiplied by 1, if not, the row is multiplied by 0. The manipulation process for the output matrix can be described as follows:

$$\overline{\boldsymbol{W}}_O = \int_0^{t_f} e^{\boldsymbol{A}^T\tau} \boldsymbol{C}^T \boldsymbol{\Theta}_{ts} \boldsymbol{C} e^{\boldsymbol{A}\tau} d\tau \tag{4.20}$$

Once a combination of sensors is chosen by the genetic algorithm to form the next

generation of subsets for fulfilling the objective function, the Gramian metrics, μ_{ts}, are calculated using $\overline{\boldsymbol{W}}_O$. This process is then repeated until the objective function, Z, is maximized. Meanwhile, additional constraints must be met. These constraints ensure uniqueness between subsets of units (*i.e.,* sensors are not reused to transmit data until each other sensor is able to transmit), and that each unit within each subset must be unique (*i.e.,* data from the same sensor should not be transmitted more than once in the same time step).

In this chapter, the built-in *MATLAB* genetic algorithm function, *ga()*, was used. This function optimizes a fitness function, Z, to solve a mixed-integer optimization problem. In the genetic algorithm function, an initial population is provided by the author as the basis of breeding and forming new generations of sensor subsets. Limitations of this function include the inability to provide a mutation rate for integer programming problems and the inability to perform crossover techniques in an integer programming problem. Therefore, the genetic algorithm is given a constraint function that maintains the uniqueness of every generation (which is desired). The initial population and each following generation contains the number of subsets for the communication network.

4.2 Methods

For this chapter, both a numerical simulation and an experimental validation are performed for the temporally decentralized wireless structural control network. The numerical simulation employs a full-scale structural model and modeled wireless communication, which are described in the following subsection. The validation for the methodology in this chapter uses an in-house small-scale structure and *Martlet* wireless sensing units to perform wireless structural control and is compared to its own computer simulation. In the numerical simulation of a full-scale structure, the simulation of the small-scale structure, and the experimental validation, a control rate of 100 Hz is used and bandwidth for the temporally decentralized communication subnetworks is divided over 7.5 ms each time step, leaving 2.5 ms for computation.

4.2.1 Numerical Simulation Study

To demonstrate the importance of communication topology in wireless estimation and control for large networks, a simulation was performed that consists of a 20 degree-of-freedom (DOF) shear structure (*i.e.,* a 20-story building), based on the second generation ASCE benchmark structure properties found in [122]. The model was scaled down with stiffness and mass equivalent to a single bay per floor. This simplification was made to better illustrate the dependence on network topology, independent from the effects of structural complexity. The modeled structure is excited by the simulated El Centro ground-motion record (Imperial Valley 5/19/40 El Centro Array #9, 180 – USGS Station 117 North-South) scaled to a peak ground acceleration of 1.0 $\frac{m}{s^2}$. The simulation uses the average acceleration method for Newmark integration, with $\beta = \frac{1}{4}$ and $\gamma = \frac{1}{2}$ [113]. The simulated structure is configured such that each floor has an available actuator that can provide up to 20 kN of control force with ideal control force output (*i.e.,* the actuator force at all steps equals the desired force calculated by LQR), along with an accelerometer for each floor that provides measurements to the Kalman estimator. The actuator location and state penalty matrices were selected to be the same for all control cases. This selection was made for consistency and to maintain stability of the decentralized controller. The system properties (*i.e.,* the stiffness and mass) are summarized in Table 4.1. A schematic of the 20-story building, with story heights of 4 m, showing the actuator and wireless sensor/accelerometer configuration is provided in Figure 4.1.

Table 4.1: Parameters of the 20-DOF structure

Floor	***Mass (kg)***	***Stiffness ($\frac{kN}{m}$)***	***Damping ($kN \cdot \frac{s}{m}$)***
20	$4.8x10^4$	$2.5x10^6$	$7.8x10^4$
19	$6x10^4$	$2.5x10^6$	$7.8x10^4$
⋮	⋮	⋮	⋮
1	$6x10^4$	$2.5x10^6$	$7.8x10^4$

Modal Frequencies (Hz)									
0.79	2.4	4.0	5.6	7.1	8.6	10.1	11.4	12.7	13.9
15.1	16.1	17.1	17.9	18.7	19.3	19.9	20.3	20.6	20.8

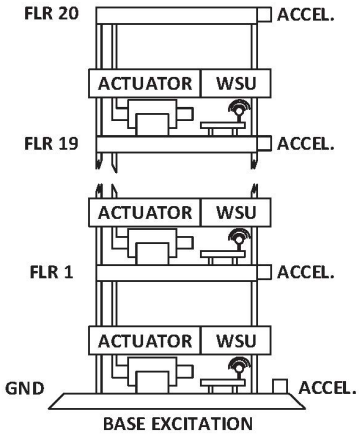

Figure 4.1: 20-DOF structure schematic

This simulation models all possible combinations of wirelessly transmitted data by accessing a library of pre-calculated Kalman estimators, emulating the on-board access to local memory for wireless units. The effectiveness of the algorithm is measured using 4 metrics: drift, $\boldsymbol{x}_d = \boldsymbol{x}_{i+1} - \boldsymbol{x}_i$, which describes the position of structural floors with the floor immediately below itself; control effort, $f_{ce} = \sqrt{\frac{\sum_{k=1}^{t} f_k^2}{t}}$, which is the root-mean-square (RMS) value for the control force time history, f_k, used to minimize response over time, t; control efficiency, $eff = \boldsymbol{x}_d\, f_{ec}$, where this is a measure of how well the control force achieved the drift reduction of a floor; and estimation error, $e = \sqrt{\frac{\sum_{k=1}^{t} (\hat{\boldsymbol{z}}_k - \boldsymbol{z}_k)^2}{t}}$ (for displacement and velocity), which is the root-mean-square error (RMSE) between the Kalman estimation of state variables and the Newmark-Beta derived state response.

4.2.2 Staggered Estimation and Control

Using the conservative transmission time for *Martlet* units, the 7.5 ms bandwidth for data communication can accommodate 5 sensor transmissions. Therefore, for the 20-DOF wireless network communicates over 4 time steps in the temporal decentralization scheme. A genetic algorithm was used to find an efficient communication pattern by maximizing μ over all 4 time steps. This staggered communication pattern was then used

in a control scheme after deriving the partially decentralized, or reduced observability Kalman estimators associated with each unique subset of units.

To compare the performance of this patterning scheme to that of other possible control schemes, other more naïve sensor combinations were also used to perform state estimation and control for comparison. As such, performance is also shown for a staggered communication pattern that has an uneven, or non-uniform Gramian-based set of subsets (*i.e.,* a scheme that forms the highest μ set of 5 sensors, followed by the second highest μ set of remaining sensors, and so forth). In addition, naïve topologies based on dividing the floors into quadrants, or evenly spacing units are also investigated. A visual representation of the four different communication patterns is shown in Figure 4.2. Finally, all of the staggered communication controllers were compared to two benchmark cases: fully-centralized and fully-decentralized control. The results are plotted and recorded in the results section utilizing performances measurements including: root-mean-square (RMS) error between state estimation and modeled structural. Drift reduction and control effort (represented by the RMS value of the control force time-history) are also compared between all schemes.

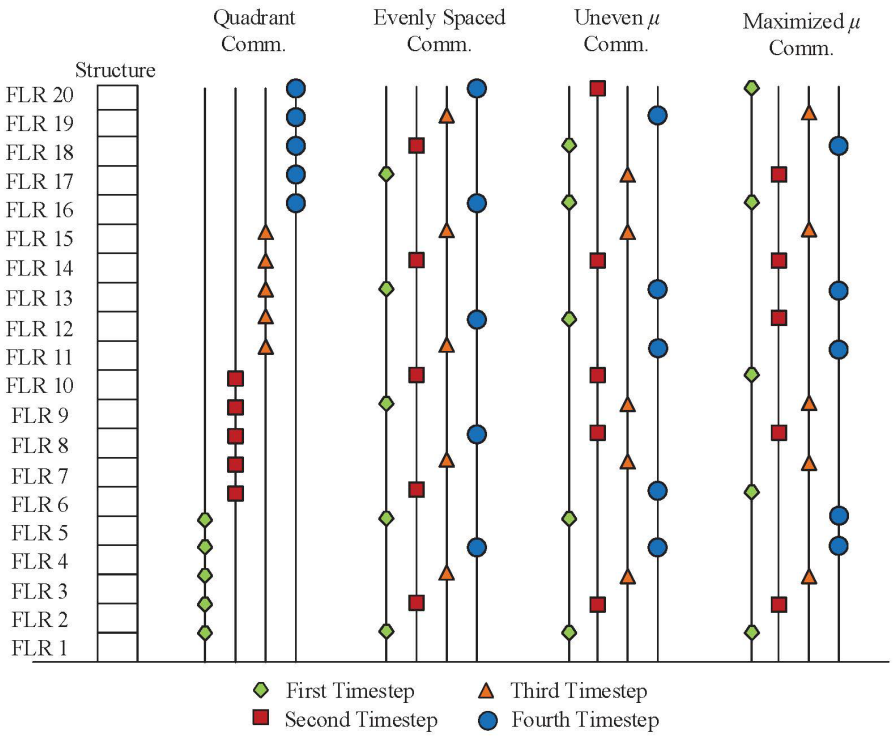

Figure 4.2: Logical and Gramian-based communication groups

4.2.3 Experimental Validation Study

Validation is accomplished using an experimental test-bed utilizing *Martlet* wireless sensing/actuation units. The test-bed uses a 9-DOF small-scale wood and aluminum shear structure that is excited by the synthesized El Centro ground-record on a Quanser Shake Table II also scaled to a peak ground acceleration of 1.0 $\frac{m}{s^2}$. A simulated 9-DOF structure is also used to compare simulation and experimental results for estimation and control. The structure in both cases employs three small-scale semi-active magneto-rheological (MR) fluid actuators that were developed in [123]. The three actuators were placed strategically using actuator placement theory on floors 1, 5, and 9. The same metric in Eq. (4.18) can be used to assess the degree of controllability given a particular configuration of actuator groups [114, 124, 125].

Each floor of the test structure, including the shake-table ground floor, has two accelerometers: one configured as a single-ended accelerometer to be used as the control

system output by a wireless sensing unit and the other which is used for verification purposes interfaces into a National Instruments (NI) DAQ NI PXIe-1071 data acquisition chassis running LabVIEW. Additionally, for validation purposes, each floor is monitored using a linear placement transducer (LPT), mounted on an external stationary reference post, that measures floor displacement through the NI PXI, but not used by the wireless sensors. The single-ended accelerometers are used within the wireless units to perform embedded Kalman state estimation. The system properties of the experimental test-bed, which are also reflected in the simulation, are summarized in Table 4.2 and the structural configuration is visually represented in Figure 4.3. The wireless units are also used to leverage control force in the MR-fluid dampers by commanding operational amplifiers after calculating the required voltage necessary to produce the desired control force.

Table 4.2: Parameters for 9-DOF Structure

Floor	*Mass (kg)*	*Stiffness* ($\frac{N}{m}$)	*Damping* ($N \cdot \frac{s}{m}$)	*Mode*	*Modal Frequency (Hz)*
9	1.38	3700	11	9	24.4
8	2.68	9000	11	8	19.5
7	1.06	5600	11	7	17.9
6	1.06	9900	11	6	13.8
5	1.38	4300	11	5	11.5
4	2.68	4200	11	4	9.4
3	1.06	3600	11	3	7.2
2	1.06	4700	11	2	4.4
1	1.38	2500	11	1	1.3

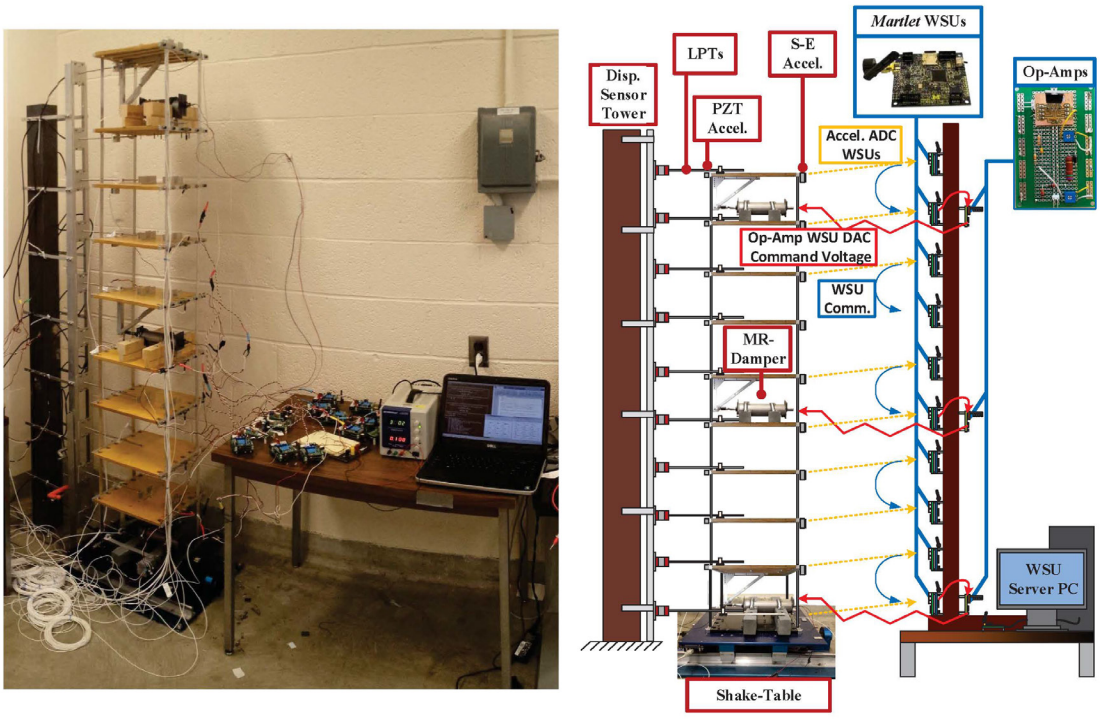

Figure 4.3: Small-scale 9-DOF testbed and schematic

In the same manner, consistent with the simulated 20-DOF structure, a genetic algorithm was used to maximize the observability of each time step for the 9-DOF experimental validation. In this chapter 10 wireless units all collect data from the aforementioned single-ended accelerometers. For performing the necessary state estimation, the ground floor wireless unit has to transmit its data to all units every time step. A control time step was chosen to be 10 ms to reasonably capture excitation frequencies within the range of modal frequencies of the 9-DOF structure. Additionally, 10 ms was chosen for the experimental validation to be consistent with the methodology used in the simulated 20-DOF case study. In 10 ms only a few units can transmit over an IEEE 802.15.4 standard implementation. It was decided for the experimental validation portion of this chapter that only 4 units could transmit per time step, one being the ground unit, to have an equal number of sensors transmitting per time step. Correspondingly, three time steps are required to cover all wireless units. For each time step a different state estimator is required to incorporate the incoming sensor data. All estimator matrices and control gains

are calculated based on a simulated 9-DOF structure that predicts structural behavior based on the structural parameters in Table 4.2.

The simulation uses the actual achieved shake-table acceleration signal recorded during the experimental test to verify the accuracy of the simulation. After the model was calibrated to match the recorded behavior of the uncontrolled experimental test-bed, simulated control tests were performed. To show centralization, control, and topology effects on performance, multiple scenarios were run including: a theoretical fully-centralized control at 100 Hz control speed; fully-decentralized control at 100 Hz; the Gramian-based control at 100 Hz; and a reduced-speed centralized control scheme at 50 Hz; and less sophisticated communication/control methods. In addition, the 9-DOF testbed validation was performed using a reduced-speed centralized control, decentralized control scheme, and an uncontrolled case. The theoretical centralized control at 100 Hz was not possible to perform experimentally due to the inability to transmit all network data in a single 10 ms time step, hence the use of the reduced-speed case. The estimators for each type of test are stored on-board prior to control testing.

4.3 Results

Sensor placement theory was used to form a set of sensor groups, over multiple time steps, which provided consistently high-quality output information while still utilizing all network sensors. A search algorithm, making use of the built-in *MATLAB* genetic algorithm function, was used to meet these constraints for two case studies: 1) a simulated 20 degree-of-freedom structure (DOF) and 2) a simulation with parameters matching the experimental 9-DOF small-scale laboratory test-bed. The most efficient and uniform multi-step communication group involving Gramian metrics, μ_{ts}, was able to attenuate seismically induced disturbances, specifically inter-story drift, comparably to centralized control, more so than other multi-step communication schemes. This staggered communication pattern outperformed decentralized control in drift reduction for both the 20-DOF and 9-DOF case. This section is laid out to first show the response reduction in the simulated 20-DOF structure using a standard LQG controller. Then each of the multi-

step communication schemes developed, to test against the sensor placement-based communication scheme, are used within the same control setup to compare how each scheme affected control performance and estimator efficiency.

4.3.1 Simulated 20 Degree-of-Freedom Structure Results

To simply demonstrate the performance of the selected structural control algorithm, Figure 4.4 shows the controlled and uncontrolled response of the simulated 20 degree-of-freedom structure. Figure 4.4 includes only three representative time-history simulated responses, at floors 1, 10, and 20 for legibility, showing the effectiveness of the controller for drift reduction.

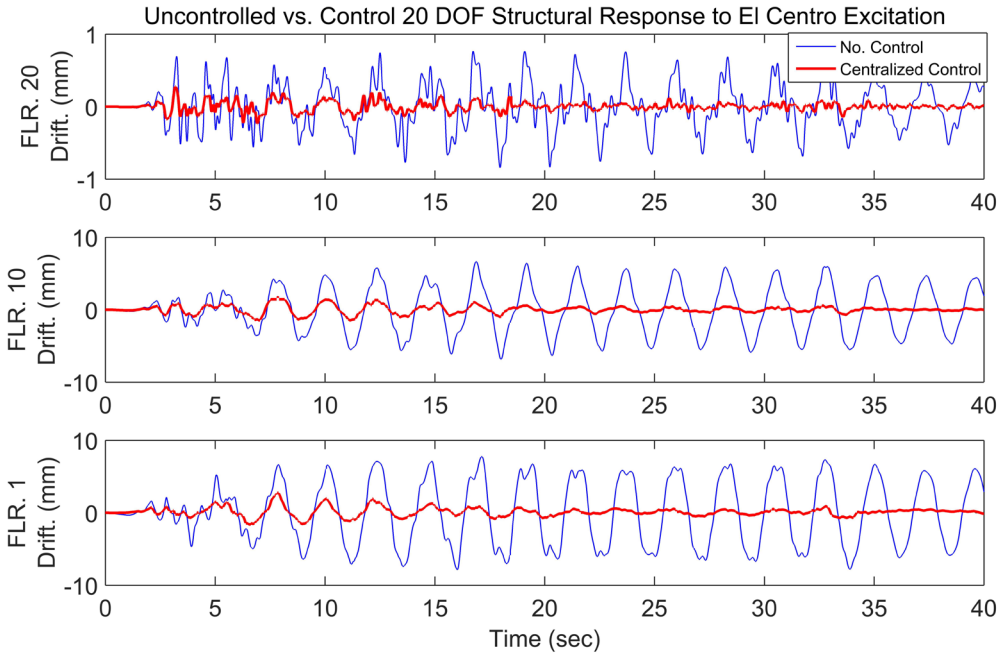

Figure 4.4: Simulated controlled and uncontrolled acceleration response of the 20-DOF structure

To show the effect on control efficiency based on centralization, Figure 5 provides the decentralized and centralized control performances benchmarked against the uncontrolled structural response. This figure shows maximum drift for the uncontrolled structure and that decentralized control is less effective than centralized control in

minimizing drift. The root-mean-square (RMS) force for each case is shown in the second subplot in Figure 4.5. Centralized control yielded RMS forces ranging from 0.5 kN from the 20th floor actuator to 6.5 kN from the 1st floor actuator, whereas decentralized control had an RMS force range from 0.6 to 8 kN, in both cases the control forces used tend to be largest near the base of the structure. Overall, decentralized control uses more control effort (kN) to achieve a lower level of drift reduction than centralized control can achieve, which is evident in the higher values seen in the efficiency metric. The increased control effort required by decentralized control may be explained by the increased estimation error, depicted in the right-hand side of Figure 4.5.

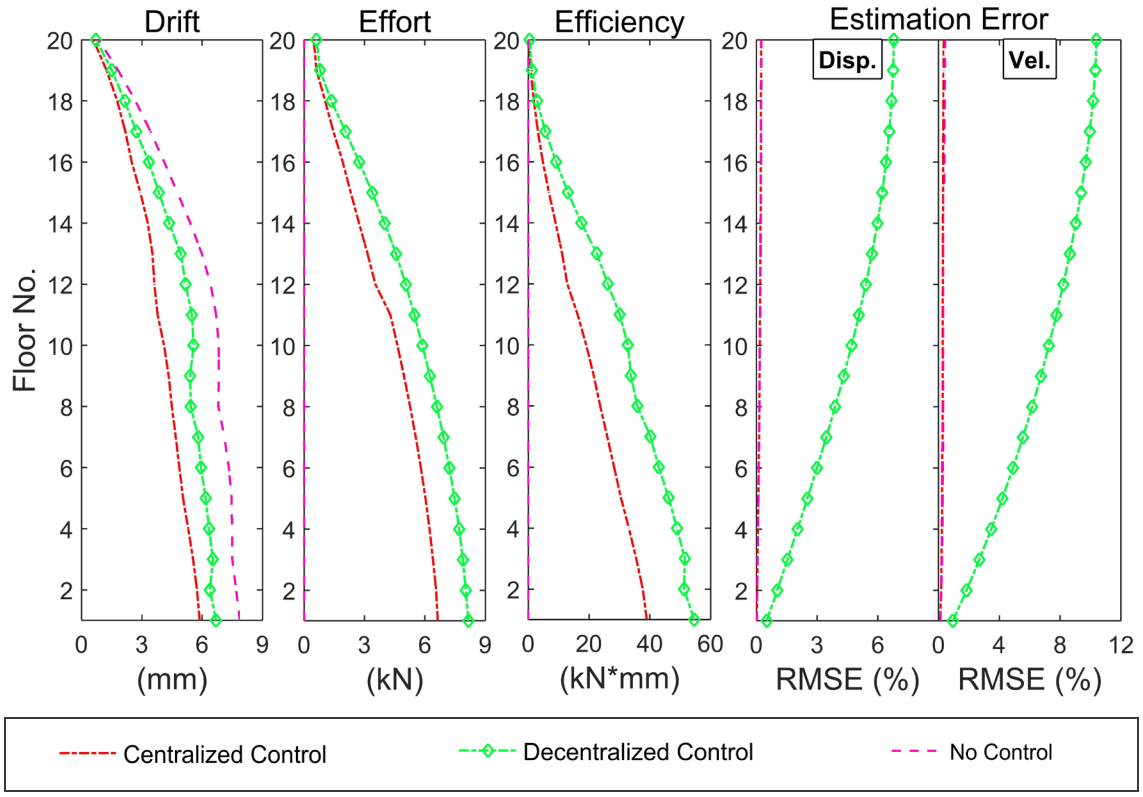

Figure 4.5: 20-DOF centralization effects on drift reduction, control effort and efficiency, and esimation error

Figure 4.6 shows the impact of communication topology on the performance of the control system in terms of drift reduction, control effort, efficiency, and estimation error. Differences between these cases can be ascribed to estimator performance. Shown in

Figure 4.6, all of the communication schemes have an estimator root-mean-square error (RMSE) that is less than 7% in displacement estimation for all floors and less than 3% in velocity estimation for each floor (except the fully decentralized case). For all cases, the error trends upward for estimating upper DOF states. The communication topology used affects the estimation error for the various staggered communication cases. Decentralized estimation exhibits the largest estimation error, with a maximum displacement estimation RMSE of 6.8% and velocity estimation RMSE of 10.5%. Centralized estimation performs the best, with maximum RMSE values of 0.2% and 0.4% for displacement and velocity estimation, respectively. The staggered communication approaches yield results that fall between the centralized and decentralized cases with the maximized Gramian (maximized μ) approach nearly equaling that of the centralized controller.

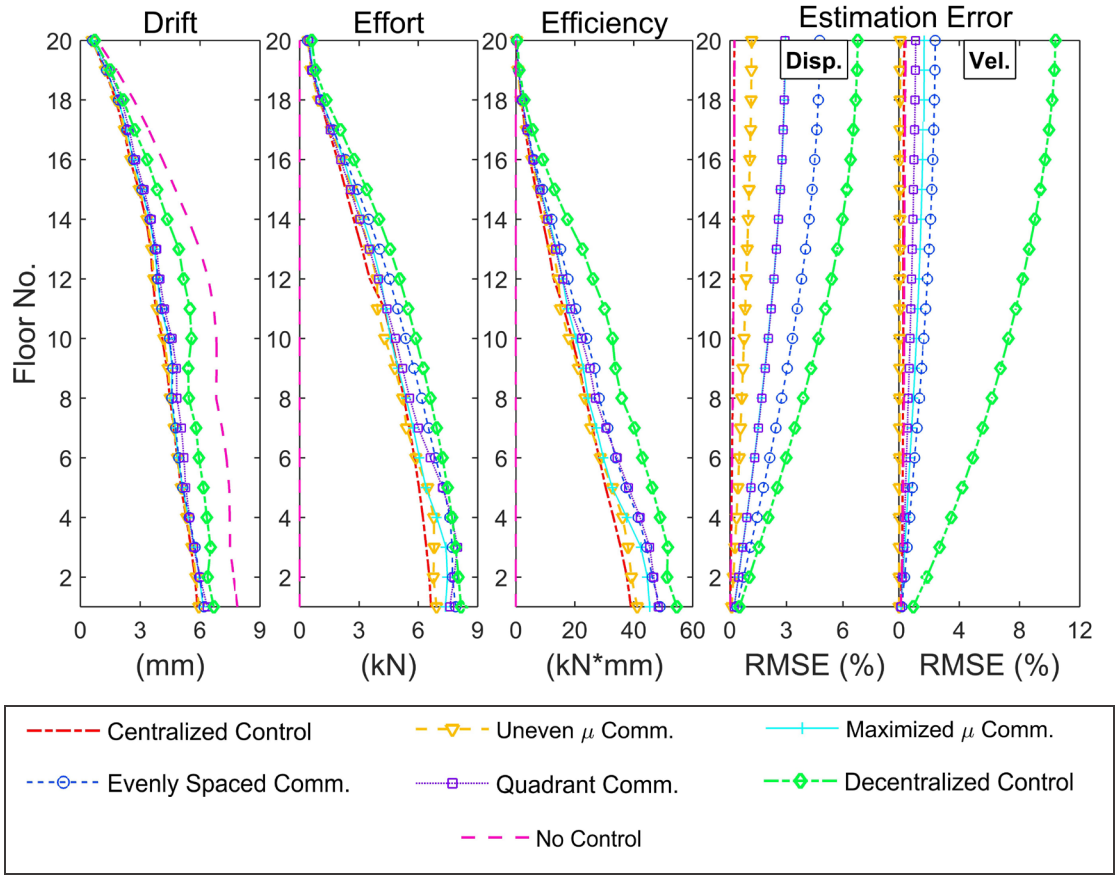

Figure 4.6: 20-DOF topology effects on drift reduction, control effor and efficiency, and estimation error

The uniform Gramian-based scheme has maximum RMSE values of 1.5% and 0.4%, and the remainder range from 3-5% and 1-3% in displacement and velocity estimation respectively. Figure 4.6 also shows that as RMSE decreases, associated with the better performing communication schemes, the control efficiency is better and the control effort is lowered. Of the staggered control approaches, the Gramian-based communication patterns used the lowest levels of RMS control force to attenuate structural response. The less sophisticated cases (*i.e.,* the evenly spaced, quadrants, and uneven/non-uniform Gramian patterns), use control force less efficiently. The less sophisticated cases and the decentralized case are overcompensating in force due to larger state estimate errors. Using all four metrics, the uniform Gramian pattern improves upon the decentralized scheme in estimation and control and behaves closely to the centralized case and the single group of best placed sensors.

4.3.2 Validation using a 9 Degree-of-Freedom Experimental Test-bed

The 9-DOF structure was used to validate the performance of temporal decentralization in an embedded wireless environment for structural control applications. The 9-DOF structural parameters were used to develop a simulation, in which simulated embedded estimation and control processes were performed. Prior to comparing control performance in simulation and experimentation, the uncontrolled structural response was measured and the accuracy of the modeled 9-DOF structure was assessed. The experimental uncontrolled acceleration response time-history to El Centro ground-record excitation and the Newmark method simulated response are shown in Figure 4.7 for floors 1, 5, and 9 of the 9-DOF structure. Overall, the modeled response of the 9-DOF structure was highly accurate, which enabled the simulated wireless communication and embedded processes.

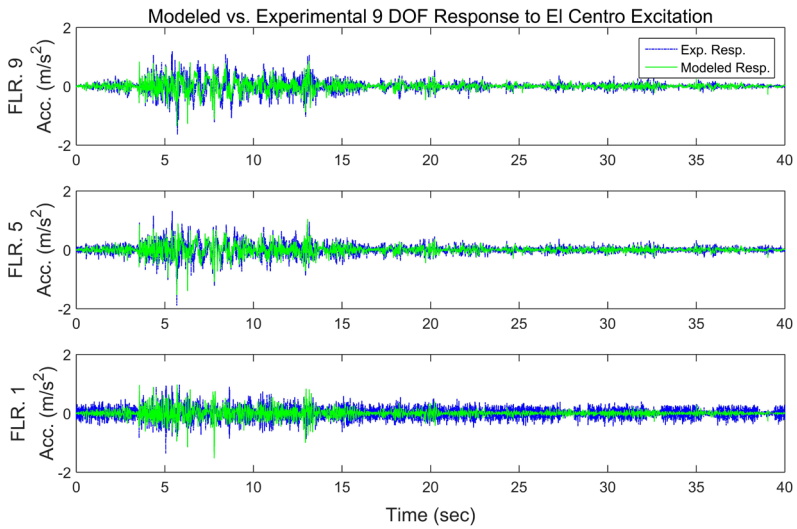

Figure 4.7: Numerical model and experimental testbed response to El Centro ground-record excitation

Simulation and experimental results for drift reduction are compared in Figure 4.8 for centralized and decentralized control benchmarked against the uncontrolled case. Figure 4.8 uses the drift, effort, efficiency, and estimation error metrics that were used in the 20-DOF simulation results (tabulated values for Figure 4.8 are shown in Tables 4.3-4.7). Due to bandwidth limitation, communication of all 10 wireless units (9 floor units and 1 ground unit) for the centralized case was not possible at 100 Hz. Therefore, simulated centralized and experimental validation were performed at 50 Hz (the fastest achievable control speed using 10 Marlet units). As anticipated, the centralized case outperformed the decentralized case in drift reduction. Drift values ranged from 0.3-1.6 mm for centralized control, 0.8-2.2 mm for decentralized control and 1.5-4.0 mm in the uncontrolled case with El Centro excitation. The efficiency metric shows that decentralized control overcompensates with control effort for erroneous state estimation. Decentralized control used RMS forces ranging from 0.8 N (9^{th} floor actuator) to 3.5 N (1^{st} floor actuator) for the experimental and simulated control test to reduce the drift. The centralized control schemes used an RMS force range of 0.5-2.7 N.

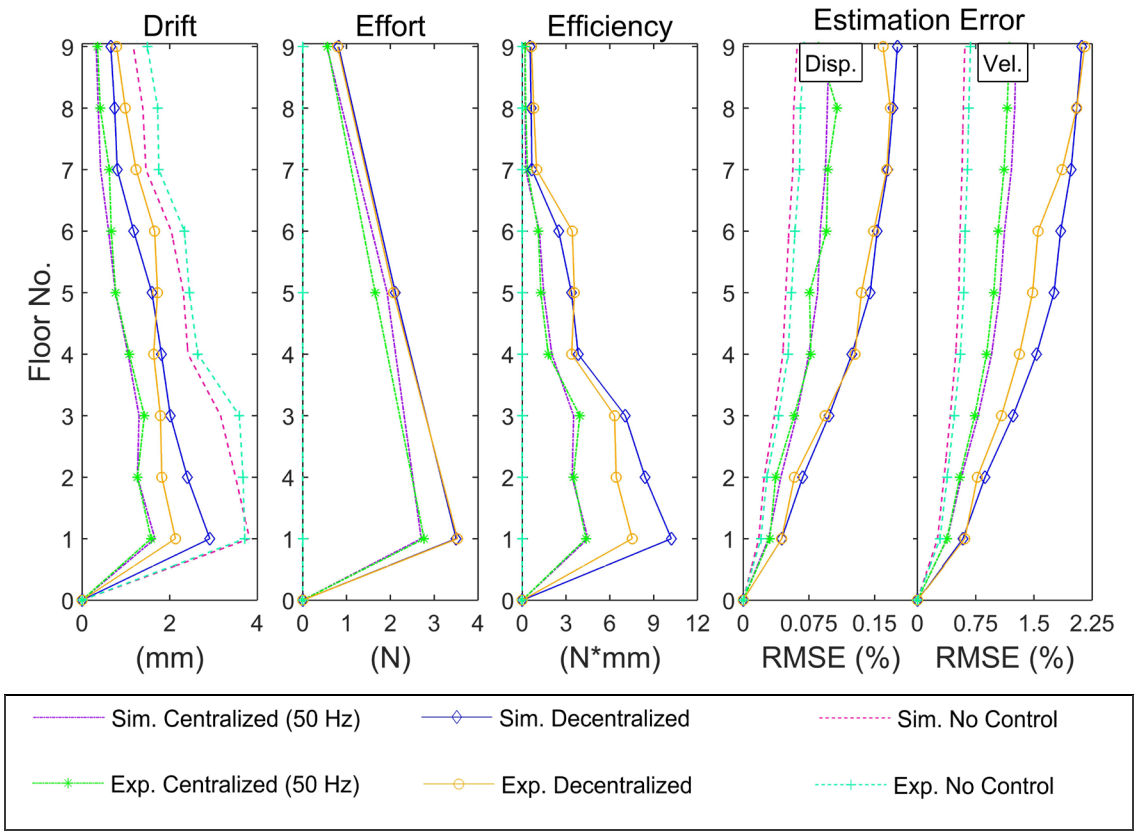

Figure 4.8: 9-DOF model validation metrics

Figure 4.9 illustrates the impact of different control schemes on drift reduction. A similar trend to the 20-DOF simulation results is displayed in Figure 4.9, where the error for state estimation increases along the height of the structure. This figure also includes the theoretical case of fully centralized control at 100 Hz for reference. The RMS force range for the centralized control scheme at 100 Hz is 0.3-1.6 N. As control speed increases for centralized control, the control effort lowers and the efficiency becomes better. The estimation error in the two centralized schemes is close which suggests that speed can also influence control efficiency.

Table 4.3: Inter-story drift (mm) values for validation results

Floor No.	*Cent. Sim*	*Cent. Exp*	*Dec. Sim*	*Dec. Exp*	*NC Sim*	*NC Exp*
9	0.32	0.35	0.66	0.79	1.17	1.49
8	0.37	0.41	0.74	0.99	1.39	1.73
7	0.42	0.62	0.80	1.23	1.46	1.75
6	0.61	0.67	1.18	1.66	2.04	2.34
5	0.76	0.77	1.59	1.72	2.31	2.45
4	1.05	1.08	1.81	1.63	2.42	2.64
3	1.30	1.42	2.02	1.79	3.16	3.59
2	1.26	1.27	2.40	1.82	3.50	3.68
1	1.66	1.58	2.92	2.13	3.82	3.71
0	0.00	0.00	0.00	0.00	0.00	0.00

Table 4.4: Control effort (N) values for validation results

Floor No.	*Cent. Sim*	*Cent. Exp*	*Dec. Sim*	*Dec. Exp*	*NC Sim*	*NC Exp*
9	0.55	0.56	0.82	0.80	0.00	0.00
8	0.55	0.56	0.82	0.80	0.00	0.00
7	0.55	0.56	0.82	0.80	0.00	0.00
6	1.93	1.65	2.11	2.07	0.00	0.00
5	1.93	1.65	2.11	2.07	0.00	0.00
4	1.93	1.65	2.11	2.07	0.00	0.00
3	2.70	2.77	3.50	3.53	0.00	0.00
2	2.70	2.77	3.50	3.53	0.00	0.00
1	2.70	2.77	3.50	3.53	0.00	0.00
0	0.00	0.00	0.00	0.00	0.00	0.00

Table 4.5: Control efficiency (N*mm) values for validation results

Floor No.	*Cent. Sim*	*Cent. Exp*	*Dec. Sim*	*Dec. Exp*	*NC Sim*	*NC Exp*
9	0.18	0.20	0.54	0.63	0.00	0.00
8	0.20	0.23	0.61	0.79	0.00	0.00
7	0.23	0.35	0.66	0.98	0.00	0.00
6	1.17	1.11	2.49	3.44	0.00	0.00
5	1.46	1.27	3.36	3.56	0.00	0.00
4	2.02	1.79	3.83	3.37	0.00	0.00
3	3.52	3.93	7.07	6.32	0.00	0.00
2	3.41	3.52	8.40	6.43	0.00	0.00
1	4.49	4.38	10.22	7.52	0.00	0.00
0	0.00	0.00	0.00	0.00	0.00	0.00

Table 4.6: Displacement-estimation error (RMSE%) values for validation results

Floor No.	*Cent. Sim*	*Cent. Exp*	*Dec. Sim*	*Dec. Exp*	*NC Sim*	*NC Exp*
9	0.098	0.086	0.176	0.160	0.062	0.070
8	0.096	0.107	0.171	0.168	0.058	0.066
7	0.094	0.097	0.165	0.164	0.057	0.064
6	0.088	0.095	0.153	0.149	0.052	0.059
5	0.085	0.076	0.145	0.135	0.049	0.055
4	0.075	0.077	0.124	0.128	0.045	0.051
3	0.061	0.058	0.098	0.094	0.036	0.041
2	0.043	0.037	0.068	0.058	0.024	0.027
1	0.029	0.030	0.044	0.044	0.018	0.020
0	0.000	0.000	0.000	0.000	0.000	0.000

Table 4.7: Velocity-estimation error (RMSE%) values for validation results

Floor No.	*Cent. Sim*	*Cent. Exp*	*Dec. Sim*	*Dec. Exp*	*NC Sim*	*NC Exp*
9	1.268	1.185	2.12	2.15	0.61	0.68
8	1.25	1.16	2.05	2.05	0.59	0.66
7	1.21	1.12	1.98	1.87	0.58	0.64
6	1.12	1.04	1.85	1.55	0.55	0.62
5	1.06	0.98	1.76	1.48	0.53	0.59
4	0.95	0.89	1.53	1.32	0.49	0.55
3	0.78	0.74	1.23	1.08	0.42	0.47
2	0.56	0.55	0.87	0.77	0.34	0.38
1	0.38	0.38	0.59	0.61	0.26	0.29
0	0.00	0.00	0.00	0.00	0.00	0.00

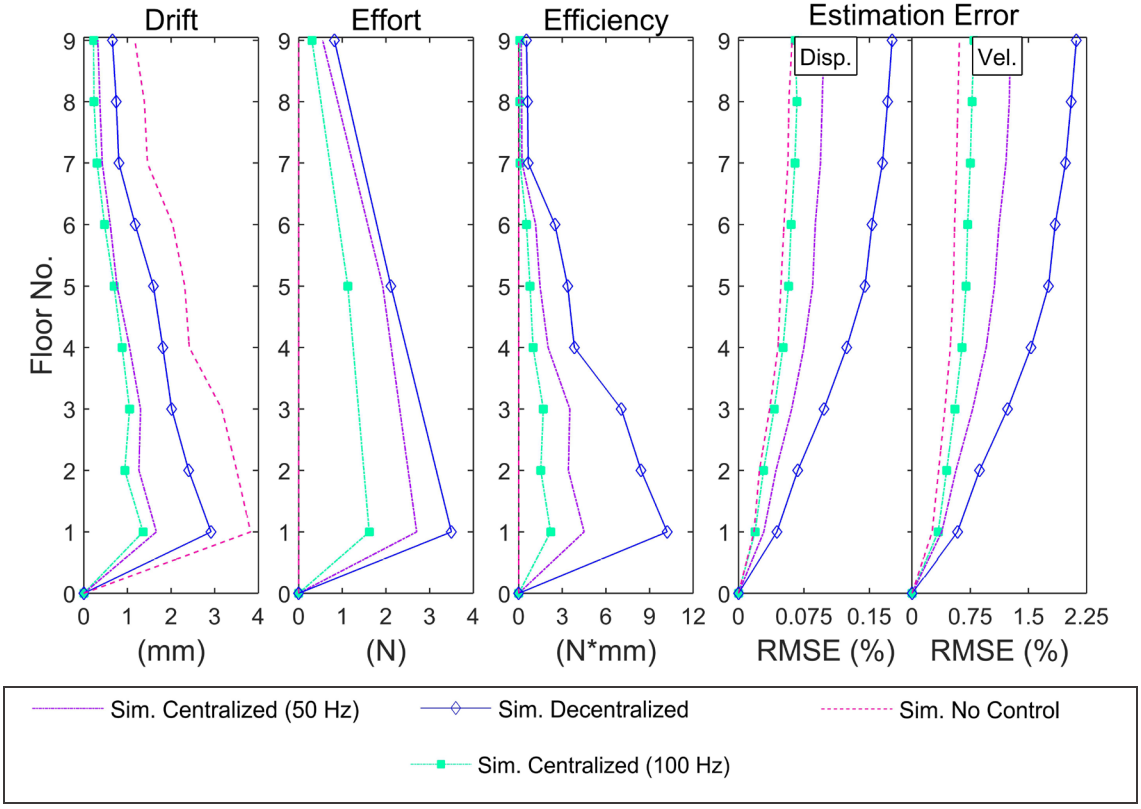

Figure 4.9: 9-DOF control effects on drift reduction, control effort and efficiency, and esimtation error

Figure 4.10 shows the effects of topology on control efficiency for the 9-DOF structure. Similar to the 20-DOF case study, the decentralized (no communication) and the

centralized (theoretical 100 Hz) schemes envelope the staggered communication control schemes across all metrics. The decentralized estimation RMSE ranges from 0.04-0.15% and 0.5-2.2% for displacement and velocity estimation, respectively. The maximum estimation errors for centralized control and throughout the staggered communication schemes for displacement estimation range from 0.06% RMSE (centralized) to 0.1% RMSE (evenly spaced communication pattern). For velocity estimation the maximum error range for these patterns is 0.7% RMSE (centralized) to 1% RMSE (evenly spaced). This figure shows that higher-quality output information (centralized estimation and uniform Gramian-based estimation) improves the state estimation, and with improved estimates, the control effort decreases. Other topologies are better than decentralized control, but not to the level of the uniform Gramian.

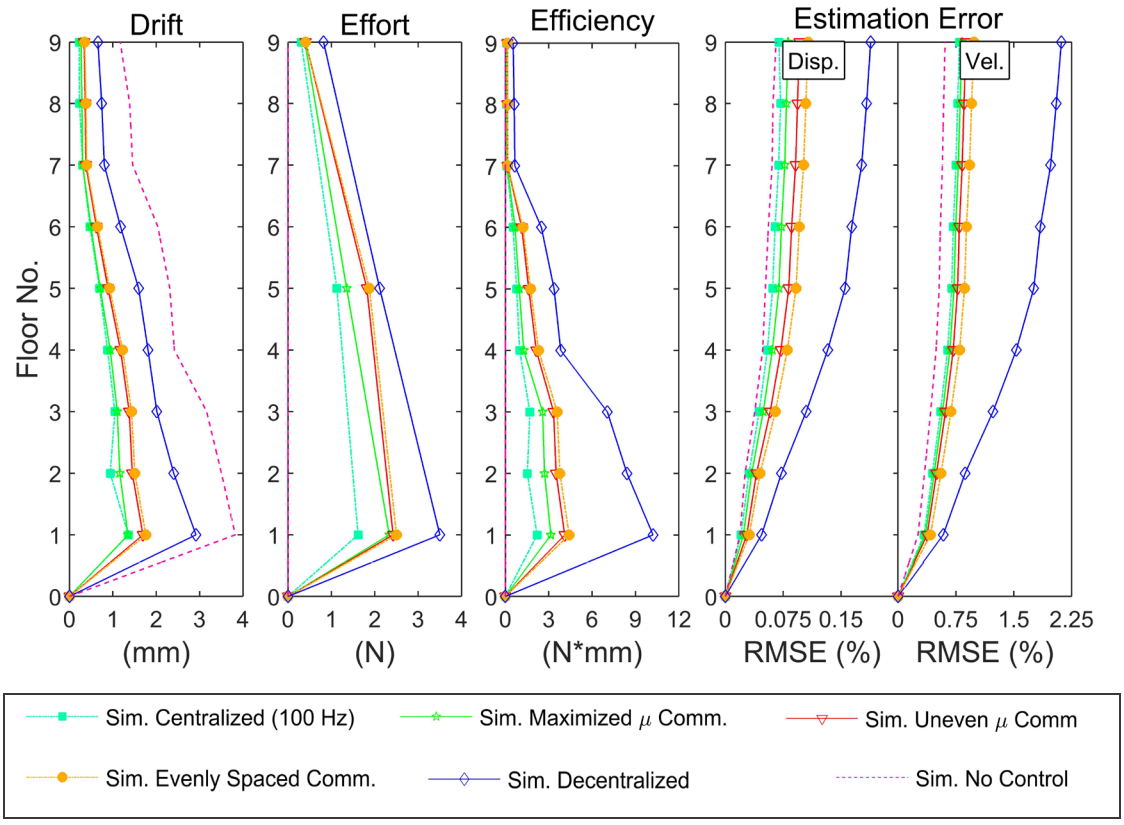

Figure 4.10: 9-DOF topology effects on drift reduction, control effort and efficiency, and estimation error

4.4 Conclusions

As wireless structural control technologies become more readily available, the issues in large scale implementation will become more apparent. Large networks must operate at higher speeds, which may prevent the entire network from transmitting important data in a single step. In this chapter, a temporal subnetworking communication scheme was explored in which wireless sensors share a saturated communication medium by making staggered broadcasts of output measurements with an effectively reduced rate while maintaining a higher sampling and control frequency than would be possible if all units were to broadcast at every step. The advantage of this approach over frequency-division subnetworking approaches is that all units in the network receive all data broadcasts from all other units. These staggered communications were found to be dependent on topology, with some combinations of units outperforming others. A staggering approach was developed, based on sensor placement theory that maximized observability of the network output at every time step in order to minimize estimator error and enhance control performance. The staggered communication approach and the associated estimator/controller performance was compared to the performance of centralized control as well as fully decentralized control. It was shown that the approach presented was able to produce control performance that was nearly as good as that of a fully-centralized controller. Less sophisticated communication patterns that were examined used less control effort and performed poorly compared to centralized and decentralized control and show the topology dependence.

5 Wireless Structural Control using Stochastic Bandwidth Allocation and Dynamic State Estimation with Measurement Fusion‡

Civil structural control systems are used to mitigate undesired dynamic response of buildings and bridges during seismic and high-wind events. Increasingly popular for civil structural control are networks of inherently-stable semi-active control devices that utilize sensor feedback to determine and command optimal control actions to reduce unwanted vibrations [24, 27]. Combined, these components require extensive cabling to be installed throughout the structure to acquire, compute, and supply signals to the various control technologies. Though these systems are effective, there are generally three challenges associated with them: 1) high installation and operation cost of the control devices and associated cabling [110]; 2) reliability over time, in part because cables and other components degrade [110]; and 3) the inability to accurately model controllable damping characteristics of smart materials [82]. Regardless of these shortcomings, semi-active devices such as rheological dampers [59, 105, 126], variable-stiffness devices [42, 43, 127], variable-orifice dampers [128], and others [28, 92] have been growing in popularity for control experimentation for civil structures.

To overcome the high cost for cable installation often associated with wired networks, the use of wireless technology have been gaining popularity research communities for civil engineering applications in the areas of damage detection and localization [1, 21], health monitoring [17-20], parameter estimation [4], and structural control [3, 15, 23, 73]. Wireless control eliminates wiring and with some technology can effectively transmit data between nodes in a structure [9], and with clear line of sight, some systems transmit data up to a kilometer away [129]. Wireless technology for structural control also has an inherent redundancy advantage over its wired counterpart, because each wireless unit associated with each sensor and actuator has its own computational core.

‡ The material contained in this chapter has been submitted to Structural Control and Health Monitoring.

Therefore, in the event of an unfortunate failure of a single computational core, the rest of the network maintains some level of control performance.

Though wireless technology overcomes some of the shortcomings of wired control, it introduces additional drawbacks hindering its acceptance into structural control methodology for field applications. An unavoidable issue that is present with all wireless technology is communication latency. Simply, it takes time for data to be relayed from one unit to the network. As structures grow in size, and the wireless networks grow to accommodate additional points of interest, and latency issues prevent the entire network from collaborating, or centralizing data, in a fast and timely manner.

This limitation is especially relevant in real-time applications, such as control, that require fast data acquisition and broadcasting to make accurate control decisions. A time division multiple access (TDMA) protocol can provide reliable communication [69], but in large it becomes impossible to transmit all data from all nodes within a useful control period. Latency, using a TDMA protocol for relaying data, governs how fast the control step can be performed, and on average this makes the control rate slow. Additionally, larger amounts of data sent in a single transmission further slows down the control step. To overcome the issue of communication latency several methods have been used, including: fully centralizing data at slower speeds [130-132], using schemes with a data loss-tolerant control algorithms [10, 16, 67], spatial decentralization without overlapping subnetworks [14], and spatial decentralization with subnetworks that share data [70, 116, 117]. To make use of smaller subsets of data in control decisions, frequency-division multiplexing is also used [71, 72]. And temporal decentralization to split up wireless transmission across multiple timesteps [133].

In the case of spatial decentralization, robust algorithms have been developed for fusing data from different high and low-cost sensors (*e.g.,* accelerometers) using a Kalman filter to estimate structural response more accurately. Researchers have had success separating sensors into groups, or neighborhoods, to reduce computation time of the network, and

to harden the wireless control network further [22, 61, 119]. Sharing data between these groups is necessary to maintain full network estimation accuracy and deciding the type/amount of data/information that should be transmitted is also important for these algorithms [134]. All of these methods have proven useful in allowing increases in the size of wireless structural control networks to be achieved without significant losses in control frequency, which would negatively affect performance. However, these methods rely on static network topologies and have no mechanism to allow the network to use any measure of information quality to dynamically prioritize data flow throughout the network.

The novel method proposed in this chapter for overcoming communication latency and speed issues in wireless structural control schemes is to allocate communication bandwidth through the use of a modified controller-aware and priority-based carrier sense multiple access with collision detection (CSMA/CD) protocol. This communication protocol will result in asynchronous data arrivals from various nodes within the network, requiring a data fusion approach within each control node, using redundant Kalman estimators, that is slightly modified from prior spatial decentralization studies. Additionally, data fusion commonly involves both state vector fusion and measurement fusion, which is computationally heavy for embedded controllers operating at high speeds. A simplified algorithm for data fusion is used that is less computationally burdensome to maintain fast wireless structural control.

This chapter contributes to the development, verification, and validation of a new means for contention-based dynamic allocation of bandwidth in large wireless structural control networks. If a data point from a particular sensor does not need to be transmitted, then it would be poor use of valuable bandwidth to transmit on a schedule. The uniqueness in this topic is the removal of a schedule and the addition of an autonomous prioritization of transmissions over saturated bandwidth where TDMA is no longer possible. Additionally, the novelty of this chapter lies in the on-demand reconfiguration of sensor groups to make use of whatever data is available in the wireless medium. In the proposed

approach wireless sensors are responsible for collecting data and determining if and when they should broadcast their data into a saturated wireless medium (*i.e.,* a communication window that has low duration and high demand for data collaboration from other units). Upon transmitting data, the unit may contend with another, therefore the wireless network must autonomously modify its CSMA back-off and delay times to prevent data collision. In this chapter, these delays are based on estimation-error residuals and observability measures. Utilizing data fusion techniques in [135-137], measurement fusion and updates will be performed using incoming data from the *neighborhood*, but conversely the proposed methods lack state transmission and state fusion, thus increasing speed. The main difference between the simplified approaches and those cited is the ability to rapidly reconfigure neighborhoods. Previous approaches have defined techniques for transmitting data and fusing it based on known neighborhoods and data distribution with guaranteed transmissions. However, computational units using these techniques could not handle data from locations outside of their neighborhoods.

This chapter is organized to first, present a short background on the standard theory used for the two main components of this chapter: a centralized linear-quadratic regulator (LQR) controller and static Kalman state estimators. Next, this chapter introduces state and measurement fusion in the form of static Kalman estimation derivation. Expressing the need to simplify computation for increasing control speed, this chapter then shows the derivation of the two proposed approaches using dynamic bandwidth allocation and describes how the estimator can be manipulated to make use of an arbitrary subset of output measurements (measurement-only fusion). Then, the subject of the verification study, a 20 degree-of-freedom (DOF) structure, is presented. Simulation results demonstrate how the two dynamic bandwidth allocation approaches perform compared to control schemes with full communication and no communication. A 9-DOF small-scale experimental test-bed is used to validate the simulation results using a network of wireless control nodes. Finally, results are presented to compare estimator/control performance and to show how priority-based transmissions affect control performance, inter-story drift, and estimation accuracy in both the 20-DOF and 9-DOF cases.

5.1 Control and Estimation with Stochastic Communication Schemes

This chapter explores the development of a method to strategically transmit data in a dynamic, non-time-budgeted manner. Sensor data received by control nodes will be used to update Kalman estimated-state vectors needed to compute local control forces using a standard LQR control gain. This section first describes the standard theory for the state-space representation of a multi-degree-of-freedom (MDOF) structure, and the standard derivation of the linear-quadratic regulator (LQR) and Kalman estimator used in this chapter are shown. Next, due to the need to handle random sets of data each time step based on the new transmission method, a Kalman estimator with state and measurement fusion is discussed. Then, the method for dynamically allocating bandwidth is discussed. Finally, simplified fusion techniques are derived to maintain computation speed for the wireless technology used in this chapter.

5.1.1 State-space Representation of a Multi-Degree-of-freedom Structure

For this section, the continuous-time dynamic equilibrium of a linear, time-invariant (LTI) lumped-mass structure with n floors, in state-space form is shown as:

$$\dot{\boldsymbol{z}}(t) = \boldsymbol{A}\boldsymbol{z}(t) + \boldsymbol{B}\boldsymbol{u}(t) + \boldsymbol{E}\ddot{x}_g(t) \tag{5.1}$$

where $\dot{\boldsymbol{z}}(\boldsymbol{t}) = \begin{Bmatrix} \boldsymbol{x} \\ \dot{\boldsymbol{x}} \end{Bmatrix} \in \mathbb{R}^{2n\times 1}$, $\boldsymbol{x} \in \mathbb{R}^{n\times 1}$ is the vector of floor displacements, $\dot{\boldsymbol{x}} \in \mathbb{R}^{n\times 1}$ is the vector of floor velocities, $\ddot{x}_g$ is the ground acceleration, and:

$$\boldsymbol{A} = \begin{bmatrix} 0 & I \\ -\boldsymbol{M}^{-1}\boldsymbol{K} & -\boldsymbol{M}^{-1}\boldsymbol{C}_d \end{bmatrix} \in \mathbb{R}^{2n\times 2\mathrm{n}} \tag{5.2}$$

$$\boldsymbol{B} = \begin{bmatrix} 0 \\ -\boldsymbol{M}^{-1}\boldsymbol{L} \end{bmatrix} \in \mathbb{R}^{2n\times m}; \boldsymbol{E} = \begin{Bmatrix} 0 \\ -\boldsymbol{1} \end{Bmatrix} \in \mathbb{R}^{2n\times 1}$$

where $\boldsymbol{I}$ is the identity matrix, $\boldsymbol{M}$ is the diagonal mass matrix, $\boldsymbol{K}$ is the dynamic stiffness matrix, $\boldsymbol{C}_d$ is the damping matrix formed using modal/Rayleigh damping [113], $\boldsymbol{L} \in \mathbb{R}^{n\times m}$ is an actuator location matrix, and m is the number of actuators. In state-space form, measurements are represented as a linear sum of the observed state response, the

influence of the control force attenuating the structural response, and the inertial acceleration:

$$\boldsymbol{y}(t) = \boldsymbol{C}\boldsymbol{z}(t) + \boldsymbol{D}\boldsymbol{u}(t) + \boldsymbol{F}\ddot{x}_g(t) \tag{5.3}$$

where $\boldsymbol{C} \in \mathbb{R}^{q\times 2n}$; $\boldsymbol{D} \in \mathbb{R}^{q\times m}$; and $\boldsymbol{F} \in \mathbb{R}^{q}$, with q being the number of observable states.

Using the zero-order hold approximation, the continuous-time state-space representation can be brought into the discrete-time domain for LTI systems as follows:

$$\boldsymbol{z}_{k+1} = \boldsymbol{\Phi}\boldsymbol{z}_k + \boldsymbol{\Gamma}\boldsymbol{u}_k + \boldsymbol{\Lambda}\ddot{\boldsymbol{x}}_{\boldsymbol{g}} \tag{5.4}$$

$$\boldsymbol{y}_k = \boldsymbol{C}\boldsymbol{z}_k + \boldsymbol{D}\boldsymbol{u}_k + \boldsymbol{F}\ddot{x}_g$$

where $\boldsymbol{\Phi} = e^{\boldsymbol{A}T_s} \in \mathbb{R}^{2n\times 2n}$; $\boldsymbol{\Gamma} = \int_0^{T_s}(e^{\boldsymbol{A}\tau}\boldsymbol{B})\,d\tau \in \mathbb{R}^{2n\times m}$; $\boldsymbol{\Lambda} = \int_0^{T_s} e^{\boldsymbol{A}\tau}\boldsymbol{E}\,d\tau \in \mathbb{R}^{2n\times 1}$; and T_s is the sampling time. The state-space model of the structure is used to derive the controller that minimizes vibrations due to seismic effects in the building.

5.1.2 Redundant Control and Estimation

In LTI systems with complete state knowledge, the linear-quadratic regulator (LQR) provides an optimal control law that trades off control effort for performance. For a discrete-time state-space model, the discrete-time LQR control solution calculates a control force trajectory that minimizes the quadratic cost function, $\boldsymbol{J}$ [114]:

$$\boldsymbol{J} = \sum_{k=0}^{\infty} \boldsymbol{z}_{\mathrm{k}}^{T}\boldsymbol{Q}\boldsymbol{z}_{\mathrm{k}} + \boldsymbol{u}^{T}\boldsymbol{R}\boldsymbol{u} \tag{5.5}$$

where $\boldsymbol{Q}$ and $\boldsymbol{R}$ are used to set importance levels on output response and control effort, respectively [104]. Using $\boldsymbol{Q} = \boldsymbol{C}_{\mathrm{LQR}}{}^{T}\boldsymbol{C}_{\mathrm{LQR}}$ ($\boldsymbol{C}_{\mathrm{LQR}} \in \mathbb{R}^{2n\times 2n}$: the linear transform $\boldsymbol{z}_{\mathrm{k}} \longrightarrow \boldsymbol{y}_{\mathrm{k}}$) and $\boldsymbol{R} \in \mathbb{R}^{m\times m}$ is a symmetric positive definite matrix which gives the control designer the ability to have target undesired vibrations and control effort, respectively. The $\boldsymbol{C}_{\mathrm{LQR}}$ matrix is used in the formulation of $\boldsymbol{Q}$ to specifically target the type of undesired response and can be configured as follows:

$$\boldsymbol{C}_{\mathrm{LQR}} = \begin{pmatrix} \boldsymbol{c}_{nxn} & \boldsymbol{0} \\ \boldsymbol{0} & \boldsymbol{I}_{nxn} \end{pmatrix} \boldsymbol{\Psi} \tag{5.6}$$

where $\boldsymbol{c} \in \mathbb{R}^{n\times n}$ is a matrix that sets up how displacement is targeted, $\boldsymbol{\Psi} = \begin{Bmatrix} \boldsymbol{\Psi}_d \\ \boldsymbol{\Psi}_v \end{Bmatrix}$ contains the weighting factors for each floors displacement, $\boldsymbol{\Psi}_d \in \mathbb{R}^{n\times 1}$, and velocity, $\boldsymbol{\Psi}_d \in \mathbb{R}^{n\times 1}$. For minimizing undesired interstory drift to reduce the possibility of collapse in a full-scale building $\boldsymbol{c}$ can be configured as follows:

$$\boldsymbol{c} = \begin{pmatrix} 1 & 0 & \cdots & 0 & 0 \\ -1 & 1 & & 0 & 0 \\ 0 & -1 & & 0 & 0 \\ \cdots & \vdots & \ddots & \vdots & \vdots \\ 0 & 0 & & 1 & 0 \\ 0 & 0 & \cdots & -1 & 1 \end{pmatrix} \tag{5.7}$$

To determine the control force trajectory two things are necessary: the control gain matrix, $\boldsymbol{G} \in \mathbb{R}^{m\times 2n}$, and the state vector, $\boldsymbol{z}_k \in \mathbb{R}^{2n\times 1}$. The control gain matrix is derived using the equation:

$$\boldsymbol{u}_k = -[[\boldsymbol{R} + \boldsymbol{\Gamma}^{\boldsymbol{T}}\boldsymbol{P}\boldsymbol{\Gamma}]^{-1}\boldsymbol{\Gamma}^{\boldsymbol{T}}\boldsymbol{P}\boldsymbol{\Phi}]\boldsymbol{z}_k = -\boldsymbol{G}\boldsymbol{z}_k \tag{5.8}$$

where $\boldsymbol{P} \in \mathbb{R}^{2n\times 2n}$ is the discrete Riccati matrix [114]:

$$\boldsymbol{P} = \boldsymbol{\Phi}^T[\boldsymbol{P} - \boldsymbol{P}\boldsymbol{\Gamma}[\boldsymbol{R} + \boldsymbol{\Gamma}^T\boldsymbol{P}\boldsymbol{\Gamma}]^{-1}\boldsymbol{\Gamma}^T\boldsymbol{P}]\boldsymbol{\Phi} + \boldsymbol{Q} \tag{5.9}$$

Eq. (5.8) requires accurate measurements or estimates of the entire state vector, $\boldsymbol{z}_k$ or $\hat{\boldsymbol{z}}_k$, respectively, in order to calculate optimal control forces. In civil structures, direct measurement of state variables is problematic, necessitating the estimation of state values from sensor measurements. When direct measurements of state variables are not available, a Kalman state estimator can be implemented to obtain $\hat{\boldsymbol{z}}_k$, which uses a series of measurements and assumes a base input of a zero-mean, broad-band excitation into the system, $\boldsymbol{w_k}$, :

$$\boldsymbol{z}_{k+1} = \boldsymbol{\Phi}\boldsymbol{z}_k + \boldsymbol{\Gamma}\boldsymbol{u}_k + \boldsymbol{\Lambda}\boldsymbol{w}_k \tag{5.10}$$

It is assumed that the output measurements of the system are corrupted by white noise, $\boldsymbol{v}_k$:

$$\boldsymbol{y}_k = \boldsymbol{C}\boldsymbol{z}_k + \boldsymbol{D}\boldsymbol{u}_k + \boldsymbol{v}_k \tag{5.11}$$

The estimator first estimates the state, $\bar{\boldsymbol{z}}_k$, of the current time step, k, using the previous estimate, $\hat{\boldsymbol{z}}_{k-1}$, and the previously applied control forces, $\boldsymbol{u}_{k-1}$:

$$\bar{\boldsymbol{z}}_k = \boldsymbol{\Phi}\hat{\boldsymbol{z}}_{k-1} + \boldsymbol{\Gamma}\boldsymbol{u}_{k-1} \tag{5.12}$$

Finally, the estimator can update this estimate using the current measurement error:

$$\hat{\boldsymbol{z}}_k = \bar{\boldsymbol{z}}_k + \boldsymbol{\mathcal{L}}_k(\boldsymbol{y}_k - \boldsymbol{C}\bar{\boldsymbol{z}}_k + \boldsymbol{D}\boldsymbol{u}_{k-1}) \tag{5.13}$$

where $\boldsymbol{\mathcal{L}}_k \in \mathbb{R}^{2n\times \mathrm{q}}$ is the time varying estimator gain matrix. The separation principle [115] allows the stable controller derived in Eqs. (5.5-5.9) to be combined with the stable estimator from Eqs. (5.10-5.13) into a stable Linear-Quadratic-Gaussian Controller where both elements are derived separately, but can be used together.

Depending on the availability of actuators and sensors, wireless units can independently collect data, possibly measuring system output and/or state variables directly, and make informed decisions to command equipped actuators. However, major issues faced by using wireless technology, such as communication latency and slow computation speed limit the bandwidth, power consumption from their typically limited power supply (*e.g.,* a battery), and loss of data over unreliable or noisy communication channels or loss due to obstructed line of sight, typically require eliminating, to some degree, communication. This typically means spatially decentralizing and distributing the wireless network into subnetworks, or fully decentralizing the network (*i.e.,* eliminating communication altogether).

5.1.3 Distributed Control using a Wireless Network

In this chapter, the term wireless distributed control refers to a wireless network that has been broken down into subnetworks where there is partial overlap of subnetworks. The

following theory is a simplification of a Kalman filter approach, specifically an optimal decentralized Kalman filter (ODKF) from [138], into a Kalman estimator with both state and measurement fusion. It should be noted that the following derivation is originally applied to subnetworks of a fixed and known size, but the intended use is for variable sized subnetworks. As is the case for a standard, centralized, Kalman estimator (defined by Eq. (5.10-5.13)), distributed control involves a prediction of the system response using the discrete state matrix $\boldsymbol{\Phi}$ and the discrete input matrix $\boldsymbol{\Gamma}$. This prediction is defined in Eq. (5.12) as $\bar{\boldsymbol{z}}_k$, but is presented as follows to demonstrate how distinct estimations are made in individual wireless units:

$$\tilde{\boldsymbol{z}}_{i_k} = \boldsymbol{\Phi}\hat{\boldsymbol{z}}_{i_{k-1}} + \boldsymbol{\Gamma}\boldsymbol{u}_{i_{k-1}} \tag{5.14}$$

Here, $\tilde{\boldsymbol{z}}_{i_k} \in \mathbb{R}^{2n\times 1}$ is the state prediction, $\hat{\boldsymbol{z}}_{i_{k-1}} \in \mathbb{R}^{2n\times 1}$ is the previous state estimate, and $\boldsymbol{u}_{i_{k-1}} \in \mathbb{R}^{n\times 1}$ is the preveiously calculated force vector, all specific to the computational core within unit i. Deviating from the traditional Kalman estimator, which does not involve data fusion, and even adding to traditional Kalman filter approaches which involve measurement fusion, the approach by Oruč [138] gains accuracy by introducing state fusion. State fusion requires all units in a subnetwork to transmit their *a priori* state vectors along with standard transmission of output measurements. Though this presents an obvious burden to the wireless units computationally, and will consume valuable transmission bandwidth, the derivation is necessary to introduce the approaches used in this chapter. Once units in a subnetwork of size N_i transmit their data (state vectors and measurements), the receiving unit(s), i, can perform an update:

$$\hat{\boldsymbol{z}}_{i_k} = \tilde{\boldsymbol{z}}_{i_k} + \sum_{j=1}^{N_i} \boldsymbol{\mathcal{M}}_{ij}\left(\hat{\boldsymbol{z}}_{j_{k-1}} - \hat{\boldsymbol{z}}_{i_{k-1}}\right) + \sum_{j=1}^{N_i} \boldsymbol{\mathcal{L}}_{ij_j}\left(y_{j_k} - \boldsymbol{C}_j\hat{\boldsymbol{z}}_{i_{k-1}}\right) \tag{5.15}$$

where $\boldsymbol{\mathcal{M}}_{ij}$ is the Kalman state gain:

$$\boldsymbol{\mathcal{M}}_{ij} = \boldsymbol{\Phi} - \boldsymbol{\mathcal{L}}_{ij}\boldsymbol{C}_{ij} - \boldsymbol{\Gamma}\boldsymbol{G} + \boldsymbol{\mathcal{L}}_{ij}\boldsymbol{D}_{ij}\boldsymbol{G} \tag{5.16}$$

$\boldsymbol{\mathcal{L}}_{ij_j}$ is the j^{th} column of a Kalman measurement gain matrix formulated using a state-space output matrix containing rows for units i and j, $\boldsymbol{C}_{ij}$ (there are N_i different $\boldsymbol{\mathcal{L}}_{ij}$ matrices for $\forall j = 1,2,\dots,i,\dots,N_i$), $\boldsymbol{C}_j$ is the j^{th} row of the output matrix, and $\boldsymbol{C}_{ij}$ and $\boldsymbol{D}_{ij}$ are the output and feedthrough matrices reduced to contain only the i^{th} and j^{th} rows. Note that the summations sum contributions of data from units 1 through N_i, which refer to units ordered numerically in the subnetwork (*i.e.,* $j = 1$ does not necessarily correspond to the unit located on the first node in the lumped-mass system). This theory was presented in a simplified form which allows the user to precalculate all $\boldsymbol{\mathcal{M}}_{ij}$ and $\boldsymbol{\mathcal{L}}_{ij}$ for a given subnetwork and store them onboard for the wireless estimation process. Though precalculation of these gain matrices is feasible, the required space for all gain matrices is immense and summation of both the state updates and measurement updates is too computationally heavy for embedded systems. Because the only the j^{th} column, $\boldsymbol{\mathcal{L}}_{ij_j}$, of a Kalman measurement matrices, $\boldsymbol{\mathcal{L}}_{ij}$, are used in the measurement update summation, full accuracy is gained once all units report their data. To alleviate some of the computation demand involved in Eq. (5.15) and to accommodate sensor data from outside of a predefined subnetwork the estimation techniques of this chapter are presented at the end of the next sub-section.

5.1.4 Wireless Control using Contention-based Techniques

In this chapter, two alternative dynamic temporal decentralization control schemes are explored to address the issue of degrading control speed with increased demand of data centralization and the associated decrease in control performance and estimation accuracy. In these approaches, control nodes transmit local sensor output measurements into a highly contended wireless medium to other units in the network. The goal is to transmit data only when necessary in order to maintain high estimation accuracy, maintain high control speed, and save on the relatively higher power demands required to transmit data. It is observed that even the fastest wireless technology for structural control applications are limited on the number of data packets from the entire network

while maintaining high control speeds. Therefore, the wireless medium, shared between all units in a large wireless network, will have to be strategically managed. In this chapter, based on available hardware limitations and desired control speed, it is expected that, at most, two wireless units will be successful at transmitting data within a single time step. To accommodate these successful transmissions each unit in the network will be equipped with a number of estimators that can estimate state vectors, $\hat{\boldsymbol{z}}_k$, for any combination of measurements. If communication is not successful by any unit, or is not required during a particular time step, each node in the system estimates states and computes control forces in a fully-decentralized setup.

Contention may occur either when units are communicating at the exact same time, or any part of their transmission window overlaps with another unit's desired window. In the event of contention, all units involved may not be able to successfully deliver their data, because the overlapping of transmission windows causes data to collide, or corrupt, and packets to drop. Fortunately, techniques exist to allow wireless technology to detect if a collision will occur, and back off and retransmit their data to avoid collision. Approaching wireless control using contention-based techniques requires investigation into the length of time that particular technology takes to relay a data packet of various lengths. With knowledge of the length of time it takes to broadcast data from a single unit, a maximum number of units can be defined that can occupy the allowed bandwidth for a specified control step. A question still remains when there is a high demand for data transmissions as to how to allow wireless units to transmit their data based on priority, autonomously, without knowing which other units are sending and when. This chapter relies on three random numbers that are generated in each wireless unit to: 1) determine if a unit should attempt to send its data; 2) determine when should each unit should begin its data transmission during the allowed time window; and 3) determine how much time should the unit back off by to retransmit in the event that it is contending with another unit (*i.e.,* back-off time to avoid data collision). These numbers should pertain to the usefulness of the measured sensor output. In this chapter, estimator residual errors and observability measures are used to determine those values.

For these random numbers, each unit examines its need to transmit data. In this chapter, the necessity to transmit data is first based on an individual unit's observability of the system response, or the impact that a unit's measurement will have when used in state estimation. A sensor group's observability is based on the work [121, 133] which defines the observability Gramian metric:

$$\bar{\mu} = \frac{2n}{trace(\overline{\boldsymbol{W}}_O^{-1})} \tag{5.17}$$

where $\overline{\boldsymbol{W}}_O^{-1}$ is defined as the inverse of the reduced observability Gramian matrix:

$$\overline{\boldsymbol{W}}_O = \int_0^{t_f} e^{\boldsymbol{A}^T\tau}\boldsymbol{C}^T\boldsymbol{\theta}\boldsymbol{C}e^{\boldsymbol{A}\tau}d\tau \tag{5.18}$$

where $\boldsymbol{\theta}$ is the diagonalization of a vector of length n, the number of degrees of freedom, containing ones and zeros in the positions of units on a structure that are actively transmitting data and not active, respectively. To define a single-sensor's observability, Eq. (5.17) and (5.18) can be manipulated so that $\boldsymbol{\theta}$ only has one active unit in its diagonal. Then, by normalizing the single-sensor observabilities by the maximum in the network a unit's observability is defined as follows:

$$\bar{\mu}_i = \frac{2n}{trace(\overline{\boldsymbol{W}}_{O_i}^{-1})\, max(\bar{\mu})} \tag{5.19}$$

The next metric to determine the necessity for a unit to transmit its data is the residual, or error between two components in the Kalman estimation step, the output measurement, $\boldsymbol{y}$, and the output estimation:

$$\hat{\boldsymbol{y}} = \hat{\boldsymbol{C}}\bar{\boldsymbol{z}}_k - \hat{\boldsymbol{D}}\boldsymbol{u}_{k-1} \tag{5.20}$$

Here $\hat{\boldsymbol{C}} = (\boldsymbol{C}^T\boldsymbol{\Theta})^T$ and $\hat{\boldsymbol{D}} = (\boldsymbol{D}^T\boldsymbol{\Theta})^T$ and are the reduced observability output and feedthrough matrices, respectively, and $\bar{\boldsymbol{z}}_k$ is the state prediction defined in Eq. (5.12). In the context of this chapter, the residual metric acts as a single unit's understanding of the accuracy of the wireless network's estimation of its nodal output. If the residual is high, then the network needs to be updated with the true measurement to regain accuracy.

To use the error between $\boldsymbol{y}$ and $\hat{\boldsymbol{y}}$ during the wireless control algorithm, when applied to civil structures, this chapter normalizes it to the reported tolerable jerk (*i.e.,* time derivative of acceleration), J, for humans, which is $2\ m/s^3$ [139]. The normalization of the measurement error is as follows and will be referred to as the jerk ratio:

$$e_i = \frac{|y_i - \hat{y}_i|}{J} f_s \tag{5.21}$$

where f_s is the frequency of control, also the sampling rate in this chapter, which is used to simply take the time derivative of the measurement residual (acceleration) to obtain the jerk residual.

This chapter uses random numbers and thresholds to decide whether or not send data. The distributions for the random number generators are modified using the two metrics defined above: the single-sensor observability metrics, $\bar{\mu}_i$**;** and instantaneous jerk ratios, e_i. The jerk ratio establishes the initial interest for a unit to transmit data. The jerk ratio is compared to a single value representing an acceptable percentage, 75%, of tolerable jerk in the structure. Next, to make the process more stochastic and to avoid over saturating the communication bandwidth, a random number is generated using a folded normal distribution. The random value is then added to the observability metric, $\bar{\mu}_i$, and compared to a threshold. Therefore, higher observability will allow the units to come closer to, if not exceed the threshold easier (*i.e.,* higher observability units will be more likely to transmit). A folded normal distribution was chosen for this decision with a threshold outside of the region of higher-likelihood random numbers to lower transmission rates; this threshold was chosen to be 1.5. In general, this value must be calibrated to fit the desired expected number of transmissions within the available data transmission window.

The next two random numbers use a uniform distribution that is directly modified by the jerk ratio and observability. These numbers are used to determine the initial transmission time for a unit attempting to transmit data, and the back-off/retransmit time for units whose data packet collides with another transmission. For the prioritization, or initial

transmission time, a uniform distribution was used. The lower bound of the distribution is $0\,ms$ (or no delay in initial transmission) and the upper bound is scaled by $\left(3\,\bar{\mu}_i'e_i'\right)ms$, where $\bar{\mu}_i' = 1 - \bar{\mu}_i$ and $e_i' = 1 - e_i$ which are the complements of the single-unit observability and jerk ratios, respectively. If the jerk ratio for a given unit and its observability are low, the initial transmission time approaches $3\,ms$ (for the technology used in this chapter $3\,ms$ is the time it takes to transmit two units' data back to back). In the event collision is detected a second uniform distribution was used to randomly select a back-off time for retransmitting data transmissions for colliding units. This second uniform distribution is scaled by $\left(1.5\,\bar{\mu}_i'e_i'\right)ms$ so that the maximum time to attempt transmitting data is $4.5\,ms$. In general, the ranges for transmission times and retransmission times should be calibrated to minimize the collision of packets. Moving forward, if the units do choose to transmit their data, and the data is successfully received by other units in the network, those units have to have a strategy for handling random output measurements.

Unlike traditional spatially decentralized control with distinct, static, subnetworks, or neighborhoods, where units only communicate information within those neighborhoods, and unlike distributed control where neighborhoods may share information using units, or neighbors, that communicate on multiple wireless channels, this chapter examines so-called dynamic neighborhoods. Dynamic neighborhoods imply that units can use data from any other unit without restriction and without prior knowledge of when it would receive data from that unit. The method for incorporating information from neighbors in distributed control relies on information, state and/or measurement fusion as defined in the previous subsection. To communicate a data packet with state variables and measurements in itself is a burden to the wireless bandwidth. The computation time to perform dynamic information fusion would also be much greater than the proposed approaches. Therefore, the formulation of the two proposed approaches can be presented which rely on an elementary fusion of measurement values only. Measurement

transmission is fast enough to not burden the bandwidth, and the associated Kalman gains are easily stored in an embedded processor.

5.1.4.1 Average Neighbor Estimation and Control

After a single or multiple unit(s) transmit data, assuming the data is valuable, as defined by the prioritizing metrics, the receiving unit has to make use of that data. The first dynamic neighborhood approach that allows units to make use of arbitrary data starts with the same state prediction defined in Eq. (5.14). Similar to the approach defined in Eq. (5.15), the following estimation relies on the summation of measurement residuals, but it removes the need to sum contributions from all units in a static neighborhood. Inspired by an iterative consensus algorithm [140] a simple measurement update is achieved by averaging the contributions from each transmitting units and the data collected by the computational unit:

$$\hat{\boldsymbol{z}}_{i_k} = \tilde{\boldsymbol{z}}_{i_k} + \frac{1}{\eta}\sum_{j=1}^{\eta} \boldsymbol{\mathcal{L}}_{ij}\left(\boldsymbol{y}_{ij} - \left(\boldsymbol{C}_{ij} - \boldsymbol{D}_{ij}\boldsymbol{G}\right)\hat{\boldsymbol{z}}_{i_{k-1}}\right) \tag{5.22}$$

where $\hat{\boldsymbol{z}}_{i_k} \in \mathbb{R}^{2n\times 1}$ is the state estimation vector for unit i, η is the number of successfully received units worth of data including the computational unit's data (*e.g.,* one unit sends its data, unit i has an $\eta = 2$), $\boldsymbol{\mathcal{L}}_{ij}$ is a Kalman measurement gain matrix formed using an output matrix with only the i^{th} and j^{th} rows, $\boldsymbol{y}_{ij}$ is a column vector with at most two measurements corresponding to the i^{th} and j^{th} measurements (*i.e.,* in the summation, the $j = i$ component uses $\boldsymbol{y}_{ii} = \boldsymbol{y}_i$, the i^{th} measurement, only), and $\hat{\boldsymbol{z}}_{i_{k-1}} \in \mathbb{R}^{2n\times 1}$ is the previous estimation of the state vector in unit i. Stability is assured in the same manner defined in Eq. (5.15) derived by the work of Oruč [138]. Unlike Eq. (5.15) this step does not rely on fusing state vectors transmitted from other units, the single state prediction is sufficient for accuracy.

5.1.4.2 Dynamic Neighborhood Estimation and Control

The next proposed approach for handling multiple measurements worth of data per timestep from outside of a predefined subnetwork consists of two faster rate Kalman estimators. The method is straightforward when compared to a standard Kalman estimator, but gains accuracy over static subnetwork estimation by incorporating random measurements. In this approach, the discrete-time state-space representation is derived using a Kalman estimation time increment that is half the magnitude of the control period. Eq. (5.14) is used for the initial state prediction, then for handling any unit's data transmitted within the first half of the control step the following measurement update is used:

$$\bar{\boldsymbol{z}}_{i_k} = \tilde{\boldsymbol{z}}_{i_k} + \begin{cases} \boldsymbol{\mathcal{L}}_i\left(\boldsymbol{y}_i - (\boldsymbol{C}_i - \boldsymbol{D}_i\boldsymbol{G})\hat{\boldsymbol{z}}_{i_{k-1}}\right) \\ \boldsymbol{\mathcal{L}}_{ij}\left(\boldsymbol{y}_{ij} - \left(\boldsymbol{C}_{ij} - \boldsymbol{D}_{ij}\boldsymbol{G}\right)\hat{\boldsymbol{z}}_{i_{k-1}}\right) \end{cases} \tag{5.23}$$

where $\bar{\boldsymbol{z}}_{i_k} \in \mathbb{R}^{2n\times 1}$ is the initial state estimation vector for unit i, the piecewise bracket indicates a conditions: if a unit did not send its data within the first half, use only the measurement from unit i, $\boldsymbol{y}_i$, and the corresponding measurement gain, $\boldsymbol{\mathcal{L}}_i$, otherwise use a vector containing the i^{th} and j^{th} measurements, $\boldsymbol{y}_{ij}$, and the corresponding 2-column gain matrix, $\boldsymbol{\mathcal{L}}_{ij}$. After the initial estimation occurs, each unit waits to receive another unit's data. After the waiting period, a secondary estimation is performed as follows:

$$\boldsymbol{z}^*_{i_k} = \boldsymbol{\Phi}\bar{\boldsymbol{z}}_{i_k} + \boldsymbol{\Gamma}\boldsymbol{u}_{i_k} \tag{5.24}$$

which is equivalent to Eq. (5.14), but using the initial estimation $\bar{\boldsymbol{z}}_{i_k}$, then an update is performed using any data that has been transmitted in the second half of the control period:

$$\hat{\boldsymbol{z}}_{i_k} = \boldsymbol{z}^*_{i_k} + \begin{cases} \boldsymbol{\mathcal{L}}_i\left(\boldsymbol{y}^*_i - (\boldsymbol{C}_i - \boldsymbol{D}_i\boldsymbol{G})\bar{\boldsymbol{z}}_{i_k}\right) \\ \boldsymbol{\mathcal{L}}_{ij}\left(\boldsymbol{y}^*_{ij} - \left(\boldsymbol{C}_{ij} - \boldsymbol{D}_{ij}\boldsymbol{G}\right)\bar{\boldsymbol{z}}_{i_k}\right) \end{cases} \tag{5.25}$$

where $\boldsymbol{y}_i^*$ and $\boldsymbol{y}_{ij}^*$ are vectors containing the resampled measurement in unit i, $\boldsymbol{y}_i^*$, and the transmitted measurement from a new unit j (not to be confused with the j^{th} unit from the initial update). Any data that is sent successfully during the end of the transmission window, that was not used in the first two estimation steps, is carried over to the next timestep and used for the initial update at that time and has a higher priority than the incoming data of the next timestep.

5.2 Methods

For this chapter, a numerical simulation of a 20 degree-of-freedom (DOF) structure was used to test the dynamic bandwidth allocation techniques and measurement fusion methods for wireless networks. The 20-DOF numerical simulation employs a full-scale structural model and simulated wireless communication. Additionally, a simulation and experimental validation were performed on a 9-DOF small-scale structure equipped with *Martlet* wireless structural control units [9]. A *Martlet* unit's processor can operate at user selected speeds between 10 and 80 MHz; it can store programs on-board with a maximum size of 2 MB (non-volatile memory) and 800 kB of volatile memory (*e.g.,* data, soft-coded parameters, *etc.*); and *Martlet* units can support a 16 GB or 32 GB Micro SD card for large data storage [9]. *The* validation study uses an in-house small-scale structure and *Martlet* wireless sensing units to perform wireless structural control and is compared to its own computer simulation. In the numerical simulation of a full-scale structure, the simulation of the small-scale structure, and the experimental validation, a control rate of 100 Hz is used and transmissions for the shared bandwidth of the wireless network are prioritized within over $7.5\,ms$ each time step, leaving $2.5\,ms$ for computation and data acquisition.

5.2.1 Large-scale Dynamic System Model Parameters

Parameters for the 20-DOF structure were obtained from a single bay of the second generation ASCE benchmark structure properties found in [122]. Reducing the 20-DOF structure to a single bay was used to better illustrate the independence of structural

complexity. The modeled structure in the simulation is excited by the simulated El Centro ground-motion record (Imperial Valley 5/19/40 El Centro Array #9, 180 – USGS Station 117 North-South) scaled to a peak ground acceleration of 1.0 m/s^2. The simulated response of the structure is approximated using the average acceleration method for Newmark integration, with $\beta = \frac{1}{4}$ and $\gamma = \frac{1}{2}$ [113]. The simulated structure is configured to have one actuator per floor with a 20 kN control force capacity and ideal control force outputs (*i.e.,* force output is LQR desired force). For simplicity the Kalman estimator uses the Newmark acceleration response at each floor (*i.e.,* simulated accelerometers) to estimate the state response. The actuator location and state penalty matrices were selected to be the same for all control cases (*e.g.,* centralized control, decentralized control, average neighbor control, and dynamic neighborhood control). This selection was made for consistency and to maintain stability of the decentralized controller. The system properties (*i.e.,* the stiffness and mass) are summarized in Table 1 and a schematic depicting the above description of the 20-DOF structure is shown in Figure 5.1.

Table 5.1: Structural parameters for the large-scale 20-DOF structure

Floor	***Mass (kg)***	***Stiffness ($\frac{kN}{m}$)***	***Damping ($kN \cdot \frac{s}{m}$)***
20	$4.8x10^4$	$2.5x10^6$	$7.8x10^4$
19	$6x10^4$	$2.5x10^6$	$7.8x10^4$
⋮	⋮	⋮	⋮
1	$6x10^4$	$2.5x10^6$	$7.8x10^4$

20 Modal Frequencies (Hz)									
0.79	2.4	4.0	5.6	7.1	8.6	10.1	11.4	12.7	13.9
15.1	16.1	17.1	17.9	18.7	19.3	19.9	20.3	20.6	20.8

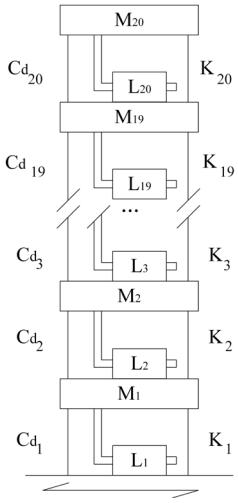

Figure 5.1: Schematic of simulation test-bed 20-DOF structure

The 20-DOF structure is controlled by each scheme for wireless transmissions, control, and estimation. Estimation is performed by accessing a library of pre-calculated Kalman measurement gains, emulating the on-board access to local memory for wireless units. The effectiveness of the algorithm is measured using 4 metrics: inter-story drift, $\boldsymbol{x}_d = \boldsymbol{x}_{i+1} - \boldsymbol{x}_i$, which describes the position of structural floors with the floor immediately below itself; control effort, $f_{ce} = \sqrt{\frac{\sum_{k=1}^{t} f_k^2}{t}}$, which is the root-mean-square (RMS) value for the control force time history, f_k, used to minimize response over time, t; control efficiency, $eff = \boldsymbol{x}_d\, f_{ec}$, where this is a measure of how well the control force achieved the drift reduction of a floor; and estimation error, $K_e = \sqrt{\frac{\sum_{k=1}^{t} (\hat{\boldsymbol{z}}_k - \boldsymbol{z}_k)^2}{t}}$ (for both the estimation of displacement and velocity), which is the root-mean-square error (RMSE) between the Kalman estimation of state variables and the Newmark-Beta derived state response.

5.2.2 Experimental Validation Platform

Validation of the dynamic bandwidth allocation control schemes is accomplished using an experimental test-bed utilizing *Martlet* wireless sensing/actuation units. The experimental 9-DOF structure was installed on a 50 cm x 50 cm Quanser Shake Table II

and excited by El Centro ground-record acceleration, scaled to a peak ground acceleration of 1.0 m/s^2, perpendicular to the weak axis of the columns using compatible software provided by the shake-table manufacturer and *SIMULINK*. The stories of the small-scale test-bed have a 30 cm x 30 cm footprint and story separation of approximately 20 cm. When assembled in the 9-DOF configuration the test-bed will have a height of approximately 1.8 m. The mass of the entire structure, including dampers, is limited to 14 kg per the shake-table specifications. The story stiffness values in this setup vary around $1000\frac{N}{m}$ when using eight 0.02 cm x 0.002 cm (weak axis) aluminum columns and the boundary conditions between the columns and floors (based on bolt tightness), and the damping is assumed to be 1.0% Rayleigh damping. There are three metal foam magneto-rheological (MR) fluid extraction-type dampers to provide lateral control. Each damper is supported by an aluminum lateral brace system. The three actuators were placed strategically on floors 1, 5, and 9 using system controllability and actuator placement theory [114, 124, 125]. *Martlet* units are used to monitor each floor and are connected to single-ended Silicon Designs Inc. piezo-electric accelerometer Model No.: 2012-002. In this setup each *Martlet* unit decides to communicate, it transmits the acceleration measurement of the current timestep to all units in the wireless network. Parameters for the small-scale 9-DOF structure are summarized in Table 5.2.

Table 5.2: Structural parameters for the small-scale 9-DOF structure

Floor	***Mass (kg)***	***Stiffness*** $(\frac{N}{m})$	***Floor***	***Damping*** $(N \cdot \frac{s}{m})$	***Mode***	***Modal Frequency (Hz)***
9	1.38	3700	9	11	9	24.4
8	2.68	9000	8	11	8	19.5
7	1.06	5600	7	11	7	17.9
6	1.06	9900	6	11	6	13.8
5	1.38	4300	5	11	5	11.5
4	2.68	4200	4	11	4	9.4
3	1.06	3600	3	11	3	7.2
2	1.06	4700	2	11	2	4.4
1	1.38	2500	1	11	1	1.3

Each *Martlet* unit calculates a desired control force based on their corresponding embedded damper Bouc-Wen look-up tables, state estimates, and feedback control gains. The analog voltage output signals of the *Martlet* units is then translated into equivalent current signals using an operation amplifier, before being supplied to one of the three dampers. After the actuated ground-record excitation and each control test, the wireless network reports its collected data to a nearby server for further analysis. In 10 ms only a few units can transmit over an IEEE 802.15.4 standard implementation. A typical timestep for the control process within a wireless unit is provided in Figure 5.2.

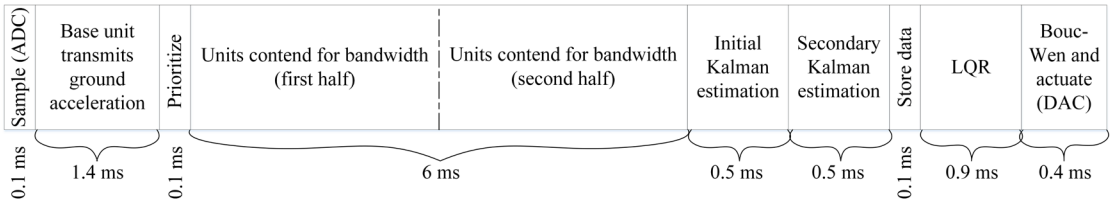

Figure 5.2: Typical timestep for embedded processes within wireless control *Martlet* units

A parallel tethered data acquisition system (National Instruments PXIe-1071 chassis running LabVIEW) records the test-bed structural response using differential PCB Piezotronics 333B50 accelerometers and MTS C-Series Core 551020 linear placement transducers (LPT) located on each floor, PCB Piezotronics 208C01 force transducer time histories, and the ground motion for validation of the wireless system performance. This experimental setup is advantageous over traditional large-scale structural control test-beds because it is affordable to assemble, reassemble, and test. Figure 5.3 shows the 9-DOF structure, the equipped dampers, accelerometers, measurement transducers, wireless units, parallel data acquisition technology, and the laboratory setup.

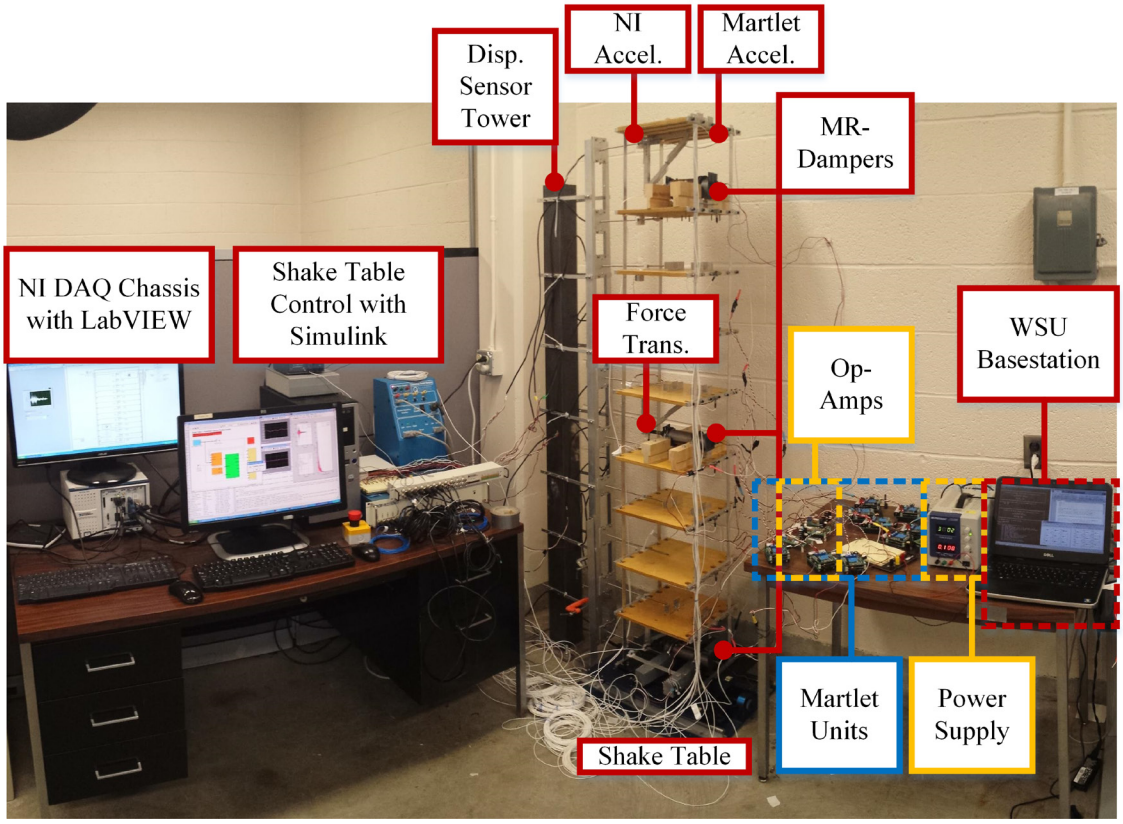

Figure 5.3: Test-bed 9-DOF small-scale structure and laboratory setup

5.2.3 Dynamic Allocation of Communication Resources

Traditionally, data in control schemes are transmitted in a timed fashion. The allocation of a transmission window is divided up between all units in the network. With dynamic allocation, such as carrier sense multiple access with collision detection (CSMA/CD) techniques, the units must decide on when to transmit data to lower the likelihood for collision. In the theory portion of this chapter, the distributions for determining if a unit needed to transmit data and transmissions times was discussed. To implement the folded normal distribution in *MATLAB* for wireless units' desire to transmit data, the absolute value of a normally distributed random number generated using the built-in function *randn()* (the seed is set to the *MATLAB* default non-negative integer). Similarly, in the simulations *rand()* is used, when modified as described in the theory section, to generate the initial transmissions and back-off delays. In the wireless *Martlet* units random

numbers for the uniform distributions were generated using the *ran3()* function, written by the authors onto the microprocessor following [141]. *ran3()* was chosen because it is identified as the more conventional method for random number generation in C (the input being an integer value seed greater than zero). The process of generating random numbers from a folded normal distribution is approximated using the absolute value of a so-called *ran3n()* function which, with a mean value of $0\ ms$ and a standard deviation of $1\ ms$ follows the form:

$$r = \sqrt{2}\, erf^{-1}(2\, ran3(s) - 1)$$

where r is the generated random value (in ms) and $erf^{-1}()$ is the inverse error function approximation from [142] which uses a uniformly distributed random number. In this chapter generated from *ran3()* for higher accuracy compared to other uniform distribution functions for C. The seed value, s, in both generators is a randomly selected non-negative, nonzero integer sent to the wireless *Martlet* units in preparation for testing.

5.3 Results

Dynamic bandwidth allocation was used to make sure data was only transmitted if the wireless network and its units felt it was necessary. Limiting transmissions based on necessity provided consistently high-quality output information to the network. A simulated 20 degree-of-freedom structure (DOF), a 9-DOF small-scale simulated structure, and an experimental 9-DOF small-scale laboratory test-bed were used to test the dynamic bandwidth allocation approach and the measurement fusion techniques for estimating state variables using randomly transmitted unit data. The two fusion techniques are used in separate control processes and inter-story drift reduction, control effort, control efficiency, and estimation accuracy are compared to centralized and fully-decentralized control. Both techniques for fusion for estimation, while using dynamic bandwidth allocation, outperformed fully-decentralized control in drift reduction for both the 20-DOF and 9-DOF cases.

5.3.1 20 Degree-of-Freedom Structure Simulation Results

Figure 5.4 shows the impact of strategic communication on the performance of the control system in terms of drift reduction, control effort, efficiency, and estimation error. Differences between centralized, fully-decentralized, and the dynamic measurement-fusion schemes, for control performance, can be ascribed to estimator performance. Shown in Figure 5.4, all of the control schemes with communication (*e.g.,* both dynamic bandwidth allocation schemes and the centralized scheme) have an estimator root-mean-square error (RMSE) that is less than 1% in displacement and velocity estimation for each floor. This result shows that, in simulation, the use of arbitrary subsets of data, transmitted based on priority, do not degrade the estimation capabilities of the wireless network. In terms of displacement drift reduction, a strategic, contention-based data sharing approach for wireless structural control networks can be almost as effective in efficiently rejecting unwanted seismic vibrations as a fully-centralized network (the fully-centralized network not being possible for wireless control at the same control frequency when the number of sensors grows large). Furthermore, the strategic and dynamic passing of information significantly improves the estimation algorithm when compared to not communicating (*i.e.,* fully-decentralized), which suggests that estimator error residuals and observability metrics are useful tools for prioritizing transmission of sensor data. For all cases, estimation error trends upward for estimating upper DOF states. Decentralized estimation exhibits the largest estimation error which is related to not having access to data from other units in the network. The maximum displacement estimation RMSE for decentralized estimation is 6.8% and the maximum decentralized velocity estimation RMSE is 10.5%. Centralized estimation performs the best, with maximum RMSE values of 0.2% and 0.4% for displacement and velocity estimation, respectively. The average neighbor estimation technique has a maximum displacement estimation RMSE of 0.5% and velocity estimation RMSE of 0.6%. Dynamic neighborhood estimation had maximum RMSE values of 0.6% and 0.7% for displacement and velocity estimation, respectively.

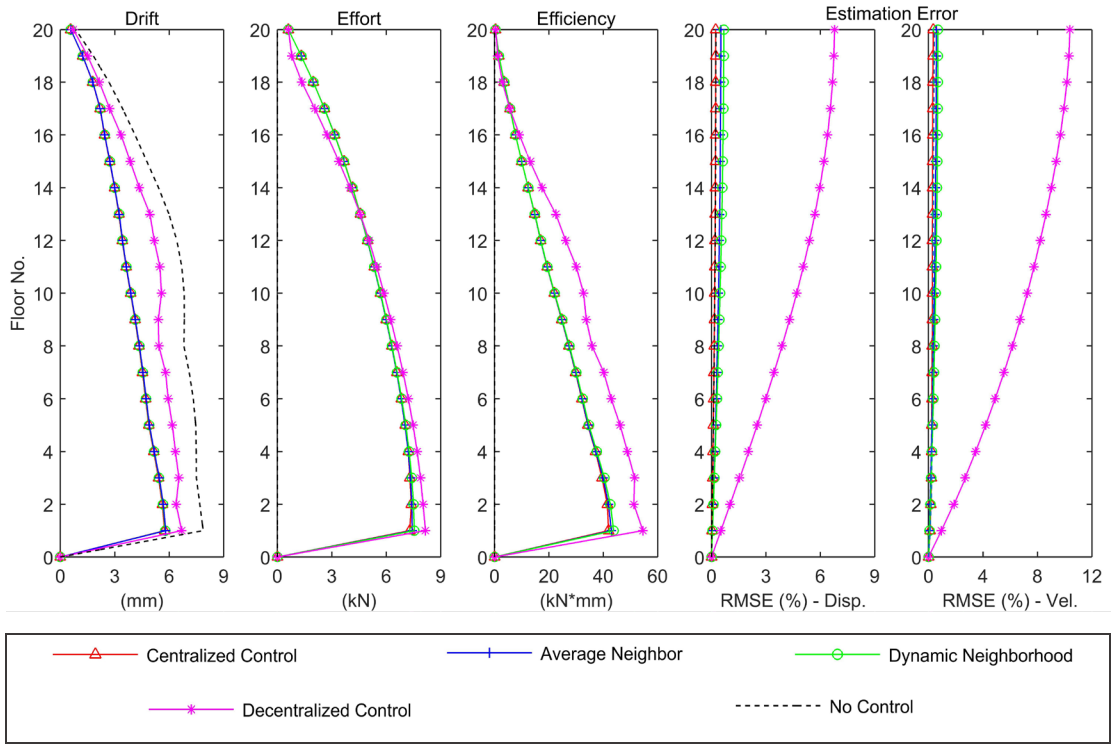

Figure 5.4: Dynamic bandwidth allocation effect on drift, control effort and efficiency, and estimation error for 20-DOF large-scale structure

Figure 5.4 also shows that as RMSE decreases as communication and the ability to handle incoming data increases. For the dynamic communication schemes, measurement-only fusion is an effective means to providing high quality data for estimation. Additionally, communication schemes with lower estimation error use lower control effort and have better control efficiency. The dynamic bandwidth and estimation approaches attenuate drift consistent to centralized control with final drift values ranging from 0.6-5.8 mm, whereas decentralized control is not as efficient reducing drift having final values ranging from 0.7-6.7 mm. The less sophisticated cases (*i.e.,* the evenly spaced, quadrants, and uneven/non-uniform Gramian patterns), use control force less efficiently. Centralized control uses a maximum control force of 7.3 kN, the average neighbor approach uses a max force of 7.4 kN, the dynamic neighborhood approach uses 7.6 kN, and fully-decentralized control uses a maximum of 8.2 kN. Overall, the dynamic bandwidth allocation schemes make use of data from any unit in the network that can contribute

high quality information, and in doing so, improve in all metrics over decentralized control.

5.3.2 9 Degree-of-Freedom Simulation and Experimental Validation Results

The 9-DOF small-scale structure was used to validate the dynamic bandwidth allocation technique and measurement fusion algorithms that are performed by wireless *Martlet* units. For the 20-DOF large-scale simulation results, estimator accuracy was shown to affect control efficiency for drift reduction. *Martlet* estimated velocity and displacement for floors 1, 5, and 9 of the 9-DOF structure are presented in Figure 5.5 overlaying the *MATLAB* simulated *Martlet* estimation process.

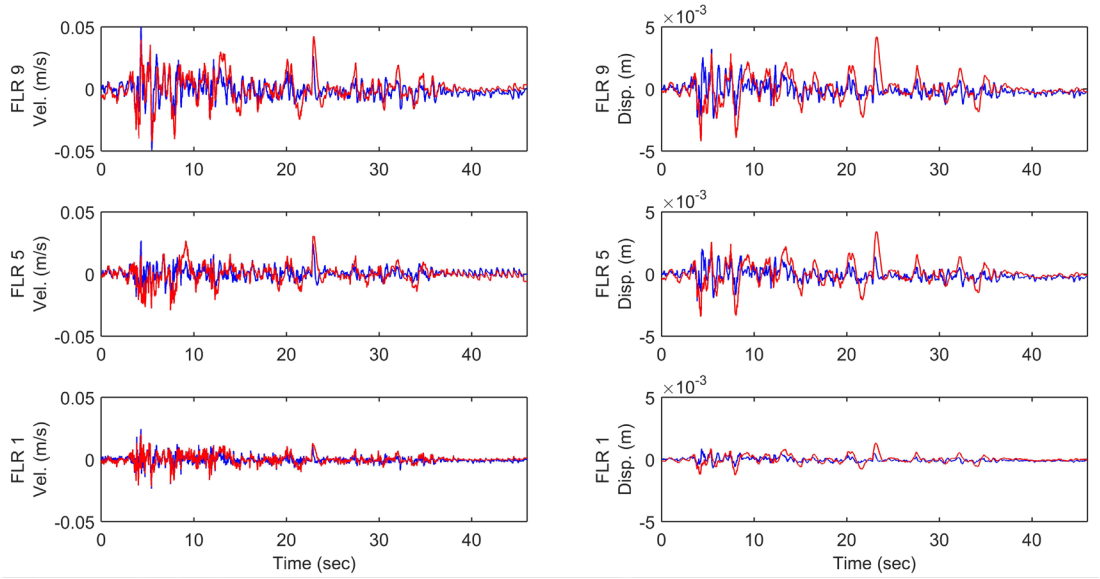

Figure 5.5: Comparison of *Martlet* average neighbor estimation (light/red) for measurement fusion and *MATLAB* simulated estimation (dark/blue) for 9-DOF small-scale structure

Simulation and experimental results for drift, effort, efficiency, and estimation error metrics, used in the 20-DOF simulation results, are presented in Figure 5.6 and Figure 5.7, respectively. Due to bandwidth limitation for the *Martlet* units' radios, fully-centralized control is not possible at 100 Hz. Therefore, simulated centralized and

experimental validation were performed at 50 Hz (the fastest achievable control speed using 10 *Marlet* units). Figure 5.6 shows the anticipated trends first observed from the 20-DOF simulation, on the 9-DOF simulated structure during control operations (*e.g.,* drift is lower using centralized control and dynamic bandwidth and fusion approaches vs. decentralized control). Again, it is found that the dynamic measurement-only fusion approaches do not destabilize state estimation within the control scheme. By providing high quality data each time step, both approaches outperform decentralized control in estimation, and by doing so, they have used control force more efficiently. The control forces used to achieve drift reduction are found to be lower when using centralized estimation and dynamic fusion estimation (both the average neighbor and dynamic neighborhood approaches). Decentralized control uses higher control force due to over estimation in state variables.

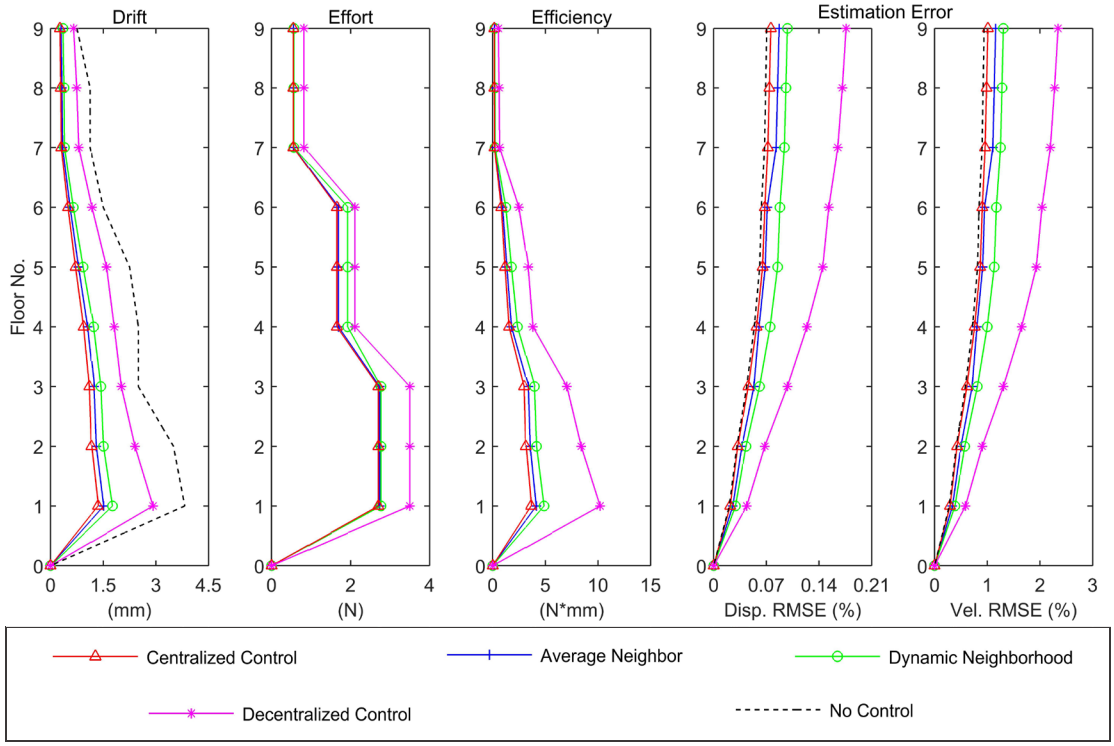

Figure 5.6: 9-DOF simulation for drift reduction, control effort and efficiency, and estimation error

For the experimental portion (metrics shown in Figure 5.7) drift values ranged from 0.2-1.4 mm for centralized control, 0.3-3.2 mm for decentralized control, 1.1-4.0 mm in the uncontrolled case with El Centro excitation. The average neighbor approach had drift values ranging from 0.2-1.6 mm (closest to centralized performance) and the dynamic neighborhood approach had drift values ranging from 0.2-2.5 mm (closer to decentralized performance). The experimental validation of the dynamic bandwidth fusion approaches shows that the average neighbor estimation scheme outperformed the dynamic neighborhood approach in drift reduction. The dynamic neighborhood approach is found to use more control force on the lower floors of the 9-DOF structure which gives is poorer efficiency. Imperfect actuators are used to control the structure and the average neighbor approach's ability to use more incoming data per time step provides higher accuracy of the estimated velocity, which lead to better selection and command of forces to be achieved by the magneto-rheological (MR) dampers. Additionally, the dynamic neighborhood approach is only capable of handling at most two measurements, whereas the average neighbor approach is setup to accommodate all transmitted measurements. However, beyond the first three floors, the estimation error decreases, thus lowering the control effort to make both fusion techniques comparable for control efficiency. The experimental validation study shows that less units can be used to centralize data and still achieve high estimation results. Overall, these approaches are effective, not only in simulation, but experimentally as well.

The efficiency metric shows that decentralized control effort is increased due to erroneous state estimation, consistent with lack of data centralization. On this smaller scale, the dynamic neighborhood approach is still better in all metrics compared to fully-decentralized control. Decentralized control used maximum forces ranging from 2.9 N (9^{th} floor actuator) to 6.9 N (1^{st} floor actuator) experimentally. The centralized control schemes used maximum forces ranging between 1.7-3.1 N from floors 1-9. Average neighbor control forces range from 1.7-3.2 N and dynamic neighborhood control forces range from 1.7-3.5 N. The decentralized estimation RMSE values range from 0.07-0.2% and 0.9-2.2% for displacement and velocity estimation, respectively. The centralized

estimation errors range from 0.02-0.07% and 0.3-0.6% for displacement and velocity estimation, respectively, and the maximum RMSE errors for average neighbor estimation is 0.8% and dynamic neighborhood estimation is 0.9% for velocity estimation. Figure 5.7 shows that higher-quality output information and quantity of information improves state estimation, and with improved estimates, the control effort decreases. From these results, on-demand reconfiguration of sensor groups to make use of available data improves estimation accuracy and therefore yields better control performance. The values found in Figures 5.6 and 5.7 are tabulated in Tables 5.3-5.7.

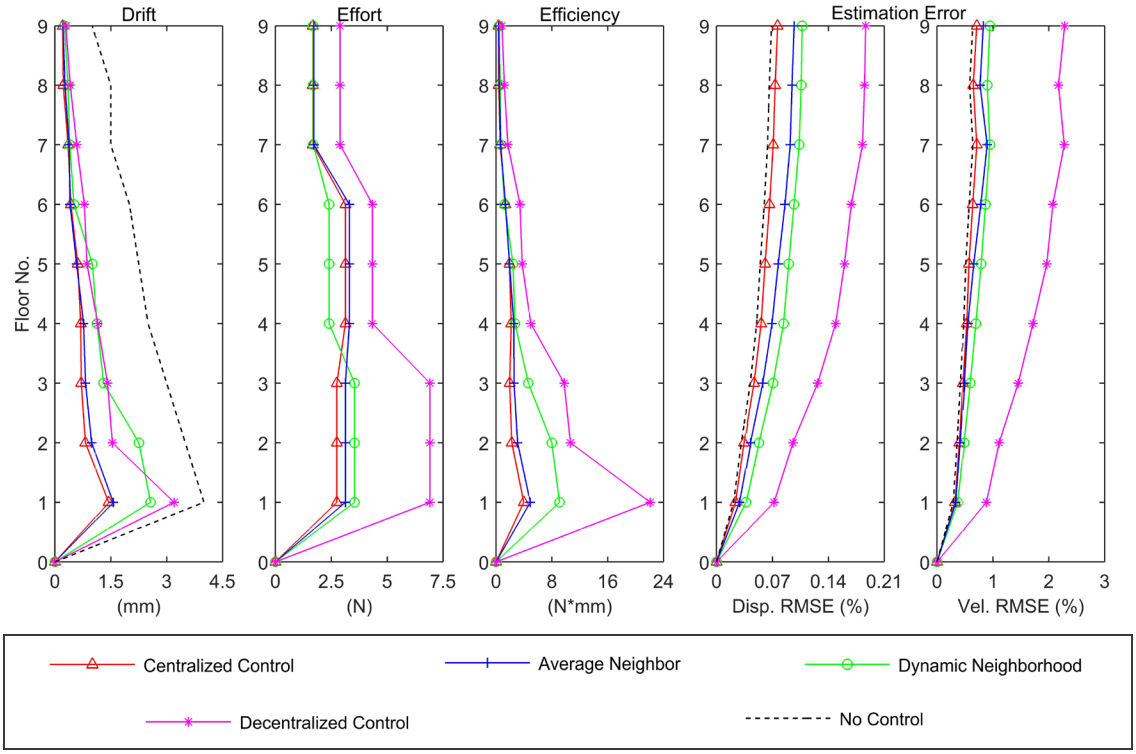

Figure 5.7: 9-DOF experimental drift reduction, control effort and efficiency, and estimation error

Table 5.3: Maximum drift values for 9-DOF simulation and experimental performance metrics

			Drift (mm)		
Floor No.	***NC Sim***	***Cent. Sim***	***Avg. Sim***	***Dyn. Sim***	***Dec. Sim***
9	0.75	0.27	0.30	0.35	0.66
8	1.13	0.29	0.32	0.38	0.75
7	1.12	0.31	0.34	0.40	0.80
6	1.50	0.49	0.56	0.65	1.18
5	2.25	0.71	0.79	0.93	1.59
4	2.50	0.94	1.05	1.23	1.81
3	2.50	1.10	1.24	1.43	2.02
2	3.50	1.16	1.30	1.51	2.40
1	3.82	1.35	1.51	1.76	2.92
0	0.00	0.00	0.00	0.00	0.00
Floor No.	***NC Exp***	***Cent. Exp***	***Avg. Exp***	***Dyn. Exp***	***Dec. Exp***
9	1.00	0.22	0.21	0.26	0.30
8	1.49	0.27	0.23	0.35	0.41
7	1.50	0.38	0.35	0.40	0.59
6	2.00	0.41	0.43	0.51	0.79
5	2.25	0.58	0.61	1.01	0.86
4	2.50	0.77	0.69	1.13	1.15
3	2.98	0.82	0.71	1.31	1.41
2	3.50	0.99	0.82	2.25	1.54
1	4.02	1.57	1.44	2.57	3.20
0	0.00	0.00	0.30	0.00	0.00

Table 5.4: Maximum force values for 9-DOF simulation and experimental performance metrics

			Effort (N)		
Floor No.	***NC Sim***	***Cent. Sim***	***Avg. Sim***	***Dyn. Sim***	***Dec. Sim***
9	0.00	0.55	0.56	0.57	0.82
8	0.00	0.55	0.56	0.57	0.82
7	0.00	0.55	0.56	0.57	0.82
6	0.00	1.65	1.69	1.93	2.11
5	0.00	1.65	1.69	1.93	2.11
4	0.00	1.65	1.69	1.93	2.11
3	0.00	2.70	2.74	2.77	3.50
2	0.00	2.70	2.74	2.77	3.50
1	0.00	2.70	2.74	2.77	3.50
0	0.00	0.00	0.00	0.00	0.00
Floor No.	***NC Exp***	***Cent. Exp***	***Avg. Exp***	***Dyn. Exp***	***Dec. Exp***
9	0.00	1.72	1.67	1.69	2.90
8	0.00	1.72	1.67	1.69	2.90
7	0.00	1.72	1.67	1.69	2.90
6	0.00	3.31	3.13	2.40	4.34
5	0.00	3.31	3.13	2.40	4.34
4	0.00	3.31	3.13	2.40	4.34
3	0.00	3.13	2.75	3.54	6.91
2	0.00	3.13	2.75	3.54	6.91
1	0.00	3.13	2.75	3.54	6.91
0	0.00	0.00	0.00	0.00	0.82

Table 5.5: Force-to-drift efficiency values for 9-DOF simulation and experimental performance metrics

	*Efficiency (N*mm)*				
Floor No.	***NC Sim***	***Cent. Sim***	***Avg. Sim***	***Dyn. Sim***	***Dec. Sim***
9	0.00	0.15	0.17	0.20	0.54
8	0.00	0.16	0.18	0.22	0.61
7	0.00	0.17	0.19	0.22	0.66
6	0.00	0.82	0.94	1.25	2.49
5	0.00	1.17	1.35	1.79	3.37
4	0.00	1.55	1.79	2.36	3.83
3	0.00	2.99	3.39	3.97	7.06
2	0.00	3.14	3.56	4.17	8.42
1	0.00	3.65	4.14	4.88	10.21
0	0.00	0.00	0.00	0.00	0.00
Floor No.	***NC Exp***	***Cent. Exp***	***Avg. Exp***	***Dyn. Exp***	***Dec. Exp***
9	0.00	0.37	0.35	0.44	0.85
8	0.00	0.47	0.38	0.59	1.19
7	0.00	0.66	0.59	0.67	1.70
6	0.00	1.34	1.34	1.23	3.43
5	0.00	1.93	1.92	2.42	3.75
4	0.00	2.54	2.17	2.72	4.97
3	0.00	2.58	1.95	4.63	9.76
2	0.00	3.09	2.25	7.99	10.66
1	0.00	4.91	3.97	9.10	22.11
0	0.00	0.00	0.00	0.00	0.00

Table 5.6: Displacement-estimation error values for 9-DOF simulation and experimental performance metrics

	Disp. Estimation Error (RMSE%)				
Floor No.	***NC Sim***	***Cent. Sim***	***Avg. Sim***	***Dyn. Sim***	***Dec. Sim***
9	0.07	0.08	0.09	0.10	0.18
8	0.07	0.07	0.09	0.10	0.17
7	0.07	0.07	0.08	0.09	0.17
6	0.06	0.07	0.07	0.09	0.15
5	0.06	0.07	0.07	0.09	0.15
4	0.05	0.06	0.06	0.08	0.12
3	0.04	0.05	0.05	0.06	0.10
2	0.03	0.03	0.04	0.04	0.07
1	0.02	0.02	0.03	0.03	0.04
0	0.00	0.00	0.00	0.00	0.00
Floor No.	***NC Exp***	***Cent. Exp***	***Avg. Exp***	***Dyn. Exp***	***Dec. Exp***
9	0.07	0.10	0.08	0.11	0.19
8	0.07	0.09	0.07	0.11	0.19
7	0.06	0.09	0.07	0.10	0.18
6	0.06	0.09	0.07	0.10	0.17
5	0.05	0.08	0.06	0.09	0.16
4	0.05	0.07	0.06	0.08	0.15
3	0.04	0.06	0.05	0.07	0.13
2	0.03	0.04	0.03	0.05	0.10
1	0.02	0.03	0.02	0.04	0.07
0	0.00	0.00	0.00	0.00	0.00

Table 5.7: Velocity-estimation error values for 9-DOF simulation and experimental performance metrics

	Vel. Estimation Error (RMSE%)				
Floor No.	***NC Sim***	***Cent. Sim***	***Avg. Sim***	***Dyn. Sim***	***Dec. Sim***
9	0.94	1.01	1.16	1.31	2.34
8	0.92	0.99	1.13	1.28	2.28
7	0.90	0.96	1.11	1.25	2.20
6	0.84	0.91	0.95	1.17	2.04
5	0.82	0.87	0.91	1.13	1.93
4	0.72	0.76	0.80	1.00	1.65
3	0.58	0.61	0.71	0.81	1.31
2	0.41	0.43	0.50	0.57	0.91
1	0.28	0.29	0.34	0.39	0.59
0	0.00	0.00	0.00	0.00	0.00
Floor No.	***NC Exp***	***Cent. Exp***	***Avg. Exp***	***Dyn. Exp***	***Dec. Exp***
9	0.64	0.83	0.71	0.95	2.28
8	0.58	0.77	0.65	0.90	2.17
7	0.64	0.90	0.71	0.95	2.28
6	0.58	0.78	0.64	0.87	2.07
5	0.51	0.66	0.57	0.79	1.96
4	0.48	0.55	0.53	0.70	1.72
3	0.42	0.49	0.46	0.59	1.45
2	0.36	0.41	0.40	0.49	1.11
1	0.29	0.34	0.32	0.37	0.88
0	0.00	0.00	0.00	0.00	0.00

5.4 Conclusions

This chapter investigated temporal decentralization using a dynamic bandwidth allocation technique to maintain fast control speeds without the need of spatial decentralization. This work focused on structural control of buildings with large control networks where normal time division approaches for budgeting data transmissions would not be feasible. The approaches used in this work allowed units to adapt based acceleration readings and reconfigure neighborhoods for fusing measurement data. Data transmissions were limited based on two criteria, nodal observability and measurement

to estimation residual jerk ratios, to prevent data collision and data loss in saturated wireless medium. This work aims to present an additional tool for wireless structural control to improve performance when communication is sparse and irregular. The approach used may be used as a stand-alone strategy or in conjunction with spatial decentralization or frequency allocation strategies. The contributions of this chapter include an algorithm for prioritizing data for transmission and fast dynamic measurement fusion schemes using a library of state estimator matrices that can accommodate data without rederiving the estimation scheme. These two contributions should be adaptable to many different size structures and applications. This chapter examined a simulated full-scale 20 degree-of-freedom structure and an experimental laboratory-scale 9 degree-of-freedom structure. The results for the dynamic fusion schemes showed a direct comparison in performance to a fully-centralized scheme and both outperformed a fully-decentralized control scheme.

6 Concluding Remarks

6.1 Summary of Dissertation

The main focus of this dissertation was to develop novel methods to maintain control speed in large wireless networks where communication latency would traditionally require wireless networks to operate at slow speeds. Though other studies have been performed that look into this issue, the methods discussed in this dissertation relied on novel approaches of static and dynamic bandwidth allocation that operated with temporally decentralized subgroups of sensors. This methodology mandated the development and validation of embedded processes for estimation and control schemes that could handle time varying sensor inputs, strategical budgeting of transmissions based on sensor group observability, and controller-aware prioritization of transmissions, all of which was conducted on a simulated large-scale structure and an experimental small-scale wireless control test-bed structure.

Semi-active damping devices are of growing in popularity within the civil engineering community. The main types of damping devices were discussed in Chapter 2 pointing out the major shortcomings associated with passive and active control devices and emphasizing the benefits semi-active devices possess. In general, wired control systems are used to provide voltage to active and semi-active devices during a control process to attenuate undesired structural response. Chapter 2 discussed that semi-active dampers, though highly attractive, are often too small to supply an appropriate control force to combat inertial forces in a structure during seismic and high-wind events. A large density of semi-active dampers (*i.e.,* a control network) is required to achieve an adequate force to control structures. Wireless control and semi-active devices are often used together due to the large amount of cabling required to power and command all semi-active devices. However, wireless technology is not well suited for real-time applications such as control, due to communication latency.

Communication latency, among other issues, such as limited power supplies to power wireless technology (*e.g.,* batteries), limited communication range, *etc.* governs how fast the wireless network can centralize data. In control applications, control speed is slowed down when traditionally time-budgeting data transmissions. To bring wireless technology for control closer to wired control systems, methods for working around communication latency and even eliminating it have been explored and reviewed in Chapter 2. These methods generally involve spatially decentralizing the wireless network, which creates subgroups of wireless units that operate, unaware of other subgroup activity and unable to retrieve data from nodes outside of subgroups. Moving past set subgroups of wireless units, other studies have looked at sharing data between groups, and even communicating data with non-time-budgeted, but rather simultaneous, methods. The shortcomings of each technique, to address communication latency, have further motivated the exploration of temporal decentralization techniques discussed in this dissertation.

Because experiments that use semi-active devices are expensive, and because the main contribution of this dissertation was to address the impact that wireless communication latency has on structural control, Chapter 3 looked at the development and use of small-scale semi-active control device and a small-scale structural control test bed. Chapter 3 discussed both the modeling and model calibration for low-force (0-10 N) double-ended piston-type magneto-rheological (MR) fluid extraction dampers. A damper was designed to exhibit the same inherent complex nonlinear hysteretic behavior comparable to a full-scale commercially available MR-fluid dampers. The MR-fluid extraction damper demonstrated the ability to reduce inter-story velocities and drift of a three degree-of-freedom (DOF) testbed structure at the scale of interest. Chapter 3 also discussed the further development of a 9-DOF testbed for use in the two studies discussed in Chapters 4 and 5. In each of the studies the MR-dampers were used to control a test-bed structures using linear-quadratic-Gaussian (LQG) control strategies.

A method of improving control speed using sensor placement techniques was explored in Chapter 4. Prior to experimental testing a simulation was developed that demonstrated how sensor placement could reduce the number of sensors that had to communicate in a wireless network employed on a 20-DOF structure. Each sensor group for transmission contained maximum system observability which aided the control performance and estimator efficiency. For this work, the performance of multiple estimators/controllers in a large wireless network was examined for a multitude of communication schemes. Many staggered communication schemes were examined and overall, the observability Gramian sensor placement technique outperformed other less sophisticated communication methods.

The work in Chapter 5 involved a method for addressing communication latency in wireless networks that are too large to operate with traditional transmission scheduling or the method discussed in Chapter 4. This chapter explored dynamic allocation by modifying a carrier sense multiple access with collision detection protocol, or carrier sense multiplexing, and added randomness to transmission times to reduce bandwidth contention. The results showed that prioritizing transmissions based on observability and measurement readings allowed temporally decentralized dynamic bandwidth allocation to improve upon fully-decentralized control. When units only transmitted when necessary, the information spread throughout the network helped to increase estimation accuracy and decrease control effort used in control tests. This work fills the gap in wireless structural control that exists when communication is sparse and irregular.

6.2 Contributions

To further promote the use of semi-active technologies, this dissertation has developed small-scale affordable semi-active dampers for experimental studies to be used with wireless technology as they go together to combat the high installation cost associated with cabling. In order to fully accept wireless technology, and therefore semi-active devices for structural control, the issue of communication latency had to be addressed further. This dissertation identified two methods that could allow wireless units to

transmit highly valuable information in the limited size communication windows to minimize the potential of wasting bandwidth and to minimize the effects of communication latency. Specifically, this dissertation acknowledged that traditional methods used to address communication latency are based on spatially dividing the control network into subgroups, which prevents the spread information throughout the structure. If the network was instead divided into groups over time, where each time group sent data to the entire network, information would always be well spread. This dissertation explored the use of sensor placement techniques to assess how valuable wireless sensor transmissions are and how the value of patterned transmissions of wireless units compared to other sensor patterns. Most interestingly, this dissertation presented a method for communicating data without a time schedule. This approach in reference is from Chapter 5, which used managed wireless communication using an extended carrier sense multiplexing approach. This has not been done for wireless structural control because it is easier to budget transmissions to have guaranteed delivery of data for centralization. However, the accompanying algorithms for handling the incoming data is able use data from any transmitting unit or units for control computation. Also, the extension to carrier sense multiplexing was knowledgeable of the control algorithm and estimated state and output values, so deciding when to retransmit data when detecting potential collisions was strategic to the ongoing process. The contributing work was all validated using wireless sensing and control technology during control experiments.

6.3 Future Work

This dissertation presented methods for improving the capabilities of wireless technology for structural control in large control networks. While the results represent that the methodology developed is feasible, future research applied to larger networks than were used in the dissertation are still warranted. Throughout the duration of this dissertation, other research studies have demonstrated interesting techniques that can be combined with the novel approaches discussed to combat communication latency. Properly

implemented, projects involving the combination of temporal and spatial decentralization with overlapping subgroups and even frequency-division multiplexing would expand the field of applications for this dissertation. Combining reduced order modeling and methods for dynamic or strategic static allocation of bandwidth might help minimize wireless unit group sizes while and calculation requirements. The model order could match the number of transmitted data points per timestep to further simplify the calculations, increase estimation efficiency, and provide grounds for examining even larger systems using the same method.

Besides simply combining methodology to improve the capabilities of wireless technology for structural control, future work is warranted to improve the specific algorithms also presented as part of this dissertation. Chapter 5 presented two algorithms for fusing measurement data from random sets of up to two incoming transmissions, this could be extended to accommodate any number of transmissions. It would be more useful to fuse state vectors if transmitted as well when making use of combined algorithm solutions to further speed up computation and communication. It is also important to consider structures that are equipped with more types of sensors, and how fusion techniques described in Chapter 5 would be applied to fusing different types of data when received, and also how different sensor data types would affect the sensor placement algorithm described in Chapter 4.

7 References

1. Hsu T.Y., Huang S.K., Lu K.-C., Loh C.-H. A damage detection algorithm integrated with a wireless sensing system. *Journal of Physics: Conference Series*. St Anne's College, University of Oxford, 2011; 012042.
2. Loh C.-H., Lynch J.P., Lu K.-C., Wang Y., Chang C.-M., Lin P.-Y., Yeh T.-H. Experimental verification of a wireless sensing and control system for structural control using MR dampers. *Earthquake Engineering & Structural Dynamics* 2007; **36**(10):1303-1328.
3. Swartz R.A. Reduced-order modal-domain structural control for seismic vibration control over wireless sensor networks. *American Control Conference (ACC)*. San Francisco, California, 2011; 2516-2521.
4. Zimmerman A.T., Shiraishi M., Swartz R.A., Lynch J.P. Automated modal parameter estimation by parallel processing within wireless monitoring systems. *Journal of Infrastructure Systems* 2008; **14**(1):102-113.
5. Jansen L.M., Dyke S.J. Semiactive control strategies for MR dampers: comparative study. *Journal of Engineering Mechanics* 2000; **126**(8):795-803.
6. Yoshida O., Dyke S.J. Seismic control of a nonlinear benchmark building using smart dampers. *Journal of engineering mechanics* 2004; **130**(4):386-392.
7. Bahar A., Pozo F., Acho L., Rodellar J., Barbat A. Semiactive control of base-isolated structures using a new inverse model of MR dampers. *Control Conference (ECC), 2009 European*. 2009; 1065-1070.
8. Swartz R.A., Jung D., Lynch J.P., Wang Y., Shi D., Flynn M.P. Design of a wireless sensor for scalable distributed in-network computation in a structural health monitoring system. *5th international workshop on structural health monitoring*. 2005; 1570-1577.
9. Kane M., Zhu D., Hirose M., Dong X., Winter B., Häckell M., Lynch J.P., Wang Y., Swartz R.A. Development of an extensible dual-core wireless sensing node for cyber-physical systems. *SPIE's 34th Annual International Symposium on Smart Structures and Materials: Nondestructive Evaluation and Health Monitoring*. 2014; 90611U-90611U-19.
10. Linderman L.E., Jo H., Spencer B.F. Low-Latency Data Acquisition Hardware for Real-Time Wireless Sensor Applications. *Sensors Journal, IEEE* 2015; **15**(3):1800-1809.
11. Law K.H., Swartz A., Lynch J.P., Wang Y. Wireless sensing and structural control strategies. *4th International Workshop on Advanced Smart Materials and Smart Structures Technologies (ANCRiSST)*. 2008; 24-25.

12. Swartz R.A., Zimmerman A., Lynch J.P. Structural health monitoring system with the latest information technologies. *Proceedings of 5th Infrastructure & Environmental Management Symposium, Yamaguchi, Japan*. 2007;

13. Wang Y., Law K.H. *Wireless sensor networks in smart structural technologies*. INTECH Open Access Publisher: 2011.

14. Law K.H., Swartz A., Lynch J.P., Wang Y. Decentralized control strategies with wireless sensing and actuation. *NFS CMMI Engineering Research and Innovation Conference*. Honolulu, Hawaii, 2009;

15. Wang Y., Swartz R.A., Lynch J.P., Law K.H., Lu K.-C., Loh C.-H. Decentralized civil structural control using real-time wireless sensing and embedded computing. *Smart Structures and Systems* 2007; **3**(3):321-340.

16. Linderman L.E., Mechitov K.A., Spencer B.F. TinyOS-based real-time wireless data acquisition framework for structural health monitoring and control. *Structural Control and Health Monitoring* 2013; **20**(6):1007-1020.

17. Chintalapudi K., Fu T., Paek J., Kothari N., Rangwala S., Caffrey J., Govindan R., Johnson E., Masri S. Monitoring civil structures with a wireless sensor network. *IEEE Internet Computing* 2006; **10**(2):26-34.

18. Tanner N.A., Wait J.R., Farrar C.R., Sohn H. Structural health monitoring using modular wireless sensors. *Journal of Intelligent Material Systems and Structures* 2003; **14**(1):43-56.

19. Rice J.A., Spencer Jr B.F. *Flexible smart sensor framework for autonomous full-scale structural health monitoring*. Newmark Structural Engineering Laboratory. University of Illinois at Urbana-Champaign.: 2009.

20. Straser E.G., Kiremidjian A.S., Meng T.H. *Modular, wireless damage monitoring system for structures*. Google Patents: 2001.

21. Lynch J.P., Sundararajan A., Law K.H., Kiremidjian A.S., Carryer E. Embedding damage detection algorithms in a wireless sensing unit for operational power efficiency. *Smart Materials and Structures* 2004; **13**(4):800.

22. Mazo M., Tabuada P. Decentralized event-triggered control over wireless sensor/actuator networks. *IEEE Transactions on Automatic Control* 2011; **56**(10):2456-2461.

23. Swartz R.A., Lynch J.P. Strategic network utilization in a wireless structural control system for seismically excited structures. *Journal of structural engineering* 2009; **135**(5):597-608.

24. Spencer Jr. B.F., Nagarajaiah S. State of the art of structural control. *Journal of Structural Engineering* 2003; **129**(7):845-856.

25. Yang J.N., Wu J.C., Kawashima K., Unjoh S. Hybrid control of seismic-excited bridge structures. *Earthquake Engineering & Structural Dynamics* 1995; **24**(11):1437-1451.

26. Soong T.T., Spencer Jr. B.F. Supplemental energy dissipation: state-of-the-art and state-of-the-practice. *Engineering Structures* 2002; **24**(3):243-259.

27. Symans M.D., Constantinou M.C. Semi-active control systems for seismic protection of structures: a state-of-the-art review. *Engineering Structures* 1999; **21**(6):469-487.

28. Rao T.R.M., Rao G.V., Rao K.S., Purushottam A. Analysis of passive and semi active controlled suspension system for ride comfort in an omnibus passing over a speed bump. *Analysis of Passive & Semi Active Controlled Suspension Systems* 2010; **5**:7-17.

29. Yang G., Spencer Jr. B.F., Carlson J.D., Sain M.K. Large-scale MR fluid dampers: Modeling and dynamic performance considerations. *Engineering Structures* 2002; **24**(3):309-323.

30. Bascom W. *A Hole in the Bottom of the Sea; The Story of the Mohole Project*. Doubleday: Garden City, NY, 1961.

31. Lee D.M., Medland I.C. Base isolation-An historical development, and the influence of higher mode responses. *Bulletin of the New Zealand National Society for Earthquake Engineering* 1978; **11**(4):219-233.

32. Kareem A., Kijewski T., Tamura Y. Mitigation of motions of tall buildings with specific examples of recent applications. *Wind and structures* 1999; **2**(3):201-251.

33. Sadek F., Mohraz B., Taylor A.W., M. C.R. *Passive Energy Dissipation Devices for Seismic Applications*. National Institute of Standards and Technology, Building and Fire Research Laboratory: 1996.

34. Rana R., Soong T. Parametric study and simplified design of tuned mass dampers. *Engineering Structures* 1998; **20**(3):193-204.

35. Kourakis I. *Structural systems and tuned mass dampers of super-tall buildings: case study of Taipei 101*. Massachusetts Institute of Technology: 2007.

36. Saaed T.E., Nikolakopoulos G., Jonasson J.-E., Hedlund H. A state-of-the-art review of structural control systems. *Journal of Vibration and Control* 2015; **21**(5):919-937.

37. Housner G.W., Bergman L.A., Caughey T.K., Chassiakos A.G., Claus R.O., Masri S.F., Skelton R.E., Soong T.T., Spencer Jr. B.F., Yao J.T.P. Structural Control: Past, Present, and Future. *Journal of Engineering Mechanics* 1997; **123**(9):897-971.

38. Friswell M.I., Inman D.J. The relationship between positive position feedback and output feedback controllers. *Smart Materials and Structures* 1999; **8**(3):285.

39. Soong T.T., Costantinou M.C. *Passive and Active Structural Vibration Control in Civil Engineering*. Springer-Verlag New York, NY, USA: 1994.

40. Cheng F.Y., Jiang H., Lou K. *Smart Structures: Innovative Systems for Seismic Response Control*. CRC Press: 2010.

41. Spencer Jr. B.F., Dyke S.J., Sain M.K. Magnetorheological dampers: a new approach to seismic protection of structures. *35th IEEE Conference on Decision and Control*. Kobe, Japan, 1996; 676-681.

42. Nagarajaiah S., Sahasrabudhe S. Seismic response control of smart sliding isolated buildings using variable stiffness systems: an experimental and numerical study. *Earthquake Engineering & Structural Dynamics* 2006; **35**(2):177-197.

43. Yang J.N., Kim J.-H., Agrawal A.K. Resetting semiactive stiffness damper for seismic response control. *Journal of Structural Engineering* 2000; **126**(12):1427-1433.

44. Zhu X., Jing X., Cheng L. Magnetorheological fluid dampers: A review on structure design and analysis. *Journal of Intelligent Material Systems and Structures* 2012; **23**(8):839-873.

45. Dyke S.J., Spencer Jr. B.F., Sain M.K., Carlson J.D. An experimental study of MR dampers for seismic protection. *Smart Materials and Structures* 1998; **7**(5):693.

46. Badel A., Sebald G., Guyomar D., Lallart M., Lefeuvre E., Richard C., Qiu J. Piezoelectric vibration control by synchronized switching on adaptive voltage sources: Towards wideband semi-active damping. *The Journal of the Acoustical Society of America* 2006; **119**(5):2815-2825.

47. Cho S.-W., Kim B.-W., Jung H.-J., Lee I.-W. Implementation of modal control for seismically excited structures using magnetorheological dampers. *Journal of Engineering mechanics* 2005; **131**(2):177-184.

48. Soong T., Reinhorn A., Wang Y., Lin R. Full scale implementation of active control. I: Design and simulation. *Journal of Structural Engineering* 1991; **117**(11):3516-3536.

49. Li H., Huo L. Advances in structural control in civil engineering in China. *Mathematical Problems in Engineering* 2010; **2010**

50. Andrawes B., DesRoches R. Unseating prevention for multiple frame bridges using superelastic devices. *Smart Materials and Structures* 2005; **14**(3):S60.

51. Ikeda Y. Active and semi-active control of buildings in Japan. *Journal of Japan Association for Earthquake Engineering* 2004; **4**(3):278-282.

52. Dyke S.J., Spencer Jr. B.F., Sain M.K., Carlson J.D. Modeling and control of magnetorheological dampers for seismic response reduction. *Smart Materials and Structures* 1996; **5**(5):565.

53. Butz T., Von Stryk O. Modelling and simulation of electro-and magnetorheological fluid dampers. *ZAMM - Journal of Applied Mathematics and Mechanics* 2002; **82**(1):3.

54. Carlson J.D. Low-cost MR fluid sponge devices. *Journal of Intelligent Material Systems and Structures* 1999; **10**(8):589-594.

55. Yan Y.X., Hui L.X., M Y., J F., Dong L.H. Dynamic response time of a metal foam magneto-rheological damper. *Smart Materials and Structures* 2013; **22**(2):1-8.

56. Wang J., Meng G. Magnetorheological fluid devices: principles, characteristics and applications in mechanical engineering. *Proceedings of the Institution of Mechanical Engineers, Part L: Journal of Materials Design and Applications* 2001; **215**(3):165-174.

57. Liu X.H., Fu Z.M., Yao X.Y., Li F. Performance of magnetorheological fluids flowing through metal foams. *Measurement Science Review* 2011; **11**(5):144-148.

58. Ahmadkhanlou F. *Design, modeling and control of magnetorheological fluid-based force feedback dampers for telerobotic systems*. The Ohio State University: 2008.

59. Kane M.B., Lynch J.P., Law K. Market-based control of shear structures utilizing magnetorheological dampers. *American Control Conference (ACC)*. San Francisco, California, 2011; 2498-2503.

60. Zivi E.L. Integrated shipboard power and automation control challenge problem. *Power Engineering Society Summer Meeting, 2002 IEEE*. 2002; 325-330.

61. Lei Y., Wu D., Liu Z. A New Decentralized Control Approach with Application to the ASCE Benchmark Control Problem under Earthquake Excitation. *Earth and Space Engineering, Science, Construction, and Operations in Challenging Environments*. 2010; 3141-3152.

62. Palacios-Quinonero F., Rossell J.M., Karimi H.R. Semi-decentralized Strategies in Structural Vibration Control. *Modeling Identification and Control* 2011; **32**(2):57-77.

63. Palacios-Quiñonero F., Rubió-Massegú J., Rossell J.M., Karimi H.R. Discrete-time multioverlapping controller design for structural vibration control of tall buildings under seismic excitation. *Mathematical Problems in Engineering* 2012; **2012**

64. Robinson C., Kumar P. Sending the most recent observation is not optimal in networked control: Linear temporal coding and towards the design of a control specific transport protocol. *46th IEEE Conference on Decision and Control*. 2007; 334-339.

65. Sun Z., Li B., Dyke S., Lu C. A novel data utilization and control strategy for wireless structural control systems with TDMA network. *ASCE International Workshop on Computing in Civil Engineering*. 2013; 23-25.

66. Rofooei F., Monajemi-Nezhad S. Decentralized control of tall buildings. *The Structural Design of Tall and Special Buildings* 2006; **15**(2):153-170.

67. Verdoljak R.D., Linderman L.E. Sparse feedback structures for wireless control of civil systems. *SPIE Smart Structures and Materials+ Nondestructive Evaluation and Health Monitoring*. 2015; 94350Z-94350Z-10.

68. Mutambara A.G. *Decentralized estimation and control for multisensor systems*. CRC press: 1998.

69. Shankar P.M. *Introduction to wireless systems*. Wiley New York: 2002.

70. Qu C., Huo L., Li H., Wang Y. A double homotopy approach for decentralized H∞ control of civil structures. *Structural Control and Health Monitoring* 2014; **21**(3):269-281.

71. Casciati S., Faravelli L., Chen Z. Frequency division multiplexing wireless connection. *2010 6th International Conference on Wireless Communications Networking and Mobile Computing (WiCOM)*. 2010; 1-4.

72. Casciati S., Chen Z. A multi-channel wireless connection system for structural health monitoring applications. *Structural Control and Health Monitoring* 2011; **18**(5):588-600.

73. Casciati S., Chen Z. An active mass damper system for structural control using real-time wireless sensors. *Structural Control and Health Monitoring* 2012; **19**(8):758-767.

74. Seto K., Mitsuta S. A new method for making a reduced-order model of flexible structures using unobservability and uncontrollability and its application in vibration control. *JSME International Journal. Ser. C, Dynamics, Control, Robotics, Design and Manufacturing* 1994; **37**(3):444-449.

75. Hori N., Seto K. Vibration Control of Flexible Space Structures Based on Reduced Order Modeling Method and Filtered LQ Control Theory. *JSME International Journal Series C* 2000; **43**(3):697-703.

76. Vaidyanathan S., Madhavan K. Reduced order design of large-scale discrete-time linear systems and its applications. *International Conference on Advances in Engineering, Science and Management (ICAESM)*. 2012; 83-87.

77. Madhavan K., Vaidyanathan S. *A Novel Design of Reduced Order Controllers Using Exponential Observers for Large-Scale Linear Discrete-Time Control Systems*. Springer: 2012.

78. Ravichandran C.S., Rani S.S., Manikandan T. Designing of PID controller for discrete time linear system using balanced approach reduced order model. *American Journal of Applied Sciences* 2007; **4**(3):155.

79. Carvalhal R., Júnior V.L., Brennam M. A comparison of two modal control strategies for the active vibration control of a truss structure. *Anais do XVIII Congresso Brasileiro de Engenharia Mecânica*. 2005;

80. Hrovat D., Barak P., Rabins M. Semi-active versus passive or active tuned mass dampers for structural control. *Journal of Engineering Mechanics* 1983; **109**(3):691-705.

81. Kurata N., Kobori T., Takahashi M., Niwa N., Midorikawa H. Actual seismic response controlled building with semi-active damper system. *Earthquake Engineering & Structural Dynamics* 1999; **28**(11):1427-1447.

82. Spencer Jr. B.F., Dyke S.J., Sain M.K., Carlson J.D. Phenomenological model for magnetorheological dampers. *Journal of Engineering Mechanics* 1997; **123**(3):230-238.

83. Jolly M.R., Bender J.W., Carlson J.D. Properties and applications of commercial magnetorheological fluids. *SPIE's 5th Annual International Symposium on Smart Structures and Materials*. San Diego, CA, 1998; 262-275.

84. Spencer Jr. B.F., Sain M.K. Controlling buildings: a new frontier in feedback. *Control Systems, IEEE* 1997; **17**(6):19-35.

85. Sassi S., Cherif K., Mezghani L., Thomas M., Kotrane A. An innovative magnetorheological damper for automotive suspension: from design to experimental characterization. *Smart Materials and Structures* 2005; **14**(4):811.

86. Ali S.F., Ramaswamy A. Hybrid structural control using magnetorheological dampers for base isolated structures. *Smart Materials and Structures* 2009; **18**(5):055011.

87. Choi S.B., Han Y.M. Hysteretic behavior of a magnetorheological fluid: experimental identification. *Acta Mechanica* 2005; **180**(1-4):37-47.

88. Klingenberg D.J. Magnetorheology: Applications and challenges. *AIChE Journal* 2001; **47**(2):246-249.

89. Dyke S.J. *Washington University Seismic Simulator Design and Construction*. NEEShub, 2015.

90. Tse T., Chang C.C. Shear-mode rotary magnetorheological damper for small-scale structural control experiments. *Journal of Structural Engineering* 2004; **130**(6):904-911.

91. Tsouroukdissian A.R., Ikhouane F., Rodellar J., Luo N. Modeling and identification of a small-scale magnetorheological damper. *Journal of Intelligent Material Systems and Structures* 2008;

92. Lin P.-Y., Chung L.-L., Loh C.-H. Semiactive control of building structures with semiactive tuned mass damper. *Computer-Aided Civil and Infrastructure Engineering* 2005; **20**(1):35-51.

93. Aydar G., Wang X., Gordaninejad F. A novel two-way-controllable magneto-rheological fluid damper. *Smart Materials and Structures* 2010; **19**(6):065024.

94. Chrzan M.J., Carlson J.D. MR fluid sponge devices and their use in vibration control of washing machines. *SPIE's 8th Annual International Symposium on Smart Structures and Materials*. Newport Beach, CA, 2001; 370-378.

95. Carlson J.D., Jolly M.R. MR fluid, foam and elastomer devices. *Mechatronics* 2000; **10**(4):555-569.

96. Spelta C., Previdi F., Savaresi S.M., Fraternale G., Gaudiano N. Control of magnetorheological dampers for vibration reduction in a washing machine. *Mechatronics* 2009; **19**(3):410-421.

97. Hoyle A., Arzanpour S., Shen Y. A novel magnetorheological damper based parallel planar manipulator design. *Smart Materials and Structures* 2010; **19**(5):055028.

98. Yi F., Dyke S.J., Caicedo J.M., Carlson J.D. Experimental verification of multiinput seismic control strategies for smart dampers. *Journal of Engineering Mechanics* 2001; **127**(11):1152-1164.

99. Liu X., Gao X., Li F., Yu H., Ye D. Shear Performance of a Metal Foam Magnetorheological Fluid Damper. 2015; **51**(1):4600107.

100. Gavin H.P., Hoagg J., Dobossy M. Optimal design of MR dampers. *US-Japan Workshop on Smart Structures for Improved Seismic Performance in Urban Regions*. Seattle, WA, 2001; 225-236.

101. Nguyen Q.H., Han Y.M., Choi S.B., Wereley N.M. Geometry optimization of MR valves constrained in a specific volume using the finite element method. *Smart Materials and Structures* 2007; **16**(6):2242.

102. Lin P.-Y., Roschke P., Loh C.-H. System identification and real application of the smart magneto-rheological damper. *International Symposium on Intelligent Control*. Limassol, Cyprus, 2005; 989-994.

103. Chassiakos A., Masri S., Smyth A., Caughey T. On-line identification of hysteretic systems. *Journal of Applied Mechanics* 1998; **65**(1):194-203.

104. Stengel R.F. *Optimal Control and Estimation*. Courier Dover Publications: 2012.

105. Lynch J.P., Wang Y., Swartz R.A., Lu K.-C., Loh C.-H. Implementation of a closed-loop structural control system using wireless sensor networks. *Structural Control and Health Monitoring* 2008; **15**(4):518-539.

106. Jordan E.C. *Reference Data for Engineers: Radio, Electronics, Computer, and Communications*. Sams: Carmel, 1991.

107. Chen S., Dong X., Kim J.-Y., Wu S., Wang Y. Design and performance validation of a compact wireless ultrasonic device for localized damage detection. *Advances in Structural Engineering* 2016; **19**(2):270-282.

108. Dong X., Chen S., Zhu D., Kane M., Wang Y., Lynch J.P. High-Speed Heterogeneous Data Acquisition using Martlet-A Next-Generation Wireless Sensing Node. *structure* 2014; **8**:9.

109. Ou J., Li H. Analysis of capability for semi-active or passive damping systems to achieve the performance of active control systems. *Structural Control and Health Monitoring* 2010; **17**(7):778-794.

110. Celebi M. *Seismic instrumentation of buildings (with emphasis on federal buildings)*. Report No. 0-7460-68170, United States Geological Survey, Menlo Park, CA: 2002.

111. Zhou G.D., Yi T.H., Zhang H., Li H.N. Energy-aware wireless sensor placement in structural health monitoring using hybrid discrete firefly algorithm. *Structural Control and Health Monitoring* 2015; **22**(4):648-666.

112. Casciati F., Faravelli L. Sensor placement driven by a model order reduction (MOR) reasoning. *Smart Structures and Systems* 2014; **13**(3):343-352.

113. Chopra A.K. *Dynamics of structures: theory and applications to earthquake engineering*. Pearson Prentice Hall: Upper Saddle River, NJ, 2011.

114. Hendricks E., Jannerup O., Sørensen P.H. *Linear systems control: deterministic and stochastic methods*. Springer Science & Business Media: 2008.

115. Callier F.M., Desoer C.A. *Linear system theory*. Springer Science & Business Media: 2012.

116. Wang Y. Time-delayed dynamic output feedback $\mathcal{H}\infty$ controller design for civil structures: A decentralized approach through homotopic transformation. *Structural Control and Health Monitoring* 2011; **18**(2):121-139.

117. Wang Y., Law K. Structural control with multi-subnet wireless sensing feedback: experimental validation of time-delayed decentralized H∞ control design. *Advances in Structural Engineering* 2011; **14**(1):25-39.

118. Wang Y., Lynch J.P., Law K.H. Decentralized $\mathcal{H}\infty$ controller design for large-scale civil structures. *Earthquake Engineering & Structural Dynamics* 2009; **38**(3):377-401.

119. Wang Y., Law K.H., Loh C.-H. Decentralized H2 control for civil structures through homotopic transformation. *Proceedings of the 5th World Conference on Structural Control and Monitoring*. 2010; 12-14.

120. Sun Z., Li B., Dyke D., Lu C. Evaluation of performances of structural control benchmark problem with time delays from wireless sensor network. *Joint Conference of the Engineering Mechanics Institute and ASCE Joint Specialty Conference on Probabilistic Mechanics and Structural Reliability*. 2012;

121. Singh A.K., Hahn J. Determining optimal sensor locations for state and parameter estimation for stable nonlinear systems. *Industrial & engineering chemistry research* 2005; **44**(15):5645-5659.

122. Spencer Jr B., Christenson R.E., Dyke S.J. Next generation benchmark control problem for seismically excited buildings. *Proceedings of the Second World Conference on Structural Control*. 1998; 1135-1360.

123. Winter B.D., Velazquez A., Swartz R.A. Low-force magneto-rheological damper design for small-scale structural control experimentation. *SPIE Smart Structures and Materials+ Nondestructive Evaluation and Health Monitoring*. 2015; 943511-943511-14.

124. Summers T.H., Cortesi F.L., Lygeros J. On submodularity and controllability in complex dynamical networks. *arXiv preprint arXiv:1404.7665* 2014;

125. Pasqualetti F., Zampieri S., Bullo F. Controllability metrics, limitations and algorithms for complex networks. *Control of Network Systems, IEEE Transactions on* 2014; **1**(1):40-52.

126. Winter B.D., Velazquez A.H., Swartz R.A. Low-Force Magneto-Rheological Damper Design for Small-Scale Structural Control Experimentation. *SPIE's 35th Annual International Symposium on Smart Structures and Materials: Nondestructive Evaluation and Health Monitoring*. 2015; Accepted.

127. Sun C., Nagarajaiah S. Study on semi-active tuned mass damper with variable damping and stiffness under seismic excitations. *Structural Control and Health Monitoring* 2014; **21**(6):890-906.

128. Ghaffarzadeh H., Dehrod E.A., Talebian N. Semi-active fuzzy control for seismic response reduction of building frames using variable orifice dampers subjected to near-fault earthquakes. *Journal of Vibration and Control* 2012:1077546312449179.

129. Kim J., Swartz A., Lynch J.P., Lee J.-J., Lee C.-G. Rapid-to-deploy reconfigurable wireless structural monitoring systems using extended-range wireless sensors. *Smart Structures and Systems* 2010; **6**(5-6):505-524.

130. Linderman L.E., Mechitov K.A., Spencer Jr B.F. *Real-time wireless data acquisition for structural health monitoring and control*. Newmark Structural Engineering Laboratory. University of Illinois at Urbana-Champaign.: 2011.

131. Ploplys N.J., Kawka P., Alleyne A.G. Closed-loop control over wireless networks. *Control Systems, IEEE* 2004; **24**(3):58-71.

132. Wang Y., Swartz R.A., Lynch J.P., Law K.H., Lu K.-C., Loh C.-H. Wireless feedback structural control with embedded computing. *Nondestructive Evaulation for Health Monitoring and Diagnostics*. San Diego, CA, 2006; 61770C-61770C-12.

133. Winter B.D., Swartz R.A. Communication patterning for multi-step TDMA bandwidth allocation using wireless structural control. *American Control Conference (ACC), 2016*. 2016; 6345-6350.

134. Durrant-Whyte H.F., Rao B., Hu H. Toward a fully decentralized architecture for multi-sensor data fusion. *Robotics and Automation, 1990. Proceedings., 1990 IEEE International Conference on*. 1990; 1331-1336.

135. Wang X., Sun T., Fan C. Neighborhood Kalman Estimation for Distributed Localization in Wireless Sensor Networks. *Mathematical Problems in Engineering* 2016; **2016**

136. Zhu B., Sinopoli B., Poolla K., Sastry S. Estimation over wireless sensor networks. *American control conference*. 2007; 2732-2737.

137. Kulkarni R.V., Venayagamoorthy G.K. Particle swarm optimization in wireless-sensor networks: A brief survey. *IEEE Transactions on Systems, Man, and Cybernetics, Part C (Applications and Reviews)* 2011; **41**(2):262-267.

138. Oruč S. *Optimal Scalable Decentralized Kalman Filter*. Eindhoven University of Technology, 2008.

139. Howkins R. Elevator ride quality–the human ride experience. *Proceedings of the ELEVCON 2006, Elevator Technology* 2006; **16**

140. Olfati-Saber R., Fax J.A., Murray R.M. Consensus and cooperation in networked multi-agent systems. *Proceedings of the IEEE* 2007; **95**(1):215-233.

141. Press W.H., Teukolsky S.A., Vetterling W.T., Flannery B.P. *Numerical recipes in C*. Cambridge university press Cambridge: 1996.

142. Abramowitz M., Stegun I.A. *Handbook of mathematical functions: with formulas, graphs, and mathematical tables*. Courier Corporation: 1964.

Appendix - Permission to Reprint Copyrighted Material

JOHN WILEY AND SONS LICENSE
TERMS AND CONDITIONS

Feb 21, 2017

This Agreement between Benjamin D Winter ("You") and John Wiley and Sons ("John Wiley and Sons") consists of your license details and the terms and conditions provided by John Wiley and Sons and Copyright Clearance Center.

License Number	4053960095898
License date	Feb 21, 2017
Licensed Content Publisher	John Wiley and Sons
Licensed Content Publication	Structural Control and Health Monitoring
Licensed Content Title	Low-force magneto-rheological damper design for small-scale structural control
Licensed Content Author	Benjamin D. Winter, R. Andrew Swartz
Licensed Content Date	Feb 16, 2017
Licensed Content Pages	1
Type of use	Dissertation/Thesis
Requestor type	Author of this Wiley article
Format	Print and electronic
Portion	Full article
Will you be translating?	No
Title of your thesis / dissertation	Limited Bandwidth Wireless Communication Strategies for Structural Control of Seismically Excited Shear Structures
Expected completion date	Mar 2017
Expected size (number of pages)	150
Requestor Location	Benjamin D Winter 1400 Townsend Drive Dow 849 HOUGHTON, MI 49931 United States Attn: Benjamin D Winter
Publisher Tax ID	EU826007151
Billing Type	Invoice

Billing Address	Benjamin D Winter 1400 Townsend Drive Dow 849 HOUGHTON, MI 49931 United States Attn: Benjamin D Winter
Total	0.00 USD

Terms and Conditions

TERMS AND CONDITIONS

This copyrighted material is owned by or exclusively licensed to John Wiley & Sons, Inc. or one of its group companies (each a"Wiley Company") or handled on behalf of a society with which a Wiley Company has exclusive publishing rights in relation to a particular work (collectively "WILEY"). By clicking "accept" in connection with completing this licensing transaction, you agree that the following terms and conditions apply to this transaction (along with the billing and payment terms and conditions established by the Copyright Clearance Center Inc., ("CCC's Billing and Payment terms and conditions"), at the time that you opened your RightsLink account (these are available at any time at http://myaccount.copyright.com).

Terms and Conditions

- The materials you have requested permission to reproduce or reuse (the "Wiley Materials") are protected by copyright.

- You are hereby granted a personal, non-exclusive, non-sub licensable (on a standalone basis), non-transferable, worldwide, limited license to reproduce the Wiley Materials for the purpose specified in the licensing process. This license, and any CONTENT (PDF or image file) purchased as part of your order, is for a one-time use only and limited to any maximum distribution number specified in the license. The first instance of republication or reuse granted by this license must be completed within two years of the date of the grant of this license (although copies prepared before the end date may be distributed thereafter). The Wiley Materials shall not be used in any other manner or for any other purpose, beyond what is granted in the license. Permission is granted subject to an appropriate acknowledgement given to the author, title of the material/book/journal and the publisher. You shall also duplicate the copyright notice that appears in the Wiley publication in your use of the Wiley Material. Permission is also granted on the understanding that nowhere in the text is a previously published source acknowledged for all or part of this Wiley Material. Any third party content is expressly excluded from this permission.

- With respect to the Wiley Materials, all rights are reserved. Except as expressly granted by the terms of the license, no part of the Wiley Materials may be copied,

modified, adapted (except for minor reformatting required by the new Publication), translated, reproduced, transferred or distributed, in any form or by any means, and no derivative works may be made based on the Wiley Materials without the prior permission of the respective copyright owner.For STM Signatory Publishers clearing permission under the terms of the STM Permissions Guidelines only, the terms of the license are extended to include subsequent editions and for editions in other languages, provided such editions are for the work as a whole in situ and does not involve the separate exploitation of the permitted figures or extracts, You may not alter, remove or suppress in any manner any copyright, trademark or other notices displayed by the Wiley Materials. You may not license, rent, sell, loan, lease, pledge, offer as security, transfer or assign the Wiley Materials on a stand-alone basis, or any of the rights granted to you hereunder to any other person.

- The Wiley Materials and all of the intellectual property rights therein shall at all times remain the exclusive property of John Wiley & Sons Inc, the Wiley Companies, or their respective licensors, and your interest therein is only that of having possession of and the right to reproduce the Wiley Materials pursuant to Section 2 herein during the continuance of this Agreement. You agree that you own no right, title or interest in or to the Wiley Materials or any of the intellectual property rights therein. You shall have no rights hereunder other than the license as provided for above in Section 2. No right, license or interest to any trademark, trade name, service mark or other branding ("Marks") of WILEY or its licensors is granted hereunder, and you agree that you shall not assert any such right, license or interest with respect thereto.

- NEITHER WILEY NOR ITS LICENSORS MAKES ANY WARRANTY OR REPRESENTATION OF ANY KIND TO YOU OR ANY THIRD PARTY, EXPRESS, IMPLIED OR STATUTORY, WITH RESPECT TO THE MATERIALS OR THE ACCURACY OF ANY INFORMATION CONTAINED IN THE MATERIALS, INCLUDING, WITHOUT LIMITATION, ANY IMPLIED WARRANTY OF MERCHANTABILITY, ACCURACY, SATISFACTORY QUALITY, FITNESS FOR A PARTICULAR PURPOSE, USABILITY, INTEGRATION OR NON-INFRINGEMENT AND ALL SUCH WARRANTIES ARE HEREBY EXCLUDED BY WILEY AND ITS LICENSORS AND WAIVED BY YOU.

- WILEY shall have the right to terminate this Agreement immediately upon breach of this Agreement by you.

- You shall indemnify, defend and hold harmless WILEY, its Licensors and their respective directors, officers, agents and employees, from and against any actual or threatened claims, demands, causes of action or proceedings arising from any breach of this Agreement by you.

- IN NO EVENT SHALL WILEY OR ITS LICENSORS BE LIABLE TO YOU OR ANY OTHER PARTY OR ANY OTHER PERSON OR ENTITY FOR ANYSPECIAL, CONSEQUENTIAL, INCIDENTAL, INDIRECT, EXEMPLARY OR PUNITIVE DAMAGES, HOWEVER CAUSED, ARISING OUT OF OR IN CONNECTION WITH THE DOWNLOADING, PROVISIONING, VIEWING OR USE OF THE MATERIALS REGARDLESS OF THE FORM OF ACTION, WHETHER FOR BREACH OF CONTRACT, BREACH OF WARRANTY, TORT, NEGLIGENCE, INFRINGEMENT OR OTHERWISE (INCLUDING, WITHOUT LIMITATION, DAMAGES BASED ON LOSS OF PROFITS, DATA, FILES, USE, BUSINESS OPPORTUNITY OR CLAIMS OF THIRD PARTIES), AND WHETHER OR NOT THE PARTY HAS BEEN ADVISED OF THE POSSIBILITY OF SUCH DAMAGES. THIS LIMITATION SHALL APPLY NOTWITHSTANDING ANY FAILURE OF ESSENTIAL PURPOSE OF ANY LIMITED REMEDY PROVIDED HEREIN.

- Should any provision of this Agreement be held by a court of competent jurisdiction to be illegal, invalid, or unenforceable, that provision shall be deemed amended to achieve as nearly as possible the same economic effect as the original provision, and the legality, validity and enforceability of the remaining provisions of this Agreement shall not be affected or impaired thereby.

- The failure of either party to enforce any term or condition of this Agreement shall not constitute a waiver of either party's right to enforce each and every term and condition of this Agreement. No breach under this agreement shall be deemed waived or excused by either party unless such waiver or consent is in writing signed by the party granting such waiver or consent. The waiver by or consent of a party to a breach of any provision of this Agreement shall not operate or be construed as a waiver of or consent to any other or subsequent breach by such other party.

- This Agreement may not be assigned (including by operation of law or otherwise) by you without WILEY's prior written consent.

- Any fee required for this permission shall be non-refundable after thirty (30) days from receipt by the CCC.

- These terms and conditions together with CCC's Billing and Payment terms and conditions (which are incorporated herein) form the entire agreement between you and WILEY concerning this licensing transaction and (in the absence of fraud) supersedes all prior agreements and representations of the parties, oral or written. This Agreement may not be amended except in writing signed by both parties. This Agreement shall be binding upon and inure to the benefit of the parties' successors, legal representatives, and authorized assigns.

- In the event of any conflict between your obligations established by these terms and conditions and those established by CCC's Billing and Payment terms and conditions, these terms and conditions shall prevail.

- WILEY expressly reserves all rights not specifically granted in the combination of (i) the license details provided by you and accepted in the course of this licensing transaction, (ii) these terms and conditions and (iii) CCC's Billing and Payment terms and conditions.

- This Agreement will be void if the Type of Use, Format, Circulation, or Requestor Type was misrepresented during the licensing process.

- This Agreement shall be governed by and construed in accordance with the laws of the State of New York, USA, without regards to such state's conflict of law rules. Any legal action, suit or proceeding arising out of or relating to these Terms and Conditions or the breach thereof shall be instituted in a court of competent jurisdiction in New York County in the State of New York in the United States of America and each party hereby consents and submits to the personal jurisdiction of such court, waives any objection to venue in such court and consents to service of process by registered or certified mail, return receipt requested, at the last known address of such party.

WILEY OPEN ACCESS TERMS AND CONDITIONS
Wiley Publishes Open Access Articles in fully Open Access Journals and in Subscription journals offering Online Open. Although most of the fully Open Access journals publish open access articles under the terms of the Creative Commons Attribution (CC BY) License only, the subscription journals and a few of the Open Access Journals offer a choice of Creative Commons Licenses. The license type is clearly identified on the article.

The Creative Commons Attribution License
The Creative Commons Attribution License (CC-BY) allows users to copy, distribute and transmit an article, adapt the article and make commercial use of the article. The CC-BY license permits commercial and non-Creative Commons Attribution Non-Commercial License.

The Creative Commons Attribution Non-Commercial (CC-BY-NC) License permits use, distribution and reproduction in any medium, provided the original work is properly cited and is not used for commercial purposes. (see below)

Creative Commons Attribution-Non-Commercial-NoDerivs License
The Creative Commons Attribution Non-Commercial-NoDerivs License (CC-BY-NC-ND) permits use, distribution and reproduction in any medium, provided